AD NUMBER

ADB254489

NEW LIMITATION CHANGE

TO

Approved for public release, distribution unlimited

FROM

Distribution authorized to U.S. Gov't. agencies only; Proprietary Info; Feb 2000. Other requests shall be referred to U.S. Army Medical Research and Materiel Command, 504 Scott Street, Ft Detrick, MD 21702-5012.

AUTHORITY

USAMRMC ltr, 28 Aug 2002

AD_____

Award Number: DAMD17-98-C-8040

TITLE: Combinatorial Strategies and Hypothesis-Based Drug Design in Drug Discovery Targeted to the Protease and Channel Activities of Botulinum Toxin A

PRINCIPAL INVESTIGATOR: Mauricio Montal, M.D., Ph.D.

CONTRACTING ORGANIZATION: University of California, San Diego
La Jolla, California 92093-0934

REPORT DATE: February 2000

TYPE OF REPORT: Midterm

PREPARED FOR: U.S. Army Medical Research and Materiel Command
Fort Detrick, Maryland 21702-5012

NOTICE

USING GOVERNMENT DRAWINGS, SPECIFICATIONS, OR OTHER DATA INCLUDED IN THIS DOCUMENT FOR ANY PURPOSE OTHER THAN GOVERNMENT PROCUREMENT DOES NOT IN ANY WAY OBLIGATE THE U.S. GOVERNMENT. THE FACT THAT THE GOVERNMENT FORMULATED OR SUPPLIED THE DRAWINGS, SPECIFICATIONS, OR OTHER DATA DOES NOT LICENSE THE HOLDER OR ANY OTHER PERSON OR CORPORATION; OR CONVEY ANY RIGHTS OR PERMISSION TO MANUFACTURE, USE, OR SELL ANY PATENTED INVENTION THAT MAY RELATE TO THEM.

LIMITED RIGHTS LEGEND

Award Number: DAMD17-98-C-8040
Organization: University of California, San Diego
Location of Limited Rights Data (Pages):

Those portions of the technical data contained in this report marked as limited rights data shall not, without the written permission of the above contractor, be (a) released or disclosed outside the government, (b) used by the Government for manufacture or, in the case of computer software documentation, for preparing the same or similar computer software, or (c) used by a party other than the Government, except that the Government may release or disclose technical data to persons outside the Government, or permit the use of technical data by such persons, if (i) such release, disclosure, or use is necessary for emergency repair or overhaul or (ii) is a release or disclosure of technical data (other than detailed manufacturing or process data) to, or use of such data by, a foreign government that is in the interest of the Government and is required for evaluational or informational purposes, provided in either case that such release, disclosure or use is made subject to a prohibition that the person to whom the data is released or disclosed may not further use, release or disclose such data, and the contractor or subcontractor or subcontractor asserting the restriction is notified of such release, disclosure or use. This legend, together with the indications of the portions of this data which are subject to such limitations, shall be included on any reproduction hereof which includes any part of the portions subject to such limitations.

THIS TECHNICAL REPORT HAS BEEN REVIEWED AND IS APPROVED FOR PUBLICATION.

_____ _____

_____ _____

REPORT DOCUMENTATION PAGE

OMB No. 074-0188

1. AGENCY USE ONLY (Leave blank)	2. REPORT DATE	3. REPORT TYPE AND DATES COVERED
	February 2000	Midterm (1 Jul 99 – 1 Jan 00)

4. TITLE AND SUBTITLE
Combinatorial Strategies and Hypothesis-Based Drug Design in Drug Discovery Targeted to the Protease and Channel Activities of Botulinum Toxin A

5. FUNDING NUMBERS
DAMD17-98-C-8040

6. AUTHOR(S)
Mauricio Montal, M.D., Ph.D.

7. PERFORMING ORGANIZATION NAME(S) AND ADDRESS(ES)
University of California, San Diego
La Jolla, California 92093-0934

E-MAIL:
montal@biomail.ucsd.edu

8. PERFORMING ORGANIZATION REPORT NUMBER

9. SPONSORING / MONITORING AGENCY NAME(S) AND ADDRESS(ES)
U.S. Army Medical Research and Materiel Command
Fort Detrick, Maryland 21702-5012

10. SPONSORING / MONITORING AGENCY REPORT NUMBER

11. SUPPLEMENTARY NOTES

12a. DISTRIBUTION / AVAILABILITY STATEMENT
Distribution authorized to U.S. Government agencies only (proprietary information, Feb 00). Other requests for this document shall be referred to U.S. Army Medical Research and Materiel Command, 504 Scott Street, Fort Detrick, Maryland 21702-5012.

12b. DISTRIBUTION CODE

13. ABSTRACT ***(Maximum 200 Words)***

The ultimate goal of this program is to understand in detail the mechanisms by which botulinum neurotoxins (BoNT) abrogate neurotransmitter release. One facet is focused on the channel-forming domain of the heavy chain (HC). The aim is to identify open channel blockers as a single class of drugs that would be effective against all BoNT isoforms. A major objective is to seek direct demonstration that the HC acts as the molecular conduit for the light chain (LC) thereby allowing the protease activity to reach the cytosol where it acts. Accordingly, purified HC is first reconstituted in lipid bilayers and the direct translocation of isolated LC through the HC channel is measured by single channel recordings and also by direct analytical determination of the LC protease activity. A second facet of the program involves the concept that the peptide products of substrate proteolysis by BoNTs uncouple excitation from secretion pointing to new means of intervention. This notion, discovered for BoNT A, appears to be valid for other BoNT isoforms thereby yielding a diverse repertoire of peptide sequences that may provide insights into the molecular interactions between partner proteins involved in membrane fusion. It is anticipated that this concerted and focused approach will uncover lead compounds that may be developed into selective drugs targeted to prevent or relieve the neurotoxic actions of BoNT.

14. SUBJECT TERMS
Botulinum neurotoxins; neurotoxicity; neurotransmission; ion channels; proteases; drug design

15. NUMBER OF PAGES
83

16. PRICE CODE

17. SECURITY CLASSIFICATION OF REPORT	18. SECURITY CLASSIFICATION OF THIS PAGE	19. SECURITY CLASSIFICATION OF ABSTRACT	20. LIMITATION OF ABSTRACT
Unclassified	Unclassified	Unclassified	Limited

NSN 7540-01-280-5500

Standard Form 298 (Rev. 2-89)
Prescribed by ANSI Std. Z39-18
298-102

FOREWORD

Opinions, interpretations, conclusions and recommendations are those of the author and are not necessarily endorsed by the U.S. Army.

MM Where copyrighted material is quoted, permission has been obtained to use such material.

___ Where material from documents designated for limited distribution is quoted, permission has been obtained to use the material.

___ Citations of commercial organizations and trade names in this report do not constitute an official Department of Army endorsement or approval of the products or services of these organizations.

N/A In conducting research using animals, the investigator(s) adhered to the "Guide for the Care and Use of Laboratory Animals," prepared by the Committee on Care and use of Laboratory Animals of the Institute of Laboratory Resources, national Research Council (NIH Publication No. 86-23, Revised 1985).

N/A For the protection of human subjects, the investigator(s) adhered to policies of applicable Federal Law 45 CFR 46.

N/A In conducting research utilizing recombinant DNA technology, the investigator(s) adhered to current guidelines promulgated by the National Institutes of Health.

N/A In the conduct of research utilizing recombinant DNA, the investigator(s) adhered to the NIH Guidelines for Research Involving Recombinant DNA Molecules.

N/A In the conduct of research involving hazardous organisms, the investigator(s) adhered to the CDC-NIH Guide for Biosafety in Microbiological and Biomedical Laboratories.

M. Monnig 1/24/2000

Award Number: DAMD17-98-C-8040

TITLE: Combinatorial Strategies and Hypothesis-Based Drug Design in Drug Discovery Targeted to the Protease and Channel Activities of Botulinum Toxin A

PRINCIPAL INVESTIGATOR: Mauricio Montal, M.D., Ph.D.

TABLE OF CONTENTS

INTRODUCTION

The ultimate goal of this program is to understand in detail the mechanisms by which botulinum neurotoxins (BoNT) abrogate neurotransmitter release. *Clostridial* neurotoxins act as sequence specific endoproteases to cleave specific constituents of the synaptic vesicle docking/fusion complex [1-6]. A widely held view considers that BoNTs enter cells via receptor-mediated endocytosis. Exposure of the holotoxin to the acidic pH of the endosomal vesicles induces a conformational change of the dichain toxin allowing the heavy chain (HC) to insert into the membrane thereby forming a channel through which the light chain (LC) protease is translocated to the cytosol where it acts [3]. This model considers a tri-modular design of the neurotoxin protein with a receptor binding domain, a translocation domain and a catalytic domain. Indeed, the crystal structures of BoNT A [7,8] and BoNT E [9] have disclosed such organization of the holotoxin and have given impetus to dissect in molecular detail the steps involved in intoxication. We have focused our efforts on two enigmatic aspects of the process: (1) The mechanism by which the HC forms the conduit for the translocation of the LC across a membrane; and (2) the contribution of the peptide products of BoNT protease activity on its substrates, namely, the components of the SNARE-complex [1-4].

That channels are formed by the HC has been surmised from evidence that the holotoxin forms channels in lipid bilayers, predominantly after exposure to an acidic pH [10-12; for review see ref. 13]. Further, a 23-mer peptide, patterned after the sequence of an amphipathic segment of the HC [659-681] predicted to self-assemble in membranes into a conductive oligomer, was shown to form channels in lipid bilayers [14]. Thus far, however, there is no evidence for the direct translocation of the LC through the putative channel and across the membrane. Several outstanding issues remain to be delineated. Key among these are the dissociation at acidic pH of the dichain toxin into its constituent LC and HC after breakdown of the disulfide bond linking them [Cys429-Cys453], the insertion of the HC monomers into the bilayer hydrophobic core, the oligomerization state of the HC when assembled into a conductive channel, the requirement of a pH gradient across the membrane, the unfolding of the LC in an acidic environment as a requirement for its passage through a narrow pore (the folded LC is 55 Å X 55 Å X 62 Å, too large

to fit through a postulated tetrameric channel of ~8 Å diameter at its widest extent), the refolding of the LC in the cytosol after its translocation. It is clear that a channel entity would constitute a critical target for intervention to abort the process of intoxication after internalization of the toxin. Screening for channel blockers continues to be a dominant aspect of the program. Thus far, the efforts were focused on the channels formed by the channel peptide alluded to before [HC, 659-681] . We plan to resume this task after establishing conditions to measure the channel activity of the isolated HC and/or the translocation domain. The most efficacious blockers will then be assayed for the ability to prevent the translocation of the LC through the channel.

This brings us to the second facet of the program. The crystal structure of a SNARE complex, a key entity involved in the specific recognition and ultimately fusion of synaptic vesicles with the neuronal plasma membrane was described [2] . The complex is formed by the specific interaction between segments of three proteins: synaptobrevin-2, a vesicle associated protein, and syntaxin-1A and SNAP-25B, two distinct proteins anchored to the plasma membrane. The SNARE complex folds into a parallel four-helical bundle with a left handed superhelical twist [2,4] : two helices are contributed by a molecule of the t-SNARE SNAP-25; the other two by synaptobrevin and syntaxin. We synthesized three peptides which correspond to sequences located in the syntaxin-1A H3 domain, the C-terminal domain of SNAP-25, and a conserved central domain of synaptobrevin-2, that exhibit a high propensity to form a minimal coiled-coil, and examined their ability to assemble into a coiled-coil using circular dichroism (CD) spectroscopy [15] . Our results with these synthetic peptides [15] are consistent with the high-resolution structure of the SNARE complex [2,4] . The four helical bundle structure of the SNARE complex may bring into juxtaposition the surfaces of the apposed vesicle and plasma membrane bilayers to facilitate fusion. How this may happen is not known, however, Ca^{2+} is required and other proteins may catalyze and confer additional specificity to the process [5,6] .

BoNTs proteolytically cleave the three proteins of the SNARE complex, consequently preventing vesicle fusion and thereby abrogating transmitter release [3] . Our program is focused on the cleavage fragments resulting from BoNT-

mediated substrate proteolysis and the emerging hypothesis that the efficacy of BoNTs as inhibitors of neurosecretion may arise from the synergistic action of cleaving the substrate and releasing peptide products that disable the fusion process by blocking specific steps of the exocytotic cascade [16-18] . Indeed, synthetic peptides corresponding to the sequences of the cleavage products of BoNT A and E act as inhibitors of neurosecretion, and mimic several aspects of the neurotoxin action *in vitro* [16-18] . Accordingly, effort has been directed to achieve the stable expression of the SNAP-25 C-terminal cleavage product of BoNT E in mammalian neurosecretory cells and to compare its activity with that of the expressed LC of BoNT E. As summarized in the BODY of the report (Section 6), we have implemented a robust assay for basal and evoked exocytosis in PC-12 cells and demonstrated the inhibitory activity of expressed BoNT A and BoNT E LCs on secretion of human growth hormone, used as the marker for secretory granules. Work in progress indicates that the conditions for peptide expression need to be optimized in order to reach levels commensurate with those necessary to achieve inhibition, as was previously demonstrated for synthetic peptides introduced into chromaffin cells after membrane permeablization, or after microinjection into *Aplysia* neurons [16-18] .

BODY

Task 1: Characterization of the ion channel of BoNT A and identification of open channel blockers.

The effort is focused on the intact HC of BoNT A reconstituted in lipid bilayers. We have used commercially available BoNT A HC from Calbiochem (Catalogue # 203652). The protein is supplied in 20 mM sodium phosphate, pH 7.5 supplemented with 10 mM mercaptoethanol. This protein exhibits a strong tendency to precipitate thereby limiting the reconstitution strategies and the range of experimental conditions necessary to explore the hypothesis formulated. We are exploring the possibility of securing cDNA clones encoding the HC in order to produce recombinant protein and to expand the range of reconstitution modalities. In an effort to overcome the precipitation problem we have started collaboration with Raymond C. Stevens, who has now moved to The Scripps Research Institute conveniently located also in La Jolla. Stevens and his group have produced recombinant translocation domain of BoNT A. This

domain is ~50 kDa and encompasses residues 488-872 of the holotoxin A sequence. This segment contains the channel-forming peptide [659-681] previously described by our group [14,19] . It also contains the elusive "belt" [492-545] , a 54-residue segment that wraps around the perimeter of the catalytic domain and, at pH 7.0, appears largely unstructured. This segment may be critical to facilitate the insertion of the translocation domain into the membrane and/or sense the pH [8] . Removal of the C-terminal ~50 kDa binding domain may reduce the tendency of the HC to aggregate and therefore lead to a reliable reconstitution scheme. Accordingly, we are in the process of producing recombinant translocation domain protein, which in due turn will be used in bilayer reconstitution experiments. An intriguing construct has also been designed aiming to examine the functional role of the "belt"; this construct is derived from the translocation domain yet it is devoid of the "belt" and the first 44-residues. The activity of the intact and the "belt-less" translocation domains will be examined after reconstitution in lipid bilayers. It will be interesting to assess if the "belt" sequence facilitates or confers membrane insertion capabilities on the translocation domain.

Reconstitution studies exploit the sensitivity of single channel recordings as an assay to uncover open channel blockers. Channel properties are characterized in terms of changes in single channel conductance, ionic selectivity, open channel lifetimes and open channel probability. Several "classes" of agents have been surveyed for open channel blocker activity based on their established efficacy against other cation-selective channel proteins. These have thus far included: Chlorpromazine, dizolcipine (MK-801) and a local anesthetic derivative of lidocaine -QX-222, all blockers of voltage-gated and ligand-gated channel proteins, as well as the antimalarial agents, chloroquine and quinacrine. The activity of these blockers will be reexamined on the reconstituted translocation domain.

A major aim consists in delineating the molecular events involved in the dissociation of the LC and the HC, the insertion of the HC into the bilayer and its assembly into a functional protein conducting channel, the direct measurement of the passage of the LC through the HC channel presumably as an unfolded polypeptide chain, the eventual refolding of the LC in a neutral pH environment and the

assay of its catalytic activity after completing the translocation steps. These studies will require the assembly of bilayers under a pH gradient (the cis-compartment at pH 4.8 and the trans-compartment at pH 7.4) aiming to mimic the conditions that may be prevalent across the endocytic vesicle. This analysis will be complemented with a determination of the pH profile for the unfolding and refolding of the LC. Such information is necessary to understand if the unfolded LC is the molecular entity that permeates across the HC channel and, if so, if it contains the inherent ability to refold a neutral pH after the translocation step is complete. As indicated, unfolding of the LC in an acidic environment may be a requirement for its passage through a pore of ~8 Å diameter (the folded LC is 55 Å X 55 Å X 62 Å), implying that refolding would occur in the cytosol after its translocation.

Another view considers that the HC may act as a chaperonin allowing the LC to unfold and refold inside a cavity formed by the HC in response to the extreme pH situations, as may occur during the transit of the toxin from the cell exterior via the endocytic pathway and then into the cytosol. A "chaperonin"-like activity of the HC may be associated with its ability to form a protein-conducting channel. Such a channel would be expected to exhibit a large conductance compatible with a wide patent pathway for the passage of the unfolded or partially folded LC. Testing this model would require using the intact HC and establishing a direct correlation between the conductance measurements in the bilayers with the actual transfer of the LC from one aqueous compartment to another. Implementation of these measurements is currently are under way.

Structure-function correlates aimed to determine reactive sites within the conductive pathway will be examined using our molecular model of the pore-forming structure [14] as well as the 3.3 Å structure obtained by the Stevens group [8]. It is anticipated that this analysis may yield insights into the structure of the binding pocket formed by the HC oligomeric pore and may outline the profile of the channel through which the LC may be translocated. This template structure may provide useful guidelines to optimize the design of pore blockers.

Two practical obstacles have hampered this facet of the program. The first concerns the availability of purified,

isolated HC and LC and the labile nature of the isolated chains. We have now collected cDNA clones for the LC of BoNT A (E. Johnson, University of Wisconsin) and BoNT E (Heiner Niemann, Medical School, Hannover, Germany) and we are producing recombinant LC. However, thus far, we have not secured clones for the HC; a request has been sent to Dr. B. Singh, University of Massachusetts Dartmouth) [20] to this effect. The second is associated with the recruitment of appropriately trained and committed personnel. Dr. Lilia Koriazova has recently joined the program. She is currently under training in the specific techniques required and implementing other components of the program, as described.

Task 2: Role of the peptide products of BoNT protease activity on neurotransmitter release.

Many studies in the past two years have examined SNARE assembly and inhibition of complex formation by these toxins in relation to the kinetics and regulation of exocytosis [21-24]. In this laboratory, *in-vitro* studies were performed examining the activity of these toxin cleavage products as potential inhibitors of exocytosis [16-18]. The 26 amino acid C-terminal peptide released by cleavage of SNAP-25 with BoNT E was introduced into permeabilized chromaffin cells as well as *Aplysia* neurons to study the impact on neurotransmitter release. It was concluded that the peptide, termed ESUP, inhibits vesicle docking and thus exocytosis by competing with SNAP-25 for coil formation within the SNARE complex. From these studies the question arose:

How does the stable expression of the SNAP-25 C-terminal cleavage product of BoNT E modulate neurosecretion in mammalian neurosecretory cells?

Approach: The 26-mer C-terminal fragment of SNAP-25 was subcloned into a mammalian expression vector, transfected into neurosecretory cells and the impact on exocytosis assessed.

Cloning: PCR primers were designed in order to clone the desired region of SNAP-25 into pCDNA3.1/ CTGFP-TOPO , a PCR cloning vector from *Invitrogen* with a C-terminal GFP (green fluorescent protein) fusion tag. Reverse primers were designed to generate either fused or unfused protein products within the vector. Fragments encoding 26 as well as 36 amino acids of the SNAP-25 C-terminus were cloned

with the idea that a longer fragment of the coil may exhibit a higher propensity for complex formation. Additionally, fragments encoding the C-terminal 26 and 36 amino acids of SNAP-25 were PCR cloned into pCR3.1-Uni, another *Invitrogen* mammalian expression vector (see Appendix 3, vector maps).

As positive controls for inhibition of exocytosis, LCs from BoNT A and E were also PCR cloned into pCDNA3.1/CTGFP-TOPO vector. Light chain A was only cloned in an unfused configuration to the GFP tag, but LC E was designed to be either fused or unfused (Stop) to the C-terminal GFP. Restriction and sequence analysis were used to confirm the identity of clones, and a good open reading frame was determined by entering the nucleotide sequence into ORF (NIH website program). Please see Appendix 1 (Primer sets) and Appendix 2 (Inventory of clones)

Cells: PC12 cells acquired from ATCC were cultured at 37°C, 5% CO_2, 80-90% humidity in high glucose DMEM (Biowhittaker) supplemented with 2 mM Glutamine, 10% Horse serum, 5% fetal bovine serum, fungizone and penicillin/streptomycin. One trypsinization step was required early in culture to disperse the cells, after which trituration through a 26 1/2 gauge needle was sufficient to disperse cells prior to plating.

Plating cells: 12-well tissue culture plates (Corning) were treated at least five hours and up to overnight at 37°C with 0.5-1 ml/well 0.2 mg/ml Poly-D-Lysine. Thereafter, wells were washed twice with sterile water and allowed to dry in the laminar flow hood. Dispersed PC12 cells were plated at a density of 0.5 - 1.0 X 10e6 cells/ml such that the total equaled ≈ 1.0 X 10e6 cells per well. These were allowed to incubate overnight before transfection.

Transfection: PC12 cells were transiently transfected with SNAP-25 fragments as well as the light chains of BoNT A and E. Control transfection vectors include pCDNA3.1+ and pCDNA3.1/CTGFP. These clones were each co-transfected with a commercially available mammalian expression vector encoding human growth hormone (pXGH5, Nichols Diagnostics) as a marker for regulated secretion/secretory granules. We adopted the method of Fisher and Burgoyne [25] using Effectene (Qiagen) as our transfection reagent. Secretion experiments were performed 72 hours post transfection.

For Effectene transfections, 0.1-0.2 µg pXGH5 and 0.2-1.1 µg test vector were transfected per well according to manufacturer's instructions. The level of hGH expression as measured by ELISA served as an index for transfection efficiency. Because Effectene is nontoxic to PC12 cells and the method allows for transfection in complete cell media, the transfection mixture was left on the cells for 48 hours before changing the media. This seemed to improve expression levels of hGH.

Secretion: Cells were stimulated to undergo exocytosis by either depolarization with 55 mM KCl in calcium secretion buffer [CaSB: NaCl 150 mM, $CaCl_2$ 2 mM, KCl 5 mM, HEPES 10 mM, pH 7.4], or stimulation with 300 µM ATP using the Krebs'-Ringer buffer (NaCl 145 mM, KCl 5mM, $MgCl_2$ 1.3 mM, NaH_2PO_4 1.2 mM, dextrose 10 mM, HEPES 20 mM, $CaCl_2$ 3 mM, pH 7.4) [25] .

Secretion was performed at room temperature for 15 min, after which the secretion supernatant was collected and frozen at -20°C. Cells were then lysed in buffer containing 1% Triton X-100 for 15 - 30 min on a rocker and the lysate was collected and frozen at -20°C. Samples were stored at -20°C until assay by ELISA for hGH .

ELISA: hGH ELISA was performed according to the manufacturer (Boehringer Mannheim/Roche, cat# 1585878). Secretion was expressed as the percentage of total hGH released; the hGH value given for the secretion supernatant was divided by the sum of the hGH values for supernatant and lysate for each well.

Results:

Summarized secretion data for ATP-stimulated exocytosis are shown below. The results indicate that in this mammalian expression system, BoNT LC A and E inhibit exocytosis, whereas the ESUPs tested have little if any effect.

ATP-evoked hGH secretion in PC12 cells transiently transfected with control vector or vector encoding BoNT LCA or LCE. Conditions were as described in the Body of the report.

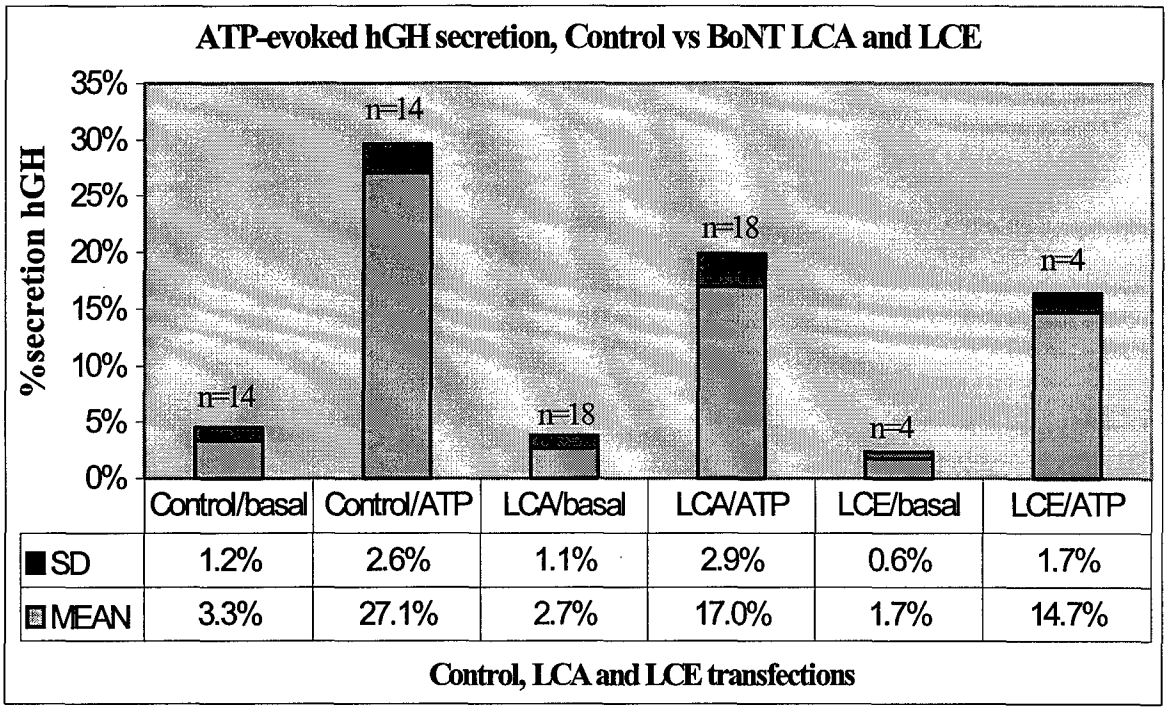

ATP-evoked hGH secretion in PC12 cells transiently transfected with control vector or vector encoding ESUP26 or ESUP36. Conditions were as described in the Body of the report.

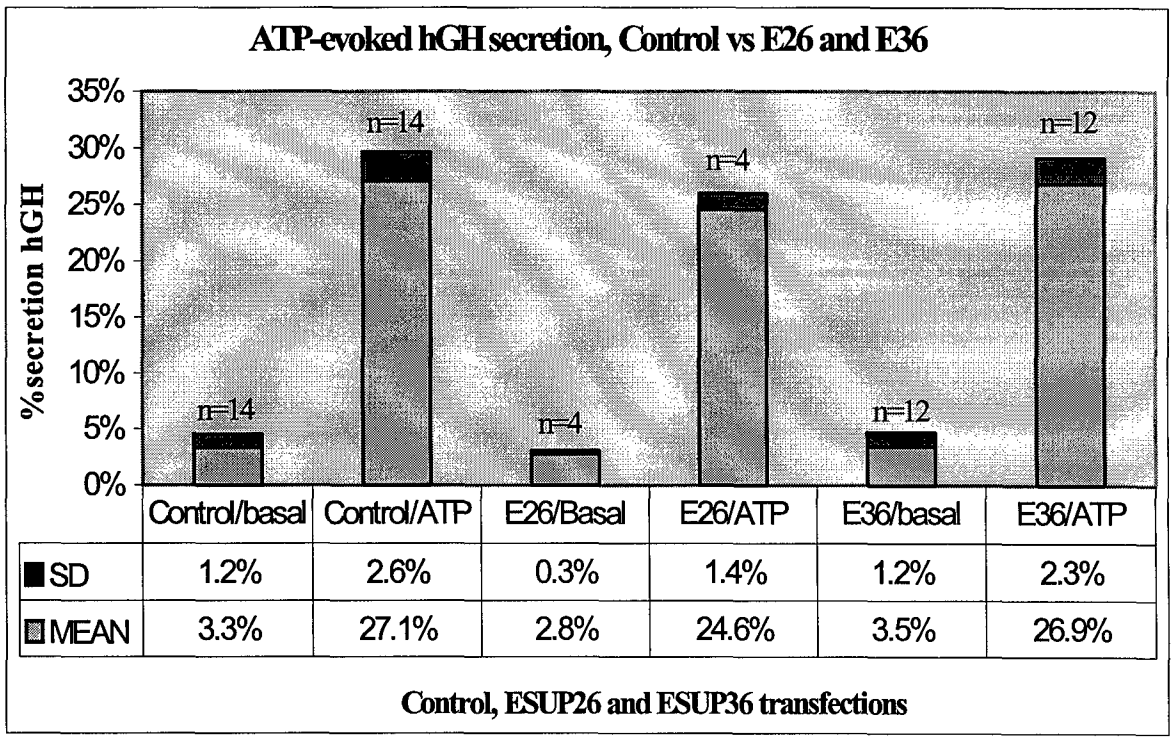

It is not clear why ESUPs are inhibitory when introduced as peptides into permeabilized cells or microinjected into neurons [16-18] but not when transfected as mammalian expression clones. One explanation could be that the quantity of ESUP produced within the cell is insufficient to render it an effective inhibitor. In the permeabilization studies, it took ~1000-fold more peptide than toxin to show a similar effect [18]. The LCs act enzymatically and therefore may not require robust expression levels to show activity. In addition to varying the amount of test vector transfected into cells, attempts were made to boost vector expression by the addition of sodium butyrate (NaBut) to transfected cells [26]. While treatment of transfected cells with NaBut increased expression of hGH significantly, it also altered the cell morphology and the nature of secretion. In some experiments, the cells appeared to "fuse" into syncitial looking "mats." In others, the secretion profiles seemed unregulated, such that basal secretion was as high as stimulated secretion. It is possible that NaBut overstimulated production of hGH to the extent that hGH was no longer secreted exclusively by the regulated exocytosis pathway. Although NaBut treatment may be a useful tool to boost vector expression, as yet we have not developed a reliable protocol for treating PC12 cells with NaButyrate without interfering with normal cell growth and secretion.

Another possibility for the inactivity of these clones is that the peptide is not being expressed or is degraded by the cell before reaching its target. In order to verify peptide expression, western blotting was performed on the secretion assay lysates using antibodies specific to the N and C terminus of SNAP-25. Although the LC transfections appear to block exocytosis by functional assay, we could not detect cleaved SNAP-25 in our lysates, nor could we detect peptide expression in the E36 transfected samples. Given that transfection efficiencies or expression may not be high enough to detect peptide product in the overall cell population, immunoprecipitation assays using the SNAP-25 antibodies will be the next effort to demonstrate peptide expression and SNAP-25 cleavage by the BoNT LCs. Northern blots or RT-PCR assays may be necessary in order to confirm mRNA expression as well. Antibodies to BoNT LCs are limited at present, but peptide antibodies are currently being raised to various regions of BoNT LC A. There are also preliminary functional data indicating that

the ESUPs are expressed: cotransfection of LC and ESUP vectors seem to show partial rescue of exocytosis. If indeed the ESUPs in question can interfere with toxin activity but do not themselves act as effective inhibitors of exocytosis, it may be necessary to examine other peptide regions and /or components of the SNARE complex as ESUPs.

In addition to transient transfection assays, we have stably transfected PC12s with pCDNA3.1/CTGFP, E36, E26 (2 clones) and LCA vectors. Cells were transfected with GenePorter (GeneTherapy Systems), expression was boosted with NaButyrate (which was discontinued due to cell fusing), and then cells were selected over several weeks using G418. Cell phenotype returned to normal during this time. Cultures were maintained as a population rather than cloning out individual cell lines. DNA was extracted from cell samples and PCR screening was done to determine if the cell DNA contained the transfect of interest. In general, one primer from the vector and one primer from the cloned insert were used. In all G418 selected cell populations except the E26 transfected cells, a single PCR product of the correct size was detected, indicating that the vector had stably integrated into the cell genome. In the E26 cells, a ladder like product was generated, suggesting that the vector has inserted in tandem or in multiple sites of the genome. It will be necessary to confirm the identity of the transfected cell DNA and PCR products by Southern blotting. Digestion of the E26 PCR product with an enzyme specific to the insert should define if the insertion is a tandem repeat. hGH transfection and secretion experiments are currently underway to determine the exocytotic capacity of these cell populations. In addition, cell lysates have been made in order to perform western blots and immunoprecipitation assays to confirm expression of the transfected genes. Northern blots and/or RT-PCR will also be performed in order to confirm mRNA expression if necessary.

As alluded to previously, the repertoire of ESUPs may be expanded to other SNARE protein peptides, such as the syntaxin region cleaved by BoNT C. Another candidate may be the N terminal segment of SNAP-25 involved in the coiled-coil SNARE complex to which Xu et al [24] raised antibodies that inhibit exocytosis. However, before embarking on further peptide design and expression, it will first be necessary to confirm ESUP expression in our system.

KEY RESEARCH ACCOMPLISHMENTS

- Activation of store-operated calcium-current in *Xenopus* oocytes requires SNAP-25 but not a diffusible messenger.

Depletion of Ca^{2+} stores in *Xenopus* oocytes activated entry of Ca^{2+} across the plasma membrane, which was measured as a current I_{SOC} in subsequently formed cell-attached patches. I_{SOC} survived excision into inside-out configuration. If cell-attached patches were formed before store depletion, I_{SOC} was activated outside but not inside the patches. I_{SOC} was potentiated by microinjection of *Clostridium* C3 transferase, which inhibits Rho GTPase, whereas I_{SOC} was inhibited by expression of wild-type or constitutively active Rho. Activation of I_{SOC} was also inhibited by *Clostridium* BoNT A and dominant-negative mutants of SNAP-25 but was unaffected by brefeldin A. These results suggest that oocyte I_{SOC} is dependent not on aqueous diffusible messengers but on SNAP-25, probably via exocytosis of membrane channels or regulatory molecules.
Cell 98:475-485 (1999)

- Electrostatic attraction at the core of membrane fusion.

SNARE proteins appear to be involved in homotypic and heterotypic membrane fusion events. The crystal structure of the synaptic SNARE complex exhibits a parallel four-helical bundle fold with two helices contributed by SNAP-25, a target SNARE (t-SNARE), and the other two by a different t-SNARE, syntaxin, and a donor vesicle SNARE (v-SNARE), synaptobrevin. The carboxy-terminal boundary of the complex, predicted to occur at the closest proximity between the apposed membranes, displays a high density of positively charged residues. This feature combined with the enrichment of negatively charged phospholipids in the cytosolic exposed leaflet of the membrane bilayer suggest that electrostatic attraction between oppositely charged interfaces may be sufficient to induce dynamic and discrete micellar discontinuities of the apposed membranes with the transient breakdown at the junction and subsequent reformation. Thus, the positively charged end of the SNARE complex in concert with Ca^{2+} may be sufficient to generate a transient "fusion pore".
FEBS Lett. 447:129-130 (1999)

- Assembly of a ternary complex by the predicted minimal coiled-coil forming domains of syntaxin, SNAP-25 and synaptobrevin.

The assembly of target (t-SNARE) and vesicle-associated (v-SNARE) proteins is a critical step for the docking of synaptic vesicles to the plasma membrane. Syntaxin-1A, SNAP-25 and synaptobrevin-2 (VAMP-2) bind to each other with high affinity, and their binding regions are predicted to form a trimeric coiled-coil. We designed three peptides which correspond to sequences located in the syntaxin-1A H3 domain, the C-terminal domain of SNAP-25, and a conserved central domain of synaptobrevin-2, that exhibit a high propensity to form a minimal trimeric coiled-coil. The peptides were synthesized by solid phase methods and their interactions were studied by CD spectroscopy. In aqueous solution, the peptides were unstructured and showed no interactions with each other. In contrast, upon addition of moderate amounts of trifluoroethanol (30%), the peptides adopted an α-helical structure and displayed both homomeric and heteromeric interactions. The interactions observed in ternary mixtures induce a stabilization of peptide structure that is greater than that predicted from individual binary interactions, suggesting the formation of a higher order structure compatible with the assembly of a trimeric coiled-coil.
J. Biol. Chem. 273:34214-34221 (1998)

- The 26-mer peptide released from SNAP-25 cleavage by botulinum neurotoxin E inhibits vesicle docking.

BoNT E cleaves SNAP-25 at the C-terminal domain releasing a 26-mer peptide. This peptide product may act as an excitation-secretion uncoupling peptide (ESUP) to inhibit vesicle fusion and thus contribute to the efficacy of BoNT E in disabling neurosecretion. We have addressed this question using a synthetic 26-mer peptide which mimics the amino acid sequence of the naturally released peptide, and is hereafter denoted as ESUP E. This synthetic peptide is a potent inhibitor of Ca^{2+}-evoked exocytosis in permeabilized chromaffin cells and reduces neurotransmitter release from identified cholinergic synapses in *in vitro* buccal ganglia of *Aplysia californica*. In chromaffin cells, both ESUP E and BoNT E abrogate the slow component of secretion without affecting the fast, Ca^{2+}-mediated fusion event. Analysis of immunoprecipitates of the synaptic ternary complex involving SNAP-25, VAMP and syntaxin demonstrates that ESUP E interferes with the assembly of the docking complex. Thus, the efficacy of BoNTs as inhibitors of neurosecretion may arise from the synergistic action of cleaving the

substrate and releasing peptide products that disable the fusion process by blocking specific steps of the exocytotic cascade.
FEBS Lett. 435:84-88 (1998)

- Structural stabilization of botulinum neurotoxins by tyrosine phosphorylation.

Tyrosine phosphorylation of BoNTs augments their proteolytic activity and thermal stability, suggesting a substantial modification of the global protein conformation. We used Fourier-Transform Infrared (FTIR) spectroscopy to study the modulation of secondary structure and thermostability of tyrosine phosphorylated BoNT A and BoNT E. Changes in the conformationally-sensitive amide I band of the infrared spectra upon phosphorylation indicated alterations in the protein secondary structure; the α-helix content increased with a concomitant decrease of less ordered structures such as turns and random coils, and without any change in β-sheet content. This change in secondary structure was accompanied by an increase in the amide II band absorbance remaining upon H-D exchange, suggesting tighter packing for the phosphorylated protein. FTIR and Differential Scanning Calorimetry (DSC) analyses of the denaturation process show that phosphorylated neurotoxins denaturated at temperatures higher than those required by nonphosphorylated species. These findings indicate that tyrosine phosphorylation induced transition to higher order and more compact structure probably imparts to the phosphorylated neurotoxins the higher catalytic activity and thermostability.
FEBS Lett. 429:78-82 (1998)

- Structural characteristics of a 23-mer channel forming peptide from botulinum neurotoxin type A.

A channel-forming peptide from the translocation domain of the HC of BoNTA has been examined by CD in order to probe transitions in secondary structure induced by environmental variables such as solvent polarity and pH. The secondary structure of the peptide is highly sensitive to solvent and pH. In aqueous solution at pH 7.0, the peptide was unstructured. In contrast, upon addition of trifluoroethanol (up to 60%), the peptide adopted a conformation compatible with a mixture of α-helix and β-sheets. At pH 3.3, the peptide exhibited primarily a β-sheet configuration at TFE concentrations below 30%, whereas it was primarily α-helical at TFE concentrations above 40%. This sensitivity to pH and solvent polarity are compatible

with the requirement of an amphipathic segment to insert into the hydrophobic core of a bilayer. Such features are consistent with the channel forming activity recorded after reconstitution of the peptide in lipid bilayers and may reflect the key contribution of this segment of the HC towards the insertion of the translocation domain into the bilayer core.

Protein Sci. 7: p.116, Abst. 361- (1998)

REPORTABLE OUTCOMES:

- Research Articles and Abstracts

1. Yao, Y., Ferrer-Montiel, A.V.F., Montal, M., and Tsien, R.Y. Activation of store-operated calcium-current in *Xenopus* oocytes requires SNAP-25 but not a diffusible messenger. **Cell** 98:475-485 (1999)

2. M. Montal. Electrostatic attraction at the core of membrane fusion. **FEBS Lett.** 447: 129-130 (1999).

3. J. M. Cànaves and M. Montal. Assembly of a Ternary Complex by the Predicted Minimal Coiled-coil-forming Domains of Syntaxin, SNAP-25, and Synaptobrevin. A circular dichroism study. **J. Biol. Chem.** 273: 34214-34221 (1998).

4. Apland, J.P., Biser, J.A., Adler, M., Ferrer-Montiel, A.V., Montal, M. and Filbert, M.G. Peptides composed of carboxy-terminal domains of SNAP-25 block acetylcholine release at an *Aplysia* synapse. **Soc. Neurosci. Abstr.** 24 (Part 1) 73, 35.1 (1998).

5. Yao, Y., Ferrer-Montiel, A.V., Montal, M., and Tsien, R.Y., Botulinum neurotoxin A inhibits capacitative Ca^{2+} influx but not Ca^{2+} release in *Xenopus* oocytes. **Soc. Neurosci. Abstr.** 24 (Part 2) 2030, 812.4 (1998).

6. Ferrer-Montiel, A.V., J.M. Merino, R. Planells-Cases, W. Sun and M. Montal. Structural determinants of the blocker binding site in glutamate and NMDA receptor channels.**Neuropharmacology** 37:139-147. (1998).

7. Encinar, J.A., Fernandez, A., Ferragut, J.A., Gonzalez-Ros, J.M., DasGupta, B.R, Montal, M, and Ferrer-Montiel-

A. Structural stabilization of botulinum neurotoxins by tyrosine phosphorylation. **FEBS Lett.** 429:78-82 (1998)

8. Byrne, M.P., Montal, M., Canaves, J. and Lebeda, F.J. Conformational changes of a channel forming peptide from the translocation domain of botulinum neurotoxin as detected by circular dichroism. **Protein Sci.** 7: p.116, Abst. 361-T (1998)

9. Apland, J.P., Biser, J.A., Adler, M. Ferrer-Montiel, A.V., Montal, M., and Filbert, M.G.Peptides that mimic the carboxy-terminal domain of SNAP-25 block acetylcholine release at an *Aplysia* synapse. **Biosci. Rev.** p.184 (1998)

10. Ferrer-Montiel, A.V., Oblatt-Montal, M., Canaves, J., and Montal, M. Botulinum neurotoxins: Modulation of protease and channel activities by tyrosine phosphorylation. **Biosci. Rev.** p.190 (1998)

11. Ferrer-Montiel, A.V., Gutierrez, L.M., Apland, J.P., Canaves, J.M., Gil, A., Viniegra, S., Biser, J.A., Adler, M. and Montal, M. The 26-mer peptide released from SNAP-25 cleavage by botulinum neurotoxin E inhibits vesicle docking. **FEBS Lett.** 435:84-88 (1998)

- Presentations:

1) Blanes-Mira, C., Gil, A., Llobregat, M., Fernandez-Ballester, G., Planells-Cases, R.,Perez-Paya, E., Canaves, J., Gutierrez, L.M., Montal, M. and Ferrer-Montiel, A. Modulation of SNAP-25-Syntaxin-VAMP complex formation and stability by small peptides. **Annual Meeting of the Spanish Biophysical Society. Alicante, Spain** (1998).

2) Apland, J.P., Biser, J.A., Adler, M. Ferrer-Montiel, A.V., Montal, M., and Filbert, M.G.Peptides that mimic the carboxy-terminal domain of SNAP-25 block acetylcholine release at an *Aplysia* synapse. **U.S. Army Medical Defense Bioscience Review. Hunt Valley, Maryland,** 31 May-4 June, 1998.

3) Ferrer-Montiel, A.V., Oblatt-Montal, M., Canaves, J., and Montal, M. Botulinum neurotoxins: Modulation of protease and channel activities by tyrosine phosphorylation. **U.S. Army Medical Defense Bioscience Review. Hunt Valley, Maryland,** 31 May-4 June, 1998.

4) Lebeda, F.J., Montal, M., Singh, B.R. and Byrne, M. Structural characteristics of a 23-mer channel forming peptide from botulinum neurotoxin type A. **Interagency Botulism Research Coordinating Committee (IBRCC). Philadelphia, Pennsylvania**, November, 1998.

5) Montal, M. Modulation of botulinum neurotoxin protease activity by tyrosine phosphorylation. **Interagency Botulism Research Coordinating Committee (IBRCC). Orlando, Florida November**, 1999.

- Patents and licenses applied for and/or issued:

U.S. Patent Application No. 08/819,286.
Title: PEPTIDE INHIBITORS OF NEUROTRANSMITTER SECRETION BY NEURONAL CELLS.
Filing Date, March 18, 1997.
Inventors: Mauricio Montal, Antonio Ferrer-Montiel and Jaume Canaves.
University of California Reference: SD 96-088

- Degrees obtained: Not applicable.
- Development of cell lines: In progress.
- Informatics: Not applicable.
- Funding applied for based on work supported by this award: Not applicable.
- Employment or research opportunities based on this award: Not applicable.

CONCLUSIONS

The thrust of this program aims to identify the role of the channel-forming domain of the HC in the intoxication process and, ultimately, to provide a potential target for drug intervention in the management of botulism based on the development of BoNT-specific channel blockers. The contribution of the cleavage products of BoNTs activity on their substrates to the global intoxication efficacy is also evaluated. A patent application, resulting from this analysis, has been submitted: it embodies the concept that the peptide products of substrate proteolysis by BoNTs can be developed into lead compounds acting as practical inhibitors of neurotransmitter secretion. Considerable progress has been achieved in both fronts of the program, as summarized in the BODY of the report and ascertained by the published work. Outstanding issues remain to be delineated concerning the molecular events involved in the

translocation of the LC across membranes and the role of the HC in the process. Similarly, expansion of the repertoire of ESUP sequences and their efficacy as inhibitors of neurosecretion in cells remains to be realized. It is anticipated that this concerted and focused program will uncover lead compounds that may be developed into selective drugs targeted to prevent, attenuate or relieve the neurotoxic action of BoNT.

REFERENCES

1) Söllner, T., Whiteheart, S.W., Brunner, M., Erdjument-Bromage, H., Geromanos, S., Tempst, P., and Rothman, J.E., 1993. Nature 362,318-324.
2) Sutton R.B., Fasshauer, D., Jahn, R. and Brunger, A.T. 1998. Nature 395, 347-353
3) Montecucco, C., and Schiavo, G. 1995.Q. Rev. Biophys. 28, 423-72.
4) Poirier, M. A., Xiao, W., Macosko,J.C., Chan, C., Shin Y.-K. and Bennett, M.K. 1998. Nature Struct. Biol. 5, 765-769.
5) Shao, X., Li, C., Fernandez, I., Zhang, X., Südhof, T.C. and Rizo, J. 1997. Neuron 18,133-142.
6) Rettig, J., Heinemann, C., Ashery, U., Sheng, Z.-H., Yokoyama, C.T., Catterall, W.A., and Neher, E. 1997. J. Neurosci. 17, 6647-6656.
7) Lacy, D.B. and Stevens, R.C. 1999. J. Mol. Biol. 291, 1091-104.
8) Lacy, D.B., Tepp, W., Cohen, A.C., DasGupta, B.R. and Stevens, R.C. 1998. Nature Struct. Biol. 5, 898-902.
9) Swaminathan, S, and Eswaramoorthy, S. 1999. Intl. Conference 1999. Basic and Therapeutic Aspects of Botulinum and Tetanus Toxins. Orlando, FL, November 16-18, 1999. Abstract, page 28.
10) Donovan, J.J. and Middlebrook, J.L. 1986. Biochemistry 25, 2872-2876.
11) Hoch, D.H., Romero-Mira, M., Ehrlich, B.E., Finkelstein, A., DasGupta, B.R., and Simpson, L. 1985. Proc. Natl. Acad. Sci. USA 82, 1692-1696.
12) Blaustein, R.O., Germann, W.J., Finkelstein, A., and DasGupta, B.R. 1987. FEBS Lett. 226, 115-120.
13) Lebeda, F.J. and Singh, B.R. 1999. J. Toxicol.-Toxin Reviews 18, 45-76.
14) Oblatt-Montal, M., Yamazaki, M., Nelson, R., and Montal, M. 1995. Protein Sci. 4,1490-1497.
15) Canaves, J.M. and Montal, M. 1998. J. Biol. Chem. 273,34214-34221.

16) Gutierrez, L.M., Canaves, J.M., Ferrer-Montiel, A.V., Reig, J.A., Montal, M. and Viniegra, S..1995. FEBS Lett. 372,39-43.
17) Gutierrez, L.M., Viniegra, S., Rueda, J., Ferrer-Montiel, A.V., Canaves, J.M. and M. Montal.1997. J. Biol. Chem. 272:2634-2639.
18) Ferrer-Montiel, A.V, Gutierrez, L.M., Apland, J.P., Canaves, J.M., Gil, A.,Viniegra, S., Biser, J.A., Adler, M. and Montal, M. 1998. FEBS Lett. 435:84-88.
19) Byrne, M.P., Lebeda, F.J., Canaves, J. and Montal, M. 1998. Protein Sci.7, p.116, ABST. 361-T.
20) Li, L. and Singh, B.R. 1999. J. Protein Chem. 18,89-95.
21) Weber, T., Zemelman, B.V., McNew, J.A., Westermann, B., Gmachl, M., Parlati, F., Söllner, T.H and Rothman, J.E. 1998. Cell 92,759-772.
22) Rizo, J. and Südhof, T.C. 1998. Nature Struct. Biol. 5, 839-842.
23) Chen, Y.A., Scales, S.J., Paytel, S.M., Doung, Y.-C., and Scheller, R.H. 1999. Cell 97,165-174.
24) Xu, T., Rammer, B., Margittal, M., Artalejo, A.R., E. Neher, and Jahn, R. 1999. Cell 99, 713-722.
25) Fisher, R.J. and Burgoyne, R.D. 1999. Pflügers Arch.-Eur. J. Physiol. 437,754-762.
26) Condreay, J.P., Witherspoon, S.M., Clay, W.C., and Kost, T.A. 1999. Proc. Natl. Acad. Sci. USA 96,127-132.

APPENDICES

APPENDIX 1

Primer sets used in cloning:

- ESUPsense and antisense, designed by Rosa Planells-Cases, used to PCR TOPO clone the 36aa C-terminus of SNAP-25 (E36) into pCDNA3.1/CTGFP-TOPO, unfused. The substrate used for PCR cloning of SNAP-25 fragments was either the human SNAP-25 clone in pGEM vector provided by Michael Wilson or the ESUP clones generated by Rosa Planells-Cases in pCINeo.

ESUPsense: 5'-GGG**GAATTC***ATG*GATACACAGAATCGC-3' contains an **EcoRI** site as well as a *start* codon. This codes for .

ESUPantisense: 5'-**CCCGGG**TCGAC*TTA*ACCACTTCCCAGCATG-3' contains **SmaI** and SalI site as well as a *stop* codon.

- ESUPForXho1 and ESUPRevX, designed by Natalie Gude, used to TOPO clone E26 into pCR3.1-Uni, unfused.

ESUPForXho1: 5'-**CTCGAG***ATG*ATC*ATGG*AGAAGGCTG-3' contains **XhoI** site and *start* codon. Note there are two possible start sites, the second of which may have a better Kozak sequence.

ESUPRevX: 5'-AGATCT*TTA*ACCACTTCCCAGC-3' contains a *stop* codon.

- ESUP25For, ESUP36For, ESUPRevFuse, designed by Natalie Gude, used to TOPOclone E25 and E36, respectively, into pCDNA3.1/CTGFP-TOPO fused to the GFP tag. Note that none of these primers contain restriction sites.

ESUP25For: 5'-**G**ATC*ATGG*AGAAGGCTGATTCC-3' contains a *start* codon and Kozak sequence recommended by Invitrogen. Also included is a 5'-**G** to optimize addition of the A overhang required in PCR cloning.

ESUP36For: 5'-**G**ATC*ATGG*ATACACAGAATCGC-3' contains the same features as ESUP25For.

ESUPRevFuse: 5'-GACCACTTCCCAGCATCTTTG-3' lacks a stop codon and also incorporates an extra residue in order to provide in frame fusion to the GFP tag.

- LCAFor2 and LCARev2, designed by Natalie Gude, used to TOPO clone the LCA into pDNA3.1/CTGFP-TOPO, unfused. The substrate used was LCA in pTrcHisA provided by Marite Bradshaw and Eric Johnson (University of Wisconsin). A primer allowing fusion to the GFP tag will be designed.

LCAFor2: 5'-*ATG*CCATTTGTTAATAAAC-3' contains a *start* codon and no restriction sites.

LCARev2: 5'-*TTATCA*CTTATTGTATCCTTTATC-3' contains two *stop* codons and no restriction sites.

- LCEFor, LCERevStop and LCERevFuse, designed by Natalie Gude, used to TOPO clone the LCE into pCDNA3.1/CTGFP-TOPO either unfused (Stop) or fused (Fuse). The substrate used was LCE in pCMV5 provided by H. Niemann (Hannover, Germany).

LCEFor: 5′-**GGTACCCGGG**GATCATGCC-3′ contains a *start* codon, partial Kozak sequence, a **5′G** recommended for PCR cloning.

Restriction sites included from the substrate include **KpnI** and **Sma1.**

LCERevStop: 5′ -**G***C TTA*CCTTATGCCTTTTAC-3′ contains a *stop* codon and a **5′G.**

LCERevFuse: 5′ -**G**CCTTATGCCTTTTACAG-3′ does not contain an in-frame stop codon and has a **5′G.**

APPENDIX 2

Current inventory of clones designed for this program:

SNAP-25 in pEGEM

ESUP in pCINeo

ESUP36 in pCDNA3.1/CTGFP-TOPO unfused

ESUP36 in pCDNA3.1/CTGFP-TOPO fused

ESUP25 in pCDNA3.1/CTGFP-TOPO fused

ESUP26 in pCR3.1-Uni

LCA in pTrcHisA

LCA in pCDNA3.1/CTGFP-TOPO unfused

LCA in pIND/V5/His unfused

LCE in pBN17

LCE in pCMV5

LCE in pCDNA3.1/CTGFP unfused

LCE in pCDNA3.1/CTGFP fused

APPENDIX 3

Vector Maps:

pcDNA3.1//CTGFP-TOPO *Invitrogen*

pIND/V5-His-TOPO *Invitrogen*

PCR′ 3.1-Uni *Invitrogen*

pTrcHisA,B,C *Invitrogen*

Vector Maps:

Comments for pcDNA3.1/CTGFP-TOPO
6157 nucleotides

CMV promoter: bases 209-863
T7 promoter/priming site: bases 863-882
Multiple cloning site: bases 908-1012
TOPO™ Cloning site: bases 953-954
GFP Reverse priming site: bases 1115-1136
GFP ORF: bases 1004-1723
pcDNA3.1/BGH reverse priming site: bases 1745-1762
BGH polyadenylation sequence: bases 1748-1975
f1 origin of replication: bases 2021-2449
SV40 promoter and origin: bases 2477-2785
Neomycin resistance gene: bases 2860-3654
SV40 polyadenylation sequence: bases 3830-3960
ColE1 origin: bases 4343-5016 (opposite strand)
Ampicillin resistance gene: bases 5161-6021 (opposite strand)

Invitrogen®

Please note that pcDNA3.1/CTGFP-TOPO is supplied linearized between bp 953 and 954. This is the TOPO™ Cloning site.

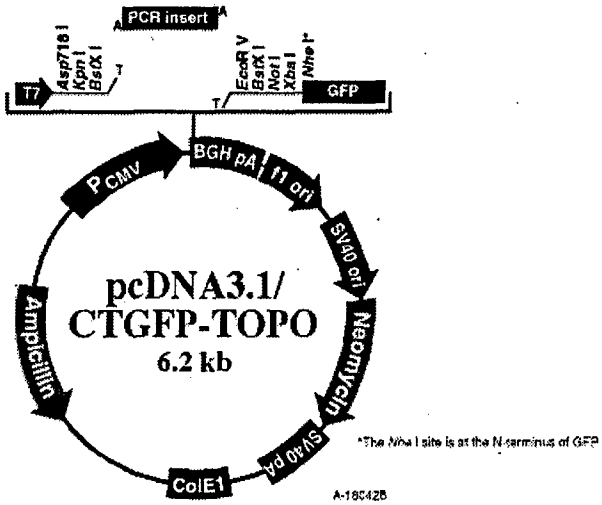

The sequence of pcDNA3.1/CTGFP-TOPO has been compiled from information in sequence databases, published sequences, and other sources. Portions of this vector have not yet been completely sequenced. If you suspect an error in the sequence, please contact Invitrogen's Technical Service Department at 800-955-6288.

U.S. Headquarters
Tel: 1-800-955-6288
Fax: 1-760-603-7201

European Headquarters
Tel: +31 (0) 594 515 175
Fax: +31 (0) 594 515 312

Comments for pIND/V5-His TOPO
5124 nucleotides

Ecdysone/glucocorticoid Response Elements (5x E/GREs): bases 12-185
Minimal Heat Shock Promoter and 5' UTR: bases 192-466
Putative Transcriptional Start: base 245
Ecdysone Forward priming site: bases 440-463
Multiple Cloning Site: bases 487-620
TOPO™ Cloning site: bases 554-555
V5 epitope: bases 621-662
Polyhistidine tag: bases 672-689
pcDNA3.1/BGH Reverse priming site: bases 712-729
BGH polyadenylation sequence: bases 715-942
f1 origin: bases 968-1416
SV40 promoter and origin: bases 1466-1752
Neomycin resistance gene ORF: bases 1827-2821
SV40 polyadenylation sequence: bases 2797-2927
ColE1 origin: bases 3310-3983
Ampicillin resistance gene ORF: bases 4128-4988

Note: The vector is supplied linearized between base pair 554 and 555. This is the TOPO™ Cloning site.

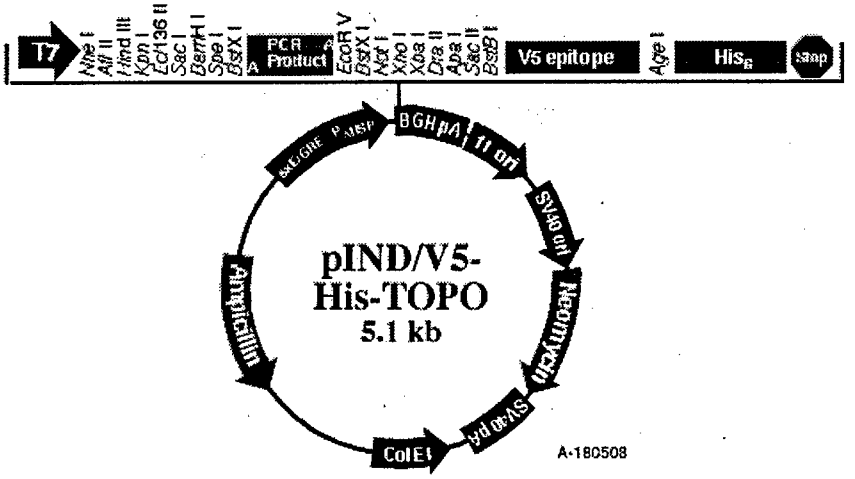

The sequence of pIND/V5-His-TOPO has been compiled from information in sequence databases, published sequences, and other sources. These vectors have not been completely sequenced. If you suspect an error in the sequences, please contact Invitrogen's Technical Services Department.

U.S. Headquarters
Tel: 1-800-955-6288
Fax: 1-760-603-7201

European Headquarters
Tel: +31 (0) 594 515 175
Fax: +31 (0) 594 515 312

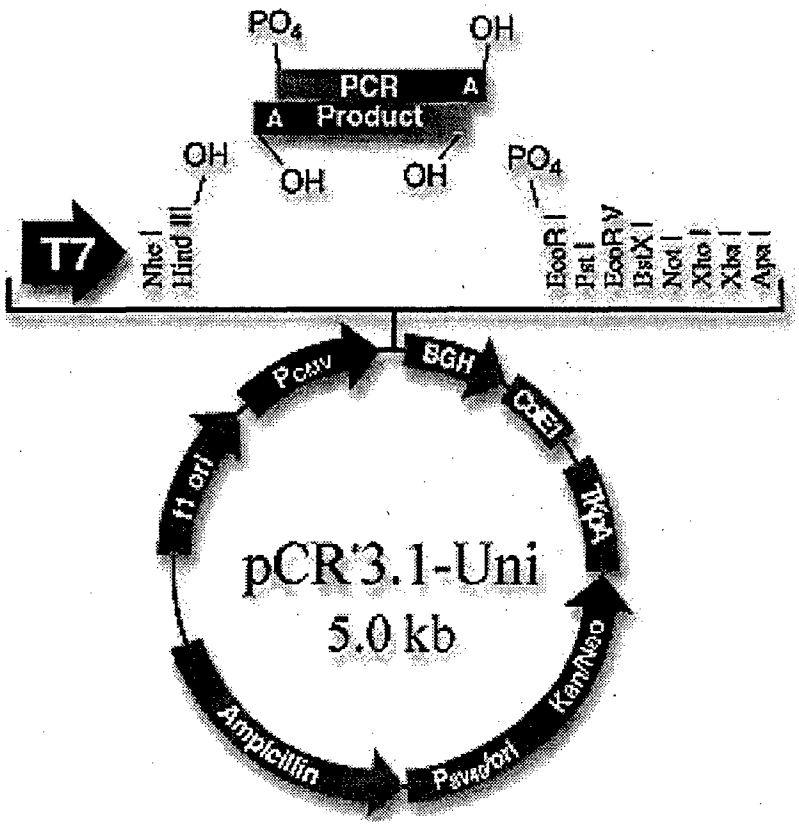
PO4
OH
PCR
A
A Product
OH
OH
OH
PO4
T7
Nhe I
Hind III
EcoR I
Pst I
EcoR V
BstX I
Not I
Xho I
Xba I
Apa I
PCMV
BGH
ColE1
f1 ori
TK-A
pCR3.1-Uni
5.0 kb
Ampicillin
Psv40ori
Kan/Neo

Comments for pTrcHis B:
4404 nucleotides

Invitrogen

Trc promoter: bases 191-221
lac operator: bases 228-248
rrnB antitermination sequences: bases 264-333
T7 gene 10 translational enhancer: bases 346-364
Ribosome binding site: bases 370-374
Mini-cistron: bases 383-409
PolyHis and enterokinase cleavage site: bases 414-504
Multiple cloning site: bases 516-554
Ampicillin resistance ORF: bases 1074-1934
lac I^q ORF: bases 3408-4395

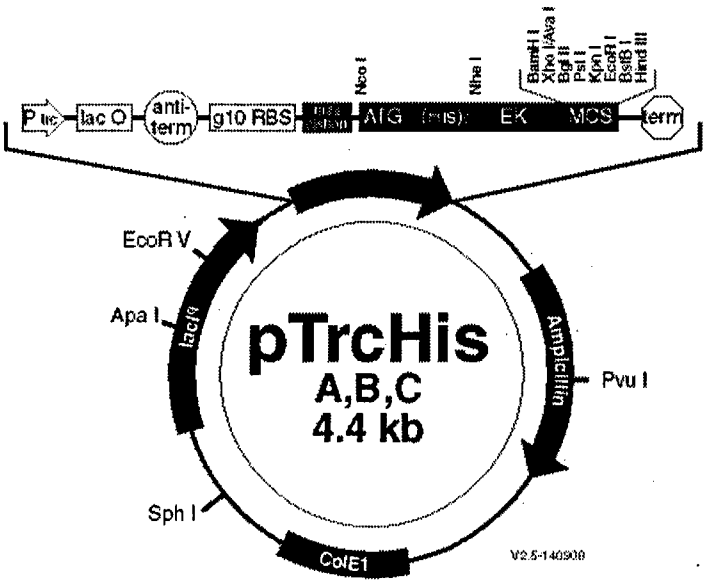

The sequence of pTrcHis has been compiled from information in sequence databases, published sequences, and other sources. This vector has not yet been completely sequenced. If you suspect an error in the sequence, please contact Invitrogen's Technical Services Department.

U.S. Headquarters
Tel: 1-800-955-6288
Fax: 1-619-597-6201

European Headquarters
Tel: +31 (0) 5945-15175
Fax: +31 (0) 5945-15312

BINDING
As requested

BIBLIOGRAPHY:

- Please see item (8), Reportable Outcomes.
- Personnel receiving pay from the research effort:
  Mauricio Montal, M.D. Ph.D., Principal Investigator
  Douglas Bei
  Natalie Gude, B.S.
  Kay Chang
  Judi Moreen
  Lilia Koriazova, Ph.D.

Quarterly Report Format

1. Contract No. DAMD 17-98-C-8040 2. Report Date January 18, 2000

3. Reporting period from October 1, 1999 to December 31, 1999

4. PI Dr. Mauricio Montal 5. Telephone No. 858-534-0931

6. Institution University of California, San Diego

7. Project Title: "Hypothesis-Based Drug Design in Drug Discovery Targeted to the Protease and Channel Activities of Botulinum Toxin A"

8. Current staff, with percent effort of each on project.

Lilia Koriazova	100 %	Kay Chang	44 %
Natalie Gude	100 %	Judi Moreen	3 %

9. Contract expenditures to date (as applicable):

	This Qtr/Cumulative		This Qtr/Cumulative
Personnel	$14360.19 / $97247.50	Travel	$1493.51 / $1493.51
Fringe Benefits	$3681.84 / $14308.79	Equipment	-0- / $13067.08
Supplies	$11970.66 / $47870.24	Other	-0- / -0-

	This Qtr/Cumulative
Subtotal	$31503.20 / $173987.12
Indirect Costs	$16476.21 / $84161.25
Fee	/
Total:	$47979.41 / $258148.37

10. Comments on administrative and logistical matters.

11. Use additional page(s), as necessary, to describe scientific progress for the quarter in terms of the tasks or objectives listed in the statement of work for this contract. Explain deviations where this isn't possible. Include data where possible.

12. Use additional page(s) to present a brief statement of plans or milestones for the next quarter.

Cell, Vol. 98, 475–485, August 20, 1999, Copyright ©1999 by Cell Press

Activation of Store-Operated Ca^{2+} Current in *Xenopus* Oocytes Requires SNAP-25 but Not a Diffusible Messenger

Yong Yao,* Antonio V. Ferrer-Montiel,†‖ Mauricio Montal,† and Roger Y. Tsien*‡§
*Department of Pharmacology
†Department of Biology
‡Howard Hughes Medical Institute
University of California, San Diego
La Jolla, California 92093-0647

Summary

Depletion of Ca^{2+} stores in *Xenopus* oocytes activated entry of Ca^{2+} across the plasma membrane, which was measured as a current I_{SOC} in subsequently formed cell-attached patches. I_{SOC} survived excision into inside-out configuration. If cell-attached patches were formed before store depletion, I_{SOC} was activated outside but not inside the patches. I_{SOC} was potentiated by microinjection of *Clostridium* C3 transferase, which inhibits Rho GTPase, whereas I_{SOC} was inhibited by expression of wild-type or constitutively active Rho. Activation of I_{SOC} was also inhibited by botulinum neurotoxin A and dominant-negative mutants of SNAP-25 but was unaffected by brefeldin A. These results suggest that oocyte I_{SOC} is dependent not on aqueous diffusible messengers but on SNAP-25, probably via exocytosis of membrane channels or regulatory molecules.

Introduction

Ca^{2+} influx across the plasma membrane can be activated by depletion of intracellular Ca^{2+} stores in many nonexcitable cells, and it is important in activation of lymphocytes, exocytosis of mast cells, and other Ca^{2+}-dependent physiological events (for recent reviews, Berridge, 1995; Lewis and Cahalan, 1995; Favre et al., 1996; Parekh and Penner, 1997; Holda et al., 1998; Putney and McKay, 1999). The mechanism by which such "capacitative" Ca^{2+} entry is activated remains controversial. Major proposals include direct interaction ("conformational coupling") between proteins in organellar and plasma membranes (Berridge, 1995), diffusible messengers or calcium influx factors (CIFs) generated by store depletion (Parekh et al., 1993; Randriamampita and Tsien, 1993; Csutora et al., 1999), metabolites of phosphoinositides, phosphorylation cascades, heterotrimeric or small G proteins (Bird and Putney, 1993; Fasolato et al., 1993), and exocytotic insertion of vesicular channels into the plasma membrane. Previous arguments for exocytosis have included inhibition of capacitative Ca^{2+} entry by intracellular GTPγS (Bird and Putney, 1993; Fasolato et al., 1993), primaquine (Somasundaram et al., 1995), and the actin-depolymerizing drug cytochalasin D (Holda and Blatter, 1997). Each of these observations is controversial. Petersen and Berridge (1995) and Gregory and Barritt (1996) showed that the GTPγS inhibition of Ca^{2+} influx into oocytes could be prevented by staurosporine. They concluded that the GTPγS effect was mediated via stimulation of kinases. The effect of primaquine has been reinterpreted as direct inhibition of the Ca^{2+} influx channels (Gregory and Barritt, 1996). Cytochalasin D has no effect on capacitative Ca^{2+} entry in NIH3T3 cells, even though it blocks agonist-dependent Ca^{2+} release (Ribeiro et al., 1997). Furthermore, none of these pharmacological interventions is particularly diagnostic for exocytosis or takes advantage of our increased understanding of the macromolecules involved in membrane trafficking. Unfortunately, the channels that mediate capacitative Ca^{2+} influx have not yet been definitively identified at the molecular level.

This study began as a reexamination of the diffusible messenger hypothesis. Channels gated directly by diffusible messengers should be activatable in cell-attached configuration, lost in excised patches, and reactivated upon cramming those inside-out patches into the cytosol of preactivated cells, as first shown for cyclic-nucleotide-gated cation channels by Kramer (1990). Parekh et al. (1993) reported analogous behavior for capacitative Ca^{2+} entry into *Xenopus* oocytes, though Ca^{2+} entry was not directly monitored but only surmised from currents of uncertain ionic basis. Recently, we showed that store-operated, capacitative Ca^{2+} currents (I_{SOC}) into whole oocytes could be directly measured by buffering cytosolic Ca^{2+} to prevent secondary currents, perfusing extracellularly with isotonic Ca^{2+} and Mg^{2+} alternately, and quantitating the difference in currents (Yao and Tsien, 1997). We have now extended this protocol to cell-attached and excised patches, hoping to solidify the evidence of Parekh et al. (1993) for a diffusible messenger. In addition, inside-out patches would be useful online detectors for the diffusible messenger(s) and would facilitate chromatographic purification and chemical identification. To our surprise, our patch-clamp findings (see Results) argued against simple mechanisms involving reversible binding of diffusible messengers.

We therefore sought experimental approaches that would be more diagnostic for an exocytotic coupling mechanism than those employed previously. We tried modulation of the small G protein Rho, because *Clostridium botulinum* C3 transferase, which specifically inactivates Rho through ADP ribosylation of Rho at Asn-41, was shown to increase insertion of the insulin-sensitive glucose transporter GLUT4 into the plasma membrane in 3T3-L1 adipocytes (Van den Berghe et al., 1996). C3 transferase also increases membrane capacitance and externalization of sodium pumps in *Xenopus* oocytes, possibly by blockade of constitutive endocytosis (Schmalzing et al., 1995).

We tested botulinum neurotoxins (BoNTs), a group of zinc endoproteases produced by bacteria of the genus *Clostridium*, because they display specific activity for a triad of protein components of the exocytic apparatus:

§To whom correspondence should be addressed (e-mail: rtsien@ucsd.edu).
‖Present address: Centro de Biologia Molecular y Celular, Universidad Miguel Hernández, C/ Monóvar s/n, 03206 Elche, Spain.

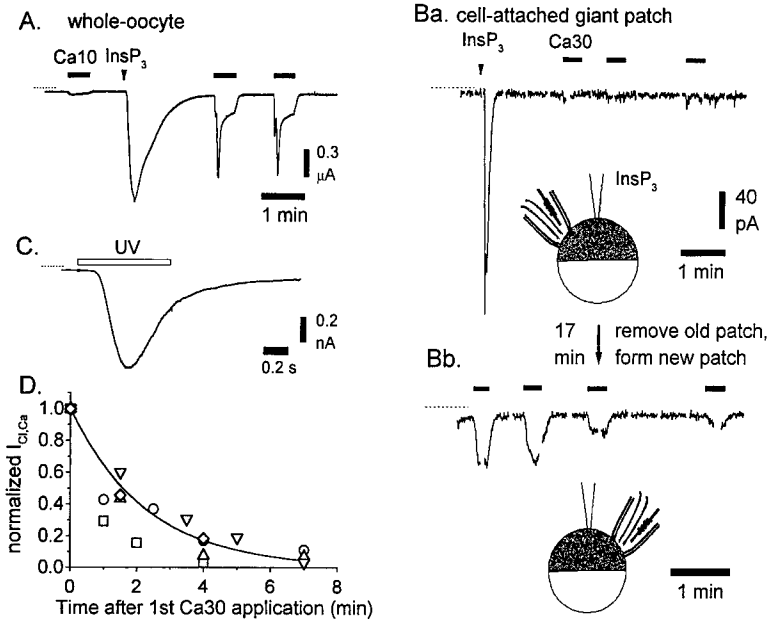

Figure 1. Blockade of Activation of Store-Operated Ca^{2+} Influx by GΩ Sealing Procedure

(A) Ca^{2+} release activated Ca^{2+} influx in oocyte recorded with two-electrode voltage clamp. Ca^{2+} influx was monitored by switching bath from Mg70 to Ca10 where indicated by heavy bars. Dotted lines in this and subsequent panels indicate zero current levels.

(Ba) Ca^{2+} release failed to activate Ca^{2+} influx in preformed cell-attached giant patch. Solution inside patch pipette was alternately changed between Mg70 and Ca30 Ringer.

(Bb) A new cell-attached giant-patch recording was made about 17 min after $InsP_3$ injection from the same oocyte. Note that the Ca^{2+} influx was recorded now in the patch formed after activation of the capacitative Ca^{2+} influx. $InsP_3$ (2 mM of 25 nl) was injected in both recordings from whole oocyte and patch as indicated by arrow heads in (A) and (B). Voltage ramps were repetitively applied during the patch recording to monitor the I-V curve. The corresponding transient currents have been blanked for clarity.

(C) $I_{Cl,Ca}$ was elicited by uncaging caged $InsP_3$ in a cell-attached giant patch. Oocyte had been loaded with 30 nl of 10 mM caged $InsP_3$.

(D) Deactivation of store-operated Ca^{2+} influx in cell-attached giant patches from $InsP_3$-loaded oocytes. Ca^{2+} influx–induced $I_{Cl,Ca}$ was measured at $V_m \approx +50$ mV and normalized to the first current amplitude. Data from five patch recordings were plotted against the time after first exposure to Ca30, among which three were made subsequently from a same oocyte. The smooth curve was a single exponential fit with a decay time constant of around 2 min.

a vesicle-associated membrane protein (VAMP or synaptobrevin), and two plasma membrane–attached proteins, SNAP-25 and syntaxin (Montecucco and Schiavo, 1995). BoNT B, D, F, and G recognize and cleave VAMP specifically. BoNT A and E cleave SNAP-25 specifically. BoNT C1 cleaves syntaxin. Binding of VAMP to syntaxin is facilitated by SNAP-25, which leads finally to fusion of vesicles with plasma membrane (Calakos and Scheller, 1996). BoNTs are widely used to block regulated exocytosis in secretory cells. Finally, dominant-negative mutants of SNAP-25 provided a molecularly independent confirmation of the BoNT A results. The combined results argue that SNAP-25 and presumably membrane trafficking play essential roles in the activation of oocyte I_{soc}.

Results

Prior Gigaseal Formation Prevents Store Depletion from Activating Ca^{2+} Entry inside but Not outside the Patch

As well-established in two-electrode voltage clamp recording (Yao and Tsien, 1997), Ca^{2+} release due to injection of $InsP_3$ invariably led to Ca^{2+} influx, which caused a Ca^{2+}-activated Cl^- current $I_{Cl,Ca}$ whenever external Ca^{2+} was present (solid horizontal bars in Figure 1A). In these cells, we did not inject Ca^{2+} chelators to buffer cytosolic Ca^{2+}, so that $I_{Cl,Ca}$ could be a maximally sensitive monitor of Ca^{2+} entry. In contrast, when currents were recorded in cell-attached giant patches, injection of a saturating dose of $InsP_3$ activated only a transient $I_{Cl,Ca}$ mediated by Ca^{2+} release, but not Ca^{2+} influx (Figure 1Ba, typical of 10 of 11 patches). Interestingly, Ca^{2+} influx could be recorded subsequently in cell-attached patches at different spots from the same oocyte (Figure 1Bb). This indicated that prior formation of a gigaohm seal blocked the coupling mechanism between store depletion and Ca^{2+} entry within the pipette, whereas Ca^{2+} entry outside the pipette activated normally.

In a separate group of experiments, TPEN (Hofer et al., 1998) was used as an independent activator to confirm the above curious finding. In two-electrode voltage clamp recordings from whole oocytes, application of 5 mM TPEN induced Ca^{2+} influx-mediated $I_{Cl,Ca}$ of 200 to 600 nA in 10 mM extracellular Ca^{2+}. This much whole-cell current should give 31–94 pA $I_{Cl,Ca}$ in giant patches of 30 μm diameter given the ratio of giant-patch to whole-cell areas, 1/6400. However, there was no detectable Ca^{2+} influx-mediated $I_{Cl,Ca}$ in 12 of 14 cell-attached giant patches under similar stimuli measured with pipettes filled with 10 mM Ca^{2+}. In the remaining two patches, the $I_{Cl,Ca}$ mediated by Ca^{2+} influx was only −3 and −5 pA, approximately one order of magnitude less than predicted from the ratio of membrane areas. This result confirmed that most cell-attached giant patches did not respond to stimuli that normally activate store-operated Ca^{2+} influx.

The plasma membrane in cell-attached patches was visibly somewhat invaginated into the patch pipette, as is common in patch clamping (Sokabe and Sachs, 1990). To estimate the diffusional distance between the stores and plasma membrane patch, oocytes were loaded with caged $InsP_3$, and the latency of $I_{Cl,Ca}$ in giant patches after UV flash was measured (Figure 1C). This latency resulted mainly from the delay time of $InsP_3$-evoked Ca^{2+} release plus time for Ca^{2+} to diffuse from the stores to plasma membrane (Parker and Ivorra, 1993). Hot spots of $InsP_3$-evoked Ca^{2+} release are normally located about 5 μm deep under the plasma membrane in oocytes (Yao et al., 1995). This distance (d) corresponds well with 30

ms latency (t) between the Ca^{2+} fluorescence signal and $I_{Cl,Ca}$, a Ca^{2+} diffusion coefficient (D) of 140 $\mu m^2 s^{-1}$, and the equation $d^2 = 6Dt$ (Allbritton et al., 1992; Parker and Ivorra, 1993). The latency of $I_{Cl,Ca}$ in giant patches after UV uncaging of $InsP_3$ was 210 ± 30 ms (n = 3). This 7-fold increase in latency corresponds to a mean effective distance of 13 μm between stores and plasma membrane. The modest increase in distance from 5 to 13 μm should not be enough to prevent diffusion of a small molecule activator.

Maintenance of Store-Operated Ca^{2+} Influx in Whole Cells, Cell-Attached, and Excised Patches

When oocytes were injected with a saturating dose of $InsP_3$, about 0.2 mM, the Ca^{2+} influx assayed by two-electrode voltage clamp recording of $I_{Cl,Ca}$ or whole-cell recording of I_{SOC} lasted >0.5 hr. However, once a patch was formed on an activated cell, $I_{Cl,Ca}$ measured from the enclosed patch as the difference of currents with 30 mM versus 0 Ca^{2+} in the pipette declined with a time constant of about 2 min. Figure 1Bb shows one example, while Figure 1D shows the pooled data from five recordings. This decay probably represented unmasking of deactivation after gigaseal formation had blocked any further activation within the patch.

The above experiments were performed with $I_{Cl,Ca}$ as the most sensitive index of Ca^{2+} entry to maximize its likelihood of detection within the patch. We were also able to detect the much smaller Ca^{2+} current itself, I_{SOC}, in similar patches if cytosolic Ca^{2+} was well buffered by EGTA injection and store depletion preceded gigaseal formation (Figure 2A). The intrapipette solution was perfused alternately with 70 mM Mg^{2+} (Mg70) and 70 mM Ca^{2+} (Ca70), and the difference of currents $I_{Ca70} - I_{Mg70}$ was taken as I_{SOC} (Yao and Tsien, 1997). In average, I_{SOC} measured in cell-attached giant membrane patches was −22.1 ± 2.7 pA (n = 32) in oocytes depleted with ionomycin, versus −3.6 ± 0.5 pA (n = 13) from control oocytes. The amplitude of I_{SOC} in preactivated patches corresponded well with that predicted from 1/6400 of the area of a whole oocyte. Ramp current traces a and b were obtained, respectively, in Mg70 and Ca70 (Figure 2Ba) and showed an I-V relation similar to that measured in whole oocytes with two-electrode voltage clamp (Yao and Tsien, 1997).

After excision of the patch into a mock intracellular Ringer with 0 Ca^{2+} and 5 mM EGTA, I_{SOC} was constant or increased with time (Figure 2A) in 12 out of 15 patches, unlike the rapid decay of Ca^{2+} entry in patches left attached to unbuffered cells (Figures 1Bb and 1D). In the other three patches, I_{SOC}-like current decayed to baseline after a few minutes. On average, this inward current was sustained for at least 4 min after patch excision (Figure 2C). In our longest recording, lasting 8 min after excision, I_{SOC} was sustained throughout. I_{SOC} in excised patches was larger and noisier at negative membrane potentials but otherwise had much the same I-V relationship (Figure 2Bb) as before excision. To verify that the former cytosolic face of the patch was truly exposed to the bath, the external solution was briefly switched to a buffer with 0.2 μM [Ca^{2+}], which activated $I_{Cl,Ca}$ as expected (Figure 2A shaded bar and I-V relation in Figure 2Bc). In oocytes without ionomycin incubation, the residual currents measured by the usual protocol ($I_{Ca70} - I_{Mg70}$) were small and not significantly affected by excision, 4.7 ± 0.7 pA (n = 6) before versus 4.8 ± 1.0 pA (n = 6) after excision.

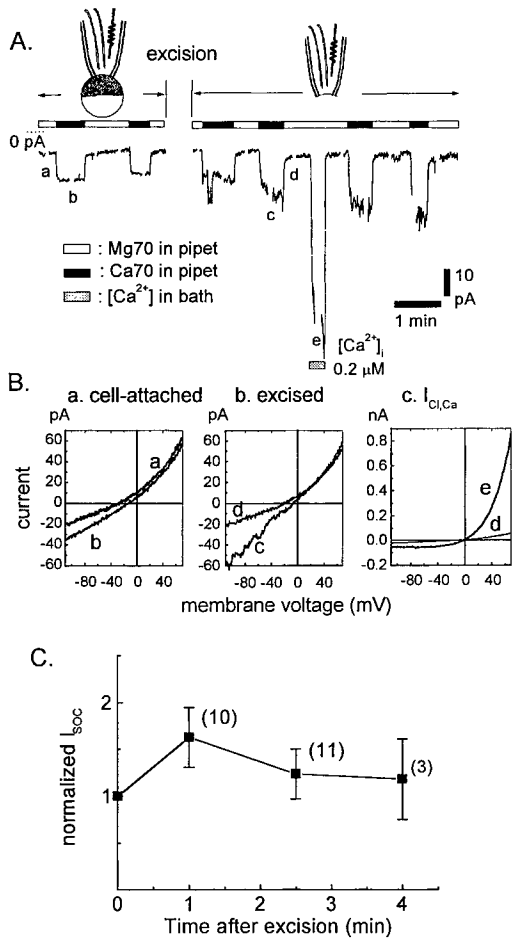

Figure 2. Survival of I_{SOC} in Inside-Out Giant Patches

(A) Store-operated Ca^{2+} current in cell-attached and inside-out giant patch. Oocyte was treated with ionomycin and injected with EGTA before patching. Pipette solution was alternately perfused with Mg70 (indicated with open bar) and Ca70 (solid bar). Voltage ramps were applied periodically to obtain the I-V curves shown in (B). The evoked current transients have been blanked for clarity.

(B) I-V curves were obtained respectively in Mg70 and Ca70 in cell-attached patch (measured at time a and b in [A]; shown in [Ba]), and in inside-out patch (c and d in [Bb]). $I_{Cl,Ca}$ was activated in excised patch by a transient increase of bath [Ca^{2+}] (e).

(C) Average of normalized I_{SOC}-like current after patch excision. The number in parentheses indicates number of patch recordings made.

Thus, seal formation on the outside of the plasma membrane inhibited activation of new I_{SOC} inside the patch but allowed preactivated I_{SOC} to continue; maintenance of such I_{SOC} did not require presence of cytosolic substances and was actually enhanced by excision. These results suggest that activation of I_{SOC} is rather localized, sensitive to membrane deformation, and unlikely to result from simple diffusion of an activator molecule. Furthermore, activation and deactivation seem to be separate processes not linked by a simple equilibrium, because different orders of manipulation can give very different results.

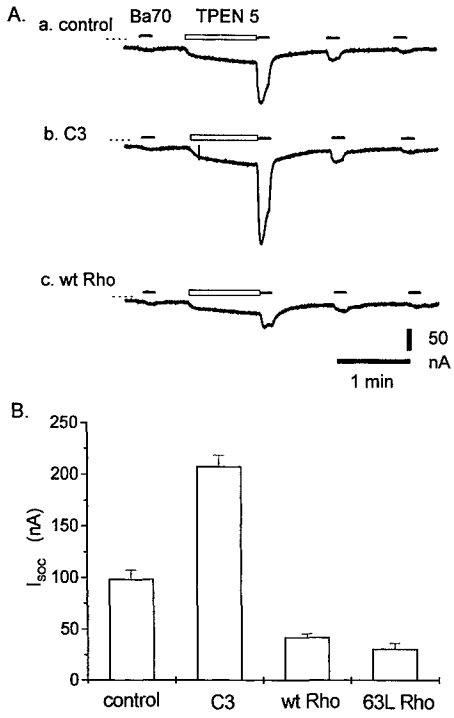

Figure 3. I_{SOC} Was Potentiated by Injection of C3 Transferase and Inhibited by Expression of Rho A

(A) I_{SOC} was induced by TPEN 5 mM in bath (open bars) and monitored by switching from Mg70 to Ba70 (solid bars). I_{SOC} evoked by TPEN was rapidly reversible. Recordings were made, respectively, in native oocyte (Aa), oocyte 1 hr after injection of C3 transferase 0.4 μM (Ab), and oocyte 6 hr after injection of 20 ng Rho A cRNA (Ac).

(B) Summary of effects on I_{SOC} of microinjected C3 transferase, expression of wild-type Rho A, and its constitutively active mutant 63L.

Regulation of Store-Operated Ca^{2+} Influx by Rho A

To examine whether the store-operated Ca^{2+} influx was affected by Rho, C3 transferase was microinjected into oocytes. In recordings illustrated in Figure 3A, Ba^{2+} current was measured to quantitate effects of C3 and Rho. Injection of Ca^{2+} chelators was omitted because activation of $I_{Cl,Ca}$ by Ba^{2+} was negligible. I_{SOC} induced by 5 mM TPEN was 98 ± 9 nA (n = 9) in control oocytes and 207 ± 11 nA (n = 7) in oocytes measured about 1–2 hr after injection of C3 (3 ng/oocyte, or 120 nM assuming uniform distribution in 1 μl cytosol), an increase of 2.1-fold ($p < 0.01$). In complementary experiments, Rho A, its constitutively active mutant (63L), and dominant-negative mutant (19N) were expressed in oocytes by injection of 20 ng of their respective cRNAs about 5 hr before recordings started. I_{SOC} was 42 ± 4 nA (n = 4) in oocytes expressed with wild-type Rho and 31 ± 6 (n = 6) with constitutively active mutant (63L), corresponding to 57% ($p < 0.01$) and 68% ($p < 0.01$) inhibition, respectively (Figure 3B). I_{SOC} remained unchanged in oocytes expressing dominant-negative mutant 19N Rho A, suggesting a large pool of endogenous Rho A existed to maintain basal activity. Injection of C3 also induced an increase of membrane capacitance. Membrane capacitance increased by about 41% in 2 hr after injection of C3 (3 ng/oocyte) (n = 7, $p < 0.01$). In contrast, no significant decrease in membrane capacitance was found to accompany inhibition of I_{SOC} in oocytes expressed with wt Rho (n = 4) and 63 L Rho (n = 6). Amplitude of I_{SOC} activated by 5 mM TPEN in the above experiments was about half of the maximum. Maximal I_{SOC} induced by a saturating dose of ionomycin (10 μM) was also enhanced about 46% (n = 9, $p < 0.01$) by C3 transferase. Oocytes from five of six animals showed a similar extent of potentiation by C3 transferase but not in the remaining one frog. This suggested that Rho played a modulatory rather than an indispensable role in activation of I_{SOC}.

Because one of the many effects of active Rho is to promote assembly of actin-myosin filaments (stress fibers), we examined whether the potentiation of I_{SOC} by C3 might simply result from the disruption of the actin-myosin assembly. Oocytes were treated with cytochalasin D (20 μg/ml) for 17 hr, at which time oocytes appeared mottled as an indication of actin depolymerization and had relative low input resistance. I_{SOC} was 118 ± 14 nA (n = 7) in control oocytes and 93 ± 17 nA (n = 7) in oocytes treated with cytochalasin D. Thus, destruction of the actin cytoskeleton by cytochalasin D slightly reduced I_{SOC}, probably by nonspecific mechanisms rather than mimicking C3 transferase, which greatly potentiated I_{SOC}. We also tried 5 μM jasplakinolide, which solidifies the actin cytoskeleton (Shurety et al., 1998). I_{SOC} was reduced from its control value of 87 ± 9.5 nA (n = 4) to 64 ± 3 nA (n = 6) during drug exposures of 0.5 or 2 hr, which were equivalent. This small reduction was significant at the p = 0.026 level and was in the same direction as, but much weaker than, the complete inhibition by 3 μM jasplakinolide of store-operated Ca^{2+} entry in cultured mammalian cells (Patterson et al., 1999 [this issue of *Cell*]).

BoNT A Inhibits Activation of Store-Operated Ca^{2+} Influx

Preinjection with 100 nM BoNT A reduced I_{SOC} by about 50% (Figures 4Aa and 4Ba) without any effect on the inward rectification or the leak current, as shown by the I-V curves in Mg70 and Ca70 (Figures 4Ab and 4Bb). BoNT A also reduced Ca^{2+} influx-dependent $I_{Cl,Ca}$ induced by ionomycin, $InsP_3$, and TPEN in 10 mM Ca_o by 89% (n = 11, $p < 0.01$), 86% (n = 4, $p < 0.01$), and 86% (n = 6, $p < 0.01$), respectively (data not shown). The more dramatic reduction in the $I_{Cl,Ca}$ compared to I_{SOC} probably reflects the nonlinear relation of the former with I_{SOC} (Yao and Tsien, 1997). No significant change in the resting potential, input resistance, and membrane capacitance were found by BoNT A. Also, BoNT A did not alter the $I_{Cl,Ca}$ transients elicited by ionomycin, $InsP_3$, or TPEN in calcium-free medium, showing that the release of Ca^{2+} from stores and the properties of $I_{Cl,Ca}$ were unaltered.

The kinetics of BoNT A action are shown in Figure 4C. The inhibition developed with an apparent single exponential time constant of 1.1 hr and reached maximum about 4 hr after BoNT A administration. I_{SOC} was 141 ± 9 nA (n = 9) in control oocytes and 72 ± 3 nA (n = 7, $p < 0.01$) in oocytes about 4 hr after injection of BoNT A. The inhibition was long-lasting and still apparent after 2 days. In a separate double-blind experiment, various doses of BoNT A were injected into oocytes. I_{SOC} was measured 4 to 7 hr after injection of 20 nl BoNT A of different concentrations. The inhibition of

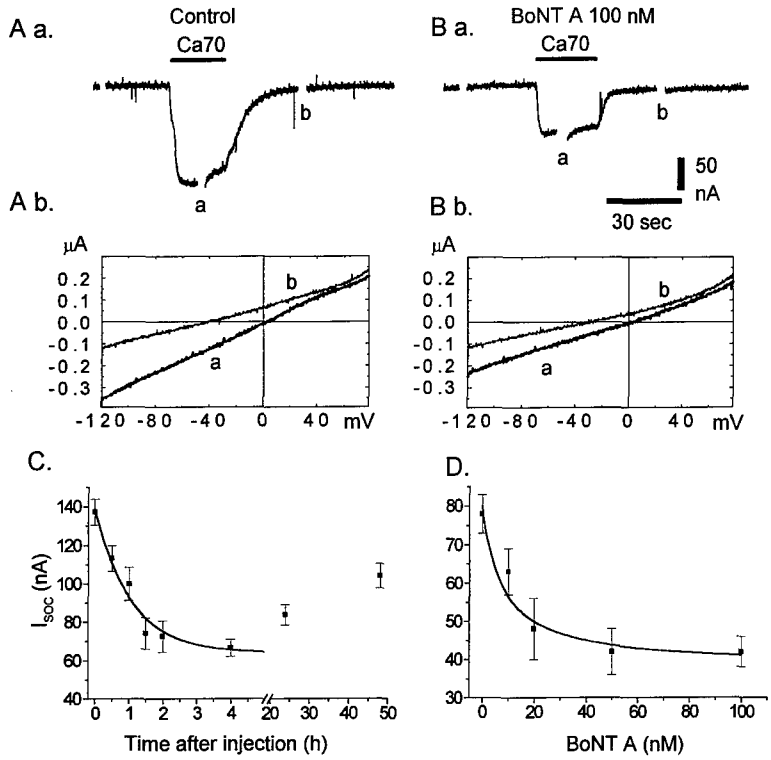

Figure 4. Inhibition of I_{SOC} by BoNT A

I_{SOC} was activated by 5 μM ionomycin followed by injection of EGTA to a final internal concentration of about 10 mM and was recorded by switching from Mg70 to Ca70 (solid bars) in a control oocyte (Aa) and an oocyte injected 4 hr earlier with 100 nM BoNT A (Ba). (Ab and Bb) The I-V relations obtained in Ca70 (a) and Mg70 (b). (C) Kinetics of BoNT A action. I_{SOC} was activated as above at different times after injection of BoNT A 100 nM. The smooth curve was the best fit to a single exponential decay with a time constant of 1.1 hr. Each data point was from more than three oocytes. (D) Dose dependence of BoNT A action. Oocytes were injected with different concentrations of BoNT A as indicated. Recordings were made 4 to 7 hr after the injections. Each data point was the average of more than four oocytes. Smooth curve was a fit to equation $(I - I_{min})/(I_{max} - I_{min}) = K_i/(K_i + [BoNT])$, with I_{max} = 80 nA, I_{min} = 38 nA, K_i = 8 nM.

I_{SOC} was found to be dose dependent on BoNT A with an apparent $K_i \approx 8$ nM (Figure 4D).

In contrast to BoNT A, BoNT B, E, and tetanus toxin had no significant effects on I_{SOC} measured about 6–8 hr after injection to final concentrations of 200 nM each. I_{SOC} was 93 ± 4 nA (n = 6) in control oocytes versus 74 ± 4 nA (n = 4), 78 ± 5 (n = 5), and 73 ± 8 (n = 6) in oocytes injected with BoNT B, E, and tetanus toxin, respectively. Unfortunately, we cannot yet test biochemically whether our toxin samples could cleave *Xenopus* oocyte SNAREs because the latter have not yet been cloned, and the antibodies we had against the mammalian proteins did not recognize their oocyte counterparts.

Blockade of I_{SOC} by Dominant-Negative Mutants of SNAP-25

Because the usual target of BoNT A is SNAP-25, we examined whether I_{SOC} activation could be similarly inhibited by dominant-negative mutants of SNAP-25. It was shown in yeast that sec9-Δ17, a C-terminal truncation of a SNAP-25 homolog, was a dominant-negative mutant (Rossi et al., 1997). According to sequence alignment (Weimbs et al., 1998) supported recently by crystal structure data (Sutton et al., 1998), yeast sec9-Δ17 corresponds to deletion of C-terminal 20 amino acids of mouse SNAP-25 (Δ20). BoNT A cleavage of mammalian SNAP-25 causes C-terminal truncation of nine amino acids (Δ9). Therefore, we made a series of C-terminal truncated SNAP-25 mutants spanning between Δ9 and Δ20 to examine whether they would have any inhibitory action on I_{SOC}. A truncated mutant SNAP-25 Δ41 was also made that corresponded to sec9-Δ38, which did not show dominant-negative effects in yeast (Rossi et al., 1997). The SNAP-25 mutants were expressed in oocytes by injection of their cRNA. I_{SOC} activated by TPEN was measured in oocytes about 14 hr after injection of 3 ng cRNA per oocyte of full-length, Δ9, Δ20, or Δ41, respectively (Figure 5). TPEN 5 mM induced about 100 nA I_{SOC} in uninjected oocytes and oocytes expressing full-length (Figure 5Aa) and Δ41 SNAP-25 (Figure 5Ac), but no I_{SOC} in oocytes expressing Δ20 (Figure 5Ab). I_{SOC} activation was inhibited by about half in oocytes expressing Δ9 cRNA. I_{SOC} activated by ionomycin was similarly inhibited by the expression of dominant-negative SNAP-25 mutants (Figure 5B). Oocytes were injected with 1 ng cRNA of each mutant per cell and recorded in 15 hr after the injection. I_{SOC} activated by 10 μM ionomycin was not affected by expression of full-length SNAP-25, but almost completely abolished by expression of Δ11, Δ14, Δ17, and Δ20 mutants. The inhibitory kinetics could be speeded up by injection of larger amounts of cRNA to express more proteins in shorter time. Thus, after injection of 30 ng of SNAP-25-Δ20, inhibition of I_{SOC} activated by ionomycin started in 2 hr and reached maximum within 4 hr after the injection (Figure 5C). While I_{SOC} was totally abolished, $I_{Cl,Ca}$ activated by ionomycin in calcium-free medium was unaffected in peak amplitude and more prolonged in oocytes expressing the dominant-negative mutant of SNAP-25, showing that inhibition of I_{SOC} was not due to any interference with Ca^{2+} release from stores. Furthermore, $I_{Cl,Ca}$ elicited by membrane depolarization (Barish, 1983) was not reduced by the dominant-negative mutants of SNAP-25. The effect of SNAP-25 on membrane turnover was assessed by capacitance measurements. A reduction of about 50% of total membrane capacitance was observed in oocytes injected with SNAP-25-Δ20 (189 ± 3 nF in control oocytes versus 96 ± 11 nF in SNAP-25-Δ20-expressed oocytes). This confirmed that the dominant-negative mutants of SNAP-25 were affecting plasma membrane turnover.

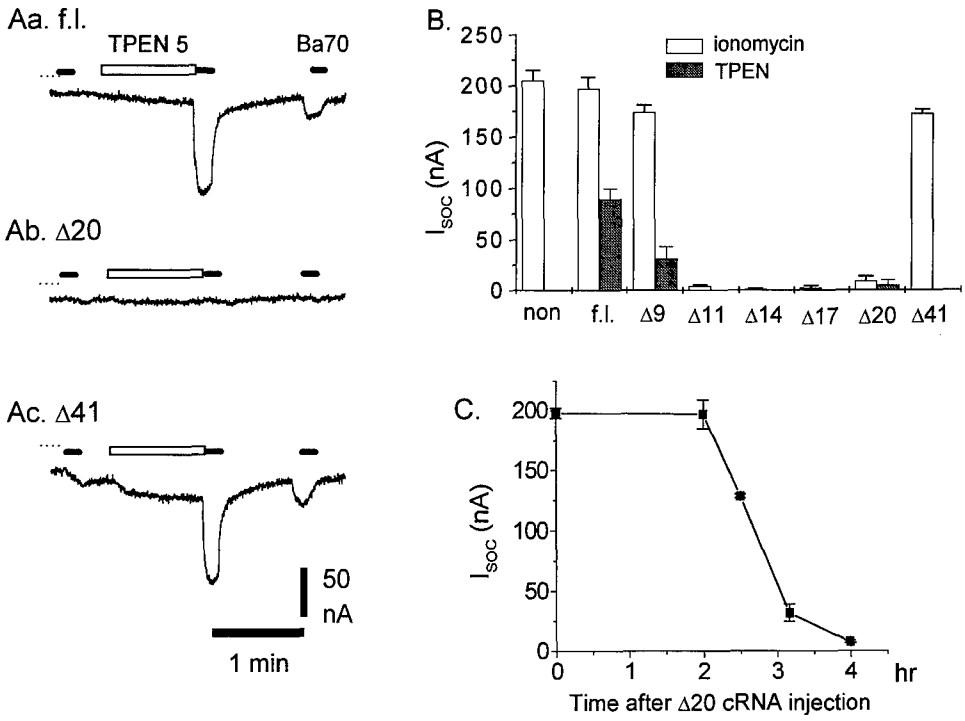

Figure 5. Prevention of I_{SOC} by C-Terminal Truncated Mutants of SNAP-25

(A) Activation of I_{SOC} by TPEN was not affected in oocytes expressing full-length (f.l.) SNAP-25 (Aa) and SNAP-25-Δ41 (Ac), but it was completely absent in oocytes expressing Δ20.

(B) Summary of inhibition of I_{SOC} by expressing SNAP-25 mutants. Activation of I_{SOC} by ionomycin (open columns) was totally abolished by expression of SNAP-25-Δ11, Δ14, Δ17, and Δ20 4 hr after injection of 30 ng cRNA, respectively. Activation of I_{SOC} by TPEN (filled columns) was inhibited by about half by expressing SNAP-25-Δ9 and was almost totally blocked by expressing Δ20 in 17 hr after injection of 3 ng cRNA each.

(C) Kinetics of I_{SOC} inhibition by expression of SNAP-25-Δ20. I_{SOC} was activated by ionomycin and measured at various times after the injection of 30 ng cRNA.

Activation of I_{SOC} Is Not Inhibited by Brefeldin A

To distinguish whether inhibition of I_{SOC} by BoNT A and dominant-negative mutants of SNAP-25 was mediated by interference with constitutive versus regulated exocytosis, we compared the effects of brefeldin A (BFA) with those of BoNT A and SNAP-25 Δ20. BFA blocks constitutive exocytosis by inhibiting protein exit from Golgi apparatus, which possibly results from BFA inhibition of guanine nucleotide exchange for ARF, a small G protein that is involved in coatomer-mediated vesicle budding from ER (Peyroche et al., 1999). Wild-type amiloride-sensitive epithelial sodium current (ENaC) expressed in *Xenopus* oocytes is inhibited by 5 μM BFA with a time constant of 3.6 hr due to blockade of constitutive insertion of ENaC channels while clathrin-mediated endocytosis remains active (Shimkets et al., 1997). We confirmed such downregulation of ENaC in oocytes by BFA as a positive control for BFA efficacy. I_{ENaC} was reduced by about 86% ($p < 10^{-10}$) by incubation of oocytes with BFA 5 μM for 7 hr. I_{SOC}, however, remained unchanged after incubation of oocytes in 5 μM BFA for 7 to 20 hr in the same batch of oocytes (Figure 6). In complete contrast to BFA, BoNT A inhibited I_{SOC} ($p < 10^{-28}$) but not I_{ENaC}. A dominant-negative SNAP-25 mutant slightly inhibited I_{ENaC} ($p = 0.014$), but to a much lesser extent than did BFA (Figure 6). In addition to the exogenous Na^+ channels, the endogenous voltage-operated Ca^{2+} channels and Ca^{2+}-activated Cl^- channels were not reduced by BoNT A and SNAP-25-Δ20 but were inhibited by BFA, though the BFA block was statistically significant only at the $p = 0.06$ level (Figure 6). These results indicated that blockade by BFA of constitutive traffic to the plasma membrane for up to 24 hr did not reduce the cells' ability to activate I_{SOC}, and inhibition of I_{SOC} by BoNT A and SNAP-25 mutants did not result from disruption of constitutive trafficking.

Discussion

Activation of the Store-Operated Ca^{2+} Current Is a Local Process that Can Show Hysteresis

Our patch-clamp experiments showed that store-operated Ca^{2+} entry was highly localizable, required store depletion to precede patch isolation, and yet survived patch excision. Thus, depletion of Ca^{2+} stores could activate Ca^{2+} influx outside but not inside a preformed gigaseal onto a 30 μm diameter patch pipette (Figures 1A and 1B). Therefore, the ability of store depletion to trigger Ca^{2+} current within the patch was disrupted by some aspect of seal formation, such as the visible invagination of the plasma membrane into the lumen of the pipette. Meanwhile, the $InsP_3$-induced increase in cytosolic $[Ca^{2+}]$ was still able to activate $I_{Cl,Ca}$ within the cell-attached patch with slightly greater latency than normal (Figure 1C). This finding showed that Ca^{2+} was still able to diffuse from the internal stores to the plasma membrane inside the gigaseal, though the mean diffusion distance had apparently been increased from the normal

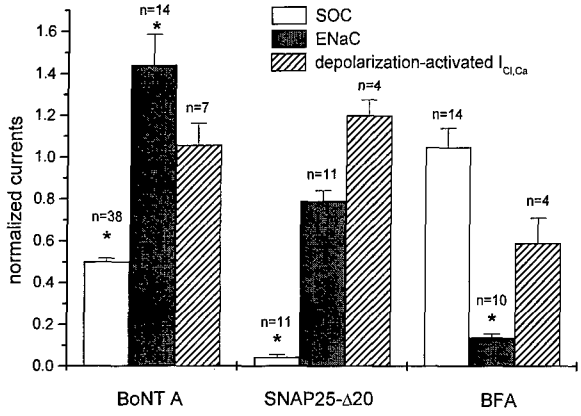

Figure 6. Comparison of Effects on I_{SOC}, I_{ENaC}, and Depolarization-Activated $I_{Cl,Ca}$ by BoNT A, SNAP-25-Δ20, and BFA

All current values measured were normalized to mean values of control groups of the same donor. The normalized currents from separate donors were averaged for statistical analysis. Groups significantly different ($p < 0.01$) from control are marked with an asterisk. Number of oocytes measured in each group is indicated on the column. I_{SOC} was activated by ionomycin and measured in Ba70. I_{ENaC} was measured in calcium-free Ringer at holding $V_m = -30$ mV as the difference in currents before and after 1 μM amiloride. Peak values of depolarization-activated $I_{Cl,Ca}$ were measured by stepping V_m to +40 mV in Ca10. It represents endogenous voltage-gated Ca^{2+} channel activity evoking $I_{Cl,Ca}$ (Barish, 1983). BoNT A was injected into oocytes to a 100–200 nM final concentration, waiting for 4 to 7 hr before recording. SNAP-25-Δ20 cRNA (30 ng) was injected into oocytes to allow protein expression for 4–6 hr. Incubations with 5 μM BFA lasted 5–20 hr before recording.

5 μm to 13 μm. Once Ca^{2+} influx was activated in the absence of or outside a gigaseal, it was readily detectable in a new cell-attached patch, showing that patch formation only obstructed initial activation rather than maintenance of the influx. Furthermore, I_{SOC} survived without diminution for minutes after excision of the patch into the inside-out configuration (Figure 2). Although one of us helped launch the idea of a diffusible CIF (Randriamampita and Tsien, 1993), we must admit that these findings argue against mediation by a CIF freely diffusible through the cytosol, because such a factor should have easily reached the plasma membrane inside the gigaseal but should have washed out immediately after excision of the patch. In a "conformational coupling" hypothesis, one would need to postulate that the protein–protein contact between the stores and plasma membrane would be easily disrupted or prevented before store depletion, but it would become robust enough after I_{SOC} activation to survive invagination and excision of the patch. In an exocytosis model, one would assume that exocytosis is locally prevented by bulging of the plasma membrane into the gigaseal. Indeed, exocytosis in mast cells is reported to be reversibly blocked by inflating the plasma membrane (Solsona et al., 1998). Whatever the model, the gigaseal results show that activation of Ca^{2+} influx can vary over distances of only a few microns, even more spatially confined than those of Petersen and Berridge (1996) or Jaconi et al. (1997), where localization was reported over distances of hundreds of microns.

These results would seem to conflict with a previous report (Figure 2, Parekh et al., 1993) in which a depletion-activated current in cell-attached patches was immediately quenched by excision from the oocyte and could be reactivated by cramming back into a stimulated cell. This current had a linear I-V curve with a reversal potential of −30 mV, was recorded in the presence of niflumic acid to block $I_{Cl,Ca}$, and had amplitudes of 10–20 pA with pipettes of ordinary micron diameters. I_{SOC} was characterized in recent two-electrode voltage clamp recording studies (Hartzell, 1996; Yao and Tsien, 1997), in which Ca^{2+} chelators instead of niflumic acid were used to abolish $I_{Cl,Ca}$ because niflumic acid was found to inhibit I_{SOC}. As expected for a highly Ca^{2+}-selective current, I_{SOC} has an inwardly rectifying I-V curve with a reversal potential >+40 mV. Giant-patch recording (Hilgemann, 1995) with 30 μm diameter pipettes and intrapipette perfusion was required to increase detection sensitivity and to record ~10 pA of I_{SOC} directly as the difference in currents between 70 and 0 mM extracellular Ca^{2+}. Therefore, the current that was quenched by excision and restored by cramming in the experiment of Parekh et al. (1993) was dominated by components other than Ca^{2+} influx.

Mechanisms of Rho A Action on I_{SOC}

Up- and downregulation of RhoA, by expression of excess Rho A or injection of *Clostridium* C3 transferase, respectively, decreased and increased the amplitude of I_{SOC} (Figure 3). Rho A is known to regulate many cell events, including cytoskeletal rearrangement and membrane trafficking (Van Aelst and D'Souza-Schorey, 1997; Hall, 1998). Because RhoA may affect both constitutive and regulated membrane trafficking, our results with C3 and RhoA provide only general evidence for the importance of trafficking in modulating capacitative Ca^{2+} entry.

Mechanisms of Action of Botulinum Neurotoxin A and SNAP-25

In this study, I_{SOC} was found to be inhibited by about 50% by BoNT A (Figures 4 and 6). This inhibition was relatively specific as endogenous $I_{Cl,Ca}$, voltage-gated Ca^{2+} current, and transfected epithelial Na^+ channels were not reduced. The time course and potency of the inhibitory action on I_{SOC} by BoNT A were similar to that described in blockade of neurotransmission of *Aplysia* synapses (Rossetto et al., 1994). Recently BoNTs have also been shown to block insulin-stimulated translocation of GLUT4 in adipocytes (Cheatham et al., 1996). The maximum inhibition of insulin-stimulated glucose uptake was 43%–51% (Tamori et al., 1996; Chen et al., 1997), quite similar to the maximal reduction of I_{SOC} in our experiments. Likewise BoNT A causes only a partial block and slowing of catecholamine release from chromaffin cells (Xu et al., 1998).

The complete inhibition of I_{SOC} by dominant-negative mutants of SNAP-25 and the biphasic length dependence of the effective truncations strongly complement the evidence from BoNT A for a crucial role for a SNAP-25 homolog in oocytes. The length dependence fits well with multiple studies showing the critical importance of the region corresponding to 9 to 26 residues from the C terminus of mammalian SNAP-25 for exocytosis and its triggering by calcium sensors (Gutierrez et al., 1995;

Rossi et al., 1997; Ferrer-Montiel et al., 1998; Huang et al., 1998; Xu et al., 1998). The partial inhibition by the Δ9 truncation fits well with the similarly partial inhibition by BoNT A, which should cut SNAP-25 at the corresponding location. The inhibition of I_{SOC} is not explainable by general interference with constitutive insertion of channels into the plasma membrane, because currents through Ca^{2+}-activated Cl^- channels, voltage-gated Ca^{2+} channels, or transfected epithelial Na^+ currents remained undiminished (Figure 6). Conversely, constitutive insertion, for example of epithelial Na^+ channels, can be inhibited by brefeldin A without any effect on I_{SOC} (Figure 6). Therefore, SNAP-25 and, presumably, regulated exocytosis are important in the process for activating I_{SOC}. We did not see any change in the I-V relation of I_{SOC} after partial inhibition by BoNT A, so we could find no evidence that SNAP-25 modifies the conductance properties of the Ca^{2+} entry channels in the way that syntaxin modulates the gating of voltage-activated Ca^{2+} channels (Bezprozvanny et al., 1995). Instead, loss of functional SNAP-25 simply reduces the amplitude of the residual I_{SOC}.

Conclusions regarding the Mechanism of Coupling

Ca^{2+} entry into oocytes can be activated by microinjection of extracts from lymphocytes or yeast in which Ca^{2+} stores have been pharmacologically or genetically depleted (Csutora et al., 1999). However, those authors acknowledged that oocytes themselves produce relatively low levels of calcium influx factor, and that the evoked influx had different properties from endogenously stimulated capacitative Ca^{2+} entry, especially in lanthanide sensitivity. Our present results come entirely from oocytes and do not rule out the potential importance of diffusible factors in other cell types. A conformational coupling hypothesis could be compatible with our data if one assumes that the link between the stores and the plasma membrane is mechanically weak before store depletion and strong afterward, and that SNAP-25 or a homolog is important for the linkage. Our results are somewhat more naturally accommodated within a model in which the channels themselves or membrane-bound activator molecules are exocytotically incorporated into the plasma membrane upon store depletion. We would argue that inhibitions by BoNT A and dominant-negative SNAP-25 are far more likely to be pharmacologically specific for SNAP-25 and exocytosis than the previous controversial effects of GTPγS, primaquine, and cytoskeletal inhibitors. Furthermore, new experiments with cytoskeletal modulation have provided fresh evidence for secretion-like coupling (Patterson et al., 1999). The major arguments against exocytosis are the lack of measurable increases in membrane capacitance before or during store-operated Ca^{2+} entry in oocytes (<1% change; preliminary data of Y. Y.) and other cell types (e.g., Fomina and Nowycky, 1999), and the lack of effect of BoNT B and E and tetanus toxin. However, the negligible capacitance increases could reflect the minuscule amount of membrane required to accommodate the channels or activators, swamped by the huge amount of concurrent exo- and endocytosis, sufficient to replace the entire oocyte plasma membrane once every day if all components mixed freely (Zampighi et al., 1999). The lack of inhibition by certain toxins might be due to imperfect homology of the relevant oocyte components to the better-studied mammalian SNAREs; we had no positive control that our toxin samples had any effect in oocytes. Nevertheless, the involvement of proteins extensively studied in exocytosis opens up many possible testable hypotheses and experiments for the future.

Experimental Procedures

Cell Preparation and Electrophysiology

Oocytes were cultured in Barth's medium supplemented with 5% horse serum to increase viability of the cells (Quick et al., 1992). Recordings were taken at least 2 hr after removal of the serum. Oocytes used to assess drug action were obtained from the same frog to reduce variability in I_{SOC}. Extracellular solution compositions and recording of whole-oocyte membrane currents with a conventional two-electrode voltage clamp were as described by Yao and Tsien (1997). Membrane potential was held at −60 mV unless otherwise specified. Capacitance of whole-oocyte plasma membrane was determined by $C_m = \int i_C\, dt/\Delta V$, where C_m is membrane capacitance, i_C capacitance current transient, ΔV membrane voltage step. C_m was averaged from ΔV of 5, 10, and 15 mV, respectively.

Giant-patch glass pipettes (#7052, O. D./I. D. 1.65/1.1, WPI, FL or borosilicate glass, O. D./I. D. 1.5/0.86 Warner Instrument Corp., Hamden, CT) were pulled to have tip openings of around 40 μm with a horizontal electrode puller (P-80/PC, Sutter Instrument Co., Novato, CA). The pipette tips were then heat-polished to give final openings of about 30 μm, which should encompass about 1/6400 of the total surface of an oocyte of 1.2 mm diameter. Thus, an oocyte with a total I_{SOC} of 100 nA should give about 16 pA through the patch assuming the channels are evenly distributed. Patch recordings made from various sites on the animal hemisphere showed no significant variation in current amplitudes. In some experiments (e.g., Figure 1), $I_{Cl,Ca}$ was measured as a more sensitive monitor of Ca^{2+} influx, because its amplitude is about an order of magnitude larger than I_{SOC} (Yao and Tsien, 1997). For intrapipette perfusion, quartz capillaries (O. D./I. D. 150/75 μm, Polymicro Technologies Inc., Phoenix, AZ) were pulled and the tips cut to about 15 to 20 μm diameter. Two capillaries were bundled with glue and inserted to within 100–200 μm of the patch pipette tip under a stereo microscope. Perfusates were passed through a 2 μm filter. Perfusates in quartz capillaries were held by suction (typically −10 mm Hg) to prevent leakage and were ejected by a positive pressure (typically 150 mm Hg). Turnover of intrapipette solutions at the membrane was typically within a few seconds. Oocyte vitelline membranes were removed in a hyperosmotic solution that contained (mM): KCl 200, $MgCl_2$ 2, KCl 1, and HEPES 5, titrated to pH 7.2 with NaOH, supplemented with EGTA 5 mM for measuring I_{SOC} or 40 μM for measuring $I_{Cl,Ca}$. Current was recorded with an Axopatch 200B amplifier (Axon Instruments, Inc., Foster City, CA), whose range of the fast capacitance compensation was expanded to 20 pF by the manufacturer. Membrane seal resistance were larger than 1 GΩ. Bath solution for excised patch recordings was a mock intracellular Ringer (IR), containing (mM): 95 KCl, 1 NaCl, 5 $MgCl_2$, 5 HEPES, titrated to pH 7.2 with NaOH, plus EGTA 5 mM and 40 μM, respectively, for recording I_{SOC} and $I_{Cl,Ca}$. Membrane potentials of the oocytes were measured to be −8.8 ± 0.5 mV (n = 4) in IR. The pipette potential was held at 50 mV after a GΩ seal was formed. A voltage ramp command from 50 to −130 mV with a duration of 0.5 s was repetitively applied at 30 s intervals to allow rapid collection of I-V relations of the current. This resulted in a final membrane potential ramp from −109 to 71 mV after summing pipette holding potential, oocyte membrane potential, and the ramp command.

All recordings were performed at room temperature (22°C ± 2°C). Data points are expressed as mean ± SE. Statistical significance of drug actions was evaluated with two-tailed Student's t test using Origin software (Microcal, Northampton, MA).

Use of TPEN to Activate Store-Operated Ca^{2+} Influx in *Xenopus* Oocytes

The usual means for dumping Ca^{2+} stores and activating I_{SOC}, such as ionomycin administration or metabolic production or microinjection of $InsP_3$, were poorly reversible. A rapidly reversible agent not requiring microinjection would be very helpful. A membrane-permeant chelator of divalent cations, TPEN, was shown recently to induce store-operated Ca^{2+} influx in mammalian cells (Hofer et al., 1998). TPEN has a low affinity for Ca^{2+} (K_D = 40 μM; Arslan et al., 1985) suitable for buffering the relatively high free Ca^{2+} concentrations in the lumen of Ca^{2+}-accumulating organelles while exerting little effect on cytosolic free Ca^{2+} (Hofer et al., 1998). The total Ca^{2+} inside the stores is conserved during application of TPEN because the TPEN–Ca^{2+} complex is impermeant (Arslan et al., 1985). When free extracellular TPEN is removed, the intraluminal TPEN–Ca^{2+} dissociates and rapidly restores intraluminal free Ca^{2+} so that deactivation of influx can be studied.

TPEN had not been previously tested in *Xenopus* oocytes but proved very useful in activating I_{SOC} because of the above advantages. TPEN was dispersed in nominally Ca^{2+}-free media and applied extracellularly to load the oocytes before restoration of normal Ca^{2+} to measure the influx. The minimum TPEN concentrations required to activate the Ca^{2+} influx varied from 0.1 to 1 mM in different batches of oocytes. Ca^{2+} influx reversed quickly after washout of TPEN from bath and could be reactivated repeatedly. Maximal Ca^{2+} influx was activated by preincubation of oocyte with TPEN for 1 min. Longer incubations with TPEN slowed the deactivation time course of the Ca^{2+} influx. An additional inward nonspecific current was present during the TPEN loading, which was not inhibited by injection of EGTA. To test whether the action of TPEN was additive to that of ionomycin, Ca^{2+} influx was first induced by TPEN and then ionomycin to obtain their individual activities in the same oocyte. Ca^{2+} influx induced by ionomycin was long-lasting. Application of TPEN after ionomycin did not induce additional Ca^{2+} influx (data not shown). Such occlusion indicates that Ca^{2+} influx induced by TPEN is through the store-operated Ca^{2+} influx pathway.

One concern with TPEN is its very high binding affinity for Zn^{2+} ($K_D = 2.63 \times 10^{-16}$ M) (Arslan et al., 1985). Also, even 5 mM TPEN only activated I_{SOC} to about half the maximal amplitude obtainable with other means for depleting stores. A new membrane-permeable Ca^{2+} chelator that has a higher affinity to Ca^{2+} and lower affinity to Zn^{2+} than TPEN would be yet better. Fortunately, inhibition of BoNTs by TPEN's chelation of Zn^{2+} is irrelevant because TPEN is only applied well after BoNT injection.

Materials

Botulinum toxin A, B, and E were kindly supplied by Dr. B. R. DasGupta (University of Wisconsin, Madison). They were dissolved at 1 mg/ml in buffer containing (mM): 150 NaCl, 10 HEPES, titrated to pH 7.0, maintained at −80°C. BoNTs were reduced with 10 or 20 mM DTT at room temperature for 1 hr before injection. Activity of BoNT A was assessed by in vitro cleavage assay of SNAP-25 (Ferrer-Montiel et al., 1996). Cytochalasin D was from Sigma. C3 transferase, amiloride, and brefeldin A were from Calbiochem Novabiochem (La Jolla, CA). One side effect of C3 transferase was a spontaneous current, dependent on extracellular Ca^{2+}, which usually developed about 1 hr or longer after the injection of C3. Intracellular injection of EGTA or exposure to TPEN suppressed the current, so it did not interfere with measurement of I_{SOC}. The origin of this curious current remained to be further characterized.

Expression Vector Construction and In Vitro Transcription

cDNAs of wild-type Rho A, its constitutively active mutant 63L, and dominant-negative mutant 19N in plasmid pCMV5 were kind gifts of Dr. G. Bokoch (Scripps Research Institute, San Diego, CA). Rho and its mutant cDNA inserts were released from pCMV5 with HindIII digestion and subcloned into pSGEM at the HindIII site. Vector pSGEM was obtained from Dr. Philipp and Dr. Flockerzi (Universität des Saarlandes, Homburg/Saar, Germany), which derived from a popular oocyte expression vector pGEMHE that contained *Xenopus* β-hemoglobin untranslated regions flanking the multiple cloning site (Liman et al., 1992). The orientation of the cDNA inserts was checked by gel electrophoresis after EcoRV digestion.

C-terminal truncated mutants of mouse SNAP-25 were created by PCR using a forward primer paired with various reverse primers that introduced a stop codon to terminate translation at different C-terminal sites of SNAP-25. The forward primer in PCR reaction had the sequence 5′-CGGGATCCGCCACCATGGCCGAGGACGCA GACATG, which contained a BamHI site and a Kozak sequence at the 5′ end of SNAP-25. The reverse primers for CΔ9, CΔ11, CΔ14, CΔ17, CΔ20, and CΔ41 were, respectively, 5′-CGGAATTCTTATTGG TTGGCTTCATCAAT, 5′-CGGAATTCTTAGGCTTCATCAATTCTGGT, 5′-CGGAATTCTTAAATTCTGGTTTTGTTGGA, 5′-CGGAATTCTTATT TGTTGGAGTCAGCCTT, 5′-CGGAATTCTTAGTCAGCCTTCTCCAT GAT, and 5′-CGGAATTCTTATAGGGCCATATGACGGAG. All reverse primers incorporated an EcoRI site and a stop codon at the 3′-end of SNAP-25. Following PCR amplification, the PCR products were gel-separated and digested with BamHI and EcoRI. The resulting PCR frgments were subcloned into the vector pSGEM between the 5′ UTR and the 3′UTR of *Xenopus* β-globin. All C-terminal truncation mutants of SNAP-25 were verified by DNA sequencing.

cDNAs of three subunits of epithelial sodium channel, α, β, γ, in plasmids pSPORT (α and γ) and pSD5 (β), were kind gifts of Dr. C. Canessa (Yale University). pSPORT-α and γ were linearized by NotI and RNA synthesized by T7 polymerase, whereas BglII and SP6 polymerase were used for pSD5-β. A mixture of the three cRNAs (0.1 or 1 ng each) was injected into each oocyte, and I_{ENaC} was measured 1–3 days later.

Capped cRNAs were synthesized using mMESSAGE mMACHINE kits from Ambion (Austin, TX). Synthetic cRNAs were resuspended in water. Aliquots of 2 μl each were stored at −80°C until injection. Typically, 20 nl RNA solution was injected into each oocyte. Concentrations of RNA were adjusted to reach the final desired mass.

Acknowledgments

We thank Dr. J. Llopis and Dr. J. Garcia-Sancho for their unpublished data and discussion, Dr. D. Hilgemann and Dr. C. C. Lu for discussion of the giant-patch recording technique, and Ms. Q. Xiong for technical assistance. This study was supported by grants to R. Y. T. from the Human Frontier Science Program (RG520/1995-M), National Institutes of Health (NS27177), and Howard Hughes Medical Institute, and a Department of the Army Medical Research Grant DAMD17-C-98-C-8040 to M. M.

Received June 8, 1999; revised July 21, 1999.

References

Allbritton, N.L., Meyer, T., and Stryer, L. (1992). Range of messenger action of calcium ion and inositol 1,4,5-trisphosphate. Science *258*, 1812–1815.

Arslan, P., Di Virgilio, F., Beltrame, M., Tsien, R.Y., and Pozzan, T. (1985). Cytosolic Ca^{2+} homeostasis in Ehrlich and Yoshida carcinomas. A new, membrane-permeant chelator of heavy metals reveals that these ascites tumor cell lines have normal cytosolic free Ca^{2+}. J. Biol. Chem. *260*, 2719–2727.

Barish, M.E. (1983). A transient calcium-dependent chloride current in the immature *Xenopus* oocytes. J. Physiol. (Lond.). *342*, 309–325.

Berridge, M.J. (1995). Capacitative calcium entry. Biochem. J. *312*, 1–11.

Bezprozvanny, I., Scheller, R.H., and Tsien, R.W. (1995). Functional impact of syntaxin on gating of N-type and Q-type calcium channels. Nature *378*, 623–626.

Bird, G.S., and Putney, J.W., Jr. (1993). Inhibition of thapsigargin-induced calcium entry by microinjected guanine nucleotide analogues. Evidence for the involvement of a small G protein in capacitative Ca^{2+} entry. J. Biol. Chem. *268*, 21486–21488.

Calakos, N., and Scheller, R.H. (1996). Synaptic vesicle biogenesis, docking, and fusion: a molecular description. Physiol. Rev. *76*, 1–29.

Cheatham, B., Volchuk, A., Kahn, C.R., Wang, L., Rhodes, C.J., and Klip, A. (1996). Insulin-stimulated translocation of GLUT4 glucose transporters requires SNARE-complex proteins. Proc. Natl. Acad. Sci. USA *93*, 15169–15173.

Chen, F., Foran, P., Shone, C.C., Foster, K.A., Melling, J., and Dolly, J.O. (1997). Botulinum neurotoxin B inhibits insulin-stimulated glucose uptake into 3T3-L1 adipocytes and cleaves cellubrevin unlike type A toxin which failed to proteolyze the SNAP-23 present. Biochemistry *36*, 5719–5728.

Csutora, P., Su, Z., Kim, H.K., Bugrim, A., Cunningham, K.W., Nuccitelli, R., Keizer, J.E., Hanley, M.R., Blalock, J.E., and Marchase, R.B. (1999). Calcium influx factor is synthesized by yeast and mammalian cells depleted of organellar calcium stores. Proc. Natl. Acad. Sci. USA *96*, 121–126.

Fasolato, C., Hoth, M., and Penner, R. (1993). A GTP-dependent step in the activation mechanism of capacitative Ca^{2+} influx. J. Biol. Chem. *268*, 20737–20740.

Favre, C.J., Nusse, O., Lew, D.P., and Krause, K.H. (1996). Store-operated Ca^{2+} influx: what is the message from the stores to the membrane? J. Lab. Clin. Med. *128*, 19–26.

Ferrer-Montiel, A.V., Canaves, J.M., DasGupta, B.R., Wilson, M.C., and Montal, M. (1996). Tyrosine phosphorylation modulates the activity of clostridial neurotoxins. J. Biol. Chem. *271*, 18322–18325.

Ferrer-Montiel, A.V., Gutierrez, L.M., Apland, J.P., Canaves, J.M., Gil, A., Viniegra, S., Biser, J.A., Adler, M., and Montal, M. (1998). The 26-mer peptide released from SNAP-25 cleavage by botulinum neurotoxin E inhibits vesicle docking. FEBS Lett. *435*, 84–88.

Fomina, A.F., and Nowycky, M.C. (1999). A current activated on depletion of intracellular Ca^{2+} stores can regulate exocytosis in adrenal chromaffin cells. J. Neurosci. *19*, 3711–3722.

Gregory, R.B., and Barritt, G.J. (1996). Store-activated Ca^{2+} inflow in *Xenopus laevis* oocytes: inhibition by primaquine and evaluation of the role of membrane fusion. Biochem. J. *319*, 755–760.

Gutierrez, L.M., Canaves, J.M., Ferrer-Montiel, A.V., Reig, J.A., Montal, M., and Viniegra, S. (1995). A peptide that mimics the carboxy-terminal domain of SNAP-25 blocks Ca^{2+}-dependent exocytosis in chromaffin cells. FEBS Lett. *372*, 39–43.

Hall, A. (1998). Rho GTPases and the actin cytoskeleton. Science *279*, 509–514.

Hartzell, H.C. (1996). Activation of different Cl currents in *Xenopus* oocytes by Ca liberated from stores and by capacitative Ca influx. J. Gen. Physiol. *108*, 157–175.

Hilgemann, D.W. (1995). The giant membrane patch. In Single-Channel Recording (2nd edition), B. Sakmann and E. Neher, eds. (New York: Plenum Press), pp. 307–327.

Hofer, A.M., Fasolato, C., and Pozzan, T. (1998). Capacitative Ca^{2+} entry is closely linked to the filling state of internal Ca^{2+} stores: a study using simultaneous measurements of I_{CRAC} and intraluminal $[Ca^{2+}]$. J. Cell Biol. *140*, 325–334.

Holda, J.R., and Blatter, L.A. (1997). Capacitative Ca^{2+} entry is inhibited in vascular endothelial cells by disruption of cytoskeletal microfilaments. FEBS Lett. *403*, 191–196.

Holda, J.R., Klishin, A., Sedova, M., Huser, J., and Blatter, L.A. (1998). Capacitative calcium entry. News Physiol. Sci. *13*, 157–163.

Huang, X., Wheeler, M.B., Kang, Y.-h., Sheu, L., Lukacs, G.L., Trimble, W.S., and Gaisano, H.Y. (1998). Truncated SNAP-25 (1–197), like botulinum neurotoxin A, can inhibit insulin secretion from HIT-T15 insulinoma cells. Mol. Endocrinol. *12*, 1060–1070.

Jaconi, M., Pyle, J., Bortolon, R., Ou, J., and Clapham, D. (1997). Calcium release and influx colocalize to the endoplasmic reticulum. Curr. Biol. *7*, 599–602.

Kramer, R.H. (1990). Patch cramming: monitoring intracellular messengers in intact cells with membrane patches containing detector ion channels. Neuron *4*, 335–341.

Lewis, R.S., and Cahalan, M.D. (1995). Potassium and calcium channels in lymphocytes. Annu. Rev. Immunol. *13*, 623–653.

Liman, E.R., Tytgat, J., and Hess, P. (1992). Subunit stoichiometry of a mammalian K+ channel determined by construction of multimeric cDNAs. Neuron *9*, 861–871.

Montecucco, C., and Schiavo, G. (1995). Structure and function of tetanus and botulinum neurotoxins. Quart. Rev. Biophys. *28*, 423–472.

Parekh, A.B., and Penner, R. (1997). Store depletion and calcium influx. Physiol. Rev. *77*, 901–930.

Parekh, A.B., Terlau, H., and Stühmer, W. (1993). Depletion of $InsP_3$ stores activates a Ca^{2+} and K^+ current by means of a phosphatase and a diffusible messenger. Nature *364*, 814–818.

Parker, I., and Ivorra, I. (1993). Confocal microfluorimetry of calcium signals evoked in *Xenopus* oocytes by photoreleased inositol trisphosphate. J. Physiol. *461*, 133–165.

Patterson, R.L., van Rossum, D.B., and Gill, D.L. (1999). Store-operated Ca^{2+} entry: evidence for a secretion-like coupling model. Cell *98*, this issue, 487–499.

Petersen, C.C.H., and Berridge, M.J. (1995). G-protein regulation of capacitative Ca^{2+} entry may be mediated by protein kinases A and C in *Xenopus* oocytes. Biochem. J. *307*, 663–668.

Petersen, C.C.H., and Berridge, M.J. (1996). Capacitative calcium entry is colocalised with calcium release in *Xenopus* oocytes: evidence against a highly diffusible calcium influx factor. Pflug. Arch. Eu. J. Physiol. *432*, 286–292.

Peyroche, A., Antonny, B., Robineau, S., Acker, J., Cherfils, J., and Jackson, C.L. (1999). Brefeldin A acts to stabilize an abortive ARF-GDP-Sec7 domain protein complex: involvement of specific residues of the Sec7 domain. Mol. Cell *3*, 275–285.

Putney, J.W., Jr., and McKay, R.R. (1999). Capacitative calcium entry channels. BioEssays *21*, 38–46.

Quick, M.W., Naeve, J., Davidson, N., and Lester, H.A. (1992). Incubation with horse serum increases viability and decreases background neurotransmitter uptake in *Xenopus* oocytes. Biotechniques *13*, 357–361.

Randriamampita, C., and Tsien, R.Y. (1993). Emptying of intracellular Ca^{2+} stores releases a novel small messenger that stimulates Ca^{2+} influx. Nature *364*, 809–814.

Ribeiro, C.M.P., Reece, J., and Putney, J.W., Jr. (1997). Role of the cytoskeleton in calcium signaling in NIH 3T3 cells: an intact cytoskeleton is required for agonist-induced $[Ca^{2+}]_i$ signaling, but not for capacitative calcium entry. J. Biol. Chem. *272*, 26555–26561.

Rossetto, O., Schiavo, G., Montecucco, C., Poulain, B., Deloye, F., Lozzi, L., and Shone, C.C. (1994). SNARE motif and neurotoxins. Nature *372*, 415–416.

Rossi, G., Salminen, A., Rice, L.M., Brünger, A.T., and Brennwald, P. (1997). Analysis of a yeast SNARE complex reveals remarkable similarity to the neuronal SNARE complex and a novel function for the C terminus of the SNAP-25 homolog, Sec9. J. Biol. Chem. *272*, 16610–16617.

Schmalzing, G., Richter, H.P., Hansen, A., Schwarz, W., Just, I., and Aktories, K., (1995). Involvement of the GTP binding protein Rho in constitutive endocytosis in *Xenopus laevis* oocytes. J. Cell Biol. *130*, 1319–1332.

Shimkets, R.A., Lifton, R.P., and Canessa, C.M. (1997). The activity of the epithelial sodium channel is regulated by clathrin-mediated endocytosis. J. Biol. Chem. *272*, 25537–25541.

Shurety, W., Stewart, N.L., and Stow, J.L. (1998). Fluid-phase markers in the basolateral endocytic pathway accumulate in response to the actin assembly-promoting drug jasplakinolide. Mol. Biol. Cell *9*, 957–975.

Sokabe, M., and Sachs, F. (1990). The structure and dynamics of patch-clamped membranes: a study using differential interference contrast light microscopy. J. Cell Biol. *111*, 599–606.

Solsona, C., Innocenti, B., and Fernandez, J.M. (1998). Regulation of exocytotic fusion by cell inflation. Biophys. J. *74*, 1061–1073.

Somasundaram, B., Norman, J.C., and Mahaut-Smith, M.P. (1995). Primaquine, an inhibitor of vesicular transport, blocks the calcium-release-activated current in rat megakaryocytes. Biochem. J. *309*, 725–729.

Sutton, R.B., Fasshauer, D., Jahn, R., and Brunger, A.T. (1998). Crystal structure of a SNARE complex involved in synaptic exocytosis at 2.4 Å resolution. Nature *395*, 347–353.

Tamori, Y., Hashiramoto, M., Araki, S., Kamata, Y., Takahashi, M., Kozaki, S, and Kasuga, M. (1996). Cleavage of vesicle-associated membrane protein (VAMP)-2 and cellubrevin on GLUT4-containing vesicles inhibits the translocation of GLUT4 in 3T3-L1 adipocytes. Biochem. Biophys. Res. Commun. *220*, 740–745.

Van Aelst, L., and D'Souza-Schorey, C. (1997). Rho GTPases and signaling networks. Genes Dev. *11*, 2295–2322.

Van den Berghe, N., Barros, L.F., van Mackelenbergh, M.G., and Krans, H.M. (1996). *Clostridium botulinum* C3 exoenzyme stimulates GLUT4-mediated glucose transport, but not glycogen synthesis, in 3T3-L1 adipocytes—a potential role of rho? Biochem. Biophys. Res. Commun. *229*, 430–439.

Weimbs, T., Mostov, K.E., Lows, S.H., and Hofmann, K. (1998). A model for structural similarity between different SNARE complexes based on sequence relationships. Trends Cell Biol. *8*, 260–262.

Xu, T., Binz, T., Niemann, H., and Neher, E. (1998). Multiple kinetic components of exocytosis distinguished by neurotoxin sensitivity. Nat. Neurosci. *1*, 192–200.

Yao, Y., and Tsien, R.Y. (1997). Calcium current activated by depletion of calcium stores in *Xenopus* oocytes. J. Gen. Physiol. *109*, 703–715.

Yao, Y., Choi, J., and Parker, I. (1995). Quantal puffs of intracellular Ca^{2+} evoked by inositol trisphosphate in *Xenopus* oocytes. J. Physiol. *482*, 533–553.

Zampighi, G.A., Loo, D.D.F., Kreman, M., Eskandari, S., and Wright, E.M. (1999). Functional and morphological correlates of connexin50 expressed in *Xenopus laevis* oocytes. J. Gen. Physiol. *113*, 507–523.

FEBS 21737

FEBS Letters 447 (1999) 129–130

Hypothesis

Electrostatic attraction at the core of membrane fusion

M. Montal*

Department of Biology, University of California San Diego, La Jolla, CA 92093, USA

Received 5 January 1999

Abstract SNARE proteins appear to be involved in homotypic and heterotypic membrane fusion events [Söllner et al. (1993) Nature 362, 318–324]. The crystal structure of the synaptic SNARE complex exhibits a parallel four-helical bundle fold with two helices contributed by SNAP-25, a target SNARE (t-SNARE), and the other two by a different t-SNARE, syntaxin, and a donor vesicle SNARE (v-SNARE), synaptobrevin. The carboxy-terminal boundary of the complex, predicted to occur at the closest proximity between the apposed membranes, displays a high density of positively charged residues. This feature combined with the enrichment of negatively charged phospholipids in the cytosolic exposed leaflet of the membrane bilayer suggest that electrostatic attraction between oppositely charged interfaces may be sufficient to induce dynamic and discrete micellar discontinuities of the apposed membranes with the transient breakdown at the junction and subsequent reformation. Thus, the positively charged end of the SNARE complex in concert with Ca^{2+} may be sufficient to generate a transient 'fusion pore'.

Key words: SNARE protein; Electrostatic attraction; Membrane fusion

1. Introduction

Neurons communicate with each other by means of neurotransmitters. Membrane fusion is essential for synaptic transmission, a process by which neurotransmitters are released from excited nerve terminals [1]. Recently, the crystal structure of a SNARE complex, a key entity involved in the specific recognition and ultimately fusion of synaptic vesicles with the neuronal plasma membrane, was described [2]. The complex is formed by the specific interaction between segments of three proteins: synaptobrevin-II, a vesicle associated protein, and syntaxin-1A and SNAP-25B, two distinct proteins anchored to the plasma membrane. The clostridial botulinum and tetanus neurotoxins proteolytically cleave these three proteins consequently preventing vesicle fusion and thereby abrogating transmitter release [3]. The SNARE complex folds into a parallel four-helical bundle with a left handed superhelical twist [2,4]: two helices are contributed by a molecule of the t-SNARE SNAP-25, the other two by synaptobrevin and syntaxin. Such a structure may bring into juxtaposition the surfaces of the apposed vesicle and plasma membrane bilayers to facilitate fusion. How this may happen is not known, however, Ca^{2+} is required and other proteins may catalyze and confer additional specificity to the process [5,6]. Here, we focus on highlighting a number of features of this fascinating structure that may provide clues to understand how it mediates bilayer fusion.

2. Electrostatic attractions between oppositely charged interfaces and fusion

A key finding emerged from electrostatic calculations that showed a conspicuous enrichment of positively charged residues at the carboxy-terminal end of the complex [2]. This boundary is assigned to be at the membrane-anchored end of the complex, and therefore, at the minimum distance between the apposed membranes. It is known that negatively charged lipids are preferentially distributed in the inner leaflet of the bilayer plasma membrane [7]. It is also well recognized that Ca^{2+} and highly basic polypeptides interact with negatively charged lipids to induce a lamellar to hexagonal phase transition with the consequent generation of local micellization foci and, if propagated, the breakdown of the bilayer structure [7–10]. And it is well established that acidic lipids are required for the insertion into and translocation across bilayers of a number of channel-forming proteins, conspicuous among them diphtheria [11] and tetanus [12] toxins, colicin [13] and Bcl-2 family proteins [14]. It appears therefore, that electrostatic interaction energy between oppositely charged interfaces might drive discrete micellizations of the apposed membranes with the transient breakdown of the hydrophobic membrane barrier and the consequent release of the transmitter. Thus, the positively charged end of the SNARE complex in concert with Ca^{2+} may be sufficient to generate a transient 'fusion pore'. This hypothesis could be tested using purified SNARE proteins reconstituted into separate bilayer vesicles of defined phospholipid composition [15]. This model system has demonstrated that SNARE proteins are necessary and sufficient for fusion in the absence of other protein components, albeit at a low rate and efficiency [15].

3. Acidic phospholipids and Ca^{2+} ions as mediators of fusion

Another striking feature of the SNARE complex is the occurrence of four shallow grooves at the surface of the helical bundle [2]. Such grooves, particularly those present at the basic charged end of the complex, may provide specific binding pockets for acidic lipids. There is structural evidence for such lipid binding pockets: the crystal structure of a type IIβ phosphatidylinositol phosphate kinase reveals an extensive flat basic surface well suited for the interfacial binding of phosphoinositides and catalysis [16]. The crystal structure of the annexin XII hexamer displays a prominent concave disc with numerous surface exposed Ca^{2+} ions on the perimeter [17].

*Fax: (1) (619) 534 0931.
E-mail: montal@biomail.ucsd.edu

0014-5793/99/$20.00
PII: S0014-5793(99)00269-0

Presumably, these Ca^{2+} ions mediate annexin binding to phosphatidylserine, its insertion into membranes and lead to channel formation and membrane fusion [18].

Specific protein-lipid interactions are considered key events in viral fusion mechanisms and the analogy to the SNARE coil-coiled complex has been drawn [15]. The recent identification of a mitochondrial v-SNARE [19] combined with the abundance of acidic lipids in mitochondrial membranes [7] raise the intriguing possibility that SNAREs could be at the fusion interface between mitochondria and other organelles, as it appears to be between yeast vacuoles [20,21]. It would be interesting to examine in molecular detail if the electrostatic attraction between oppositely charged interfaces is sufficient to induce dynamic and discrete micellar discontinuities of the apposed membranes with the transient breakdown at the junction and subsequent reformation. Attention to Ca^{2+} as a mediator of protein-lipid interactions at membrane fusion interfaces is worth revisiting in view of the new structural information.

Acknowledgements: Our research is supported by grants from the U.S. Public Health Service (GM-49711, GM-56538), the Department of the Army Medical Research (DAMD 17-98-C-8040), and the U.S. Army Research Office (DAAG55-98-1-0106).

References

[1] Söllner, T., Whiteheart, S.W., Brunner, M., Erdjument-Bromage, H., Geromanos, S., Tempst, P. and Rothman, J.E. (1993) Nature 362, 318–324.
[2] Sutton, R.B., Fasshauer, D., Jahn, R. and Brunger, A.T. (1998) Nature 395, 347–353.
[3] Montecucco, C. and Schiavo, G. (1995) Q. Rev. Biophys. 28, 423–472.
[4] Poirier, M.A., Xiao, W., Macosko, J.C., Chan, C., Shin, Y.-K. and Bennett, M.K. (1998) Nature Struct. Biol. 5, 765–769.
[5] Shao, X., Li, C., Fernandez, I., Zhang, X., Südhof, T.C. and Rizo, J. (1997) Neuron 18, 133–142.
[6] Rettig, J., Heinemann, C., Ashery, U., Sheng, Z.-H., Yokoyama, C.T., Catterall, W.A. and Neher, E. (1997) J. Neurosci. 17, 6647–6656.
[7] De Kruijff, B. (1997) Nature 386, 129–130.
[8] Sherwood, D. and Montal, M. (1975) Biophys. J. 15, 417–434.
[9] Montal, M. (1972) J. Membr. Biol. 7, 245–266.
[10] Siegel, D.P. and Epand, R.M. (1997) Biophys. J. 73, 3089–3111.
[11] Donovan, J.J., Simon, M.I. and Montal, M. (1982) Nature 298, 669–672.
[12] Gambale, F. and Montal, M. (1988) Biophys. J. 53, 771–783.
[13] Zakharov, S.D., Lindeberg, M., Griko, Y., Salamon, Z., Tollin, G., Prendergast, F.G. and Cramer, W.A. (1998) Proc. Natl. Acad. Sci. USA 95, 4282–4287.
[14] Schendel, S.L., Xie, Z., Oblatt-Montal, M., Matsuyama, S., Montal, M. and Reed, J.C. (1997) Proc. Natl. Acad. Sci. USA 93, 5113–5118.
[15] Weber, T., Zemelman, B.V., McNew, J.A., Westermann, B., Gmachl, M., Parlati, F., Söllner, T.H. and Rothman, J.E. (1998) Cell 92, 759–772.
[16] Rao, V.D., Misra, S., Boronenkov, I.V., Anderson, R.A. and Hurley, J.H. (1998) Cell 94, 829–829.
[17] Luecke, H., Chang, B.T., Maillard, W.S., Schlapfer, D.D. and Haigler, H.T. (1995) Nature 378, 512–515.
[18] Langen, R., Isas, J.M., Hubbell, W.L. and Haigler, H.T. (1998) Proc. Natl. Acad. Sci. USA 95, 14060–14065.
[19] Isenmann, S., Khew-Goodall, Y., Gamble, J., Vadas, M. and Wattenberg, B.W. (1998) Mol. Biol. Cell 9, 1649–1660.
[20] Ungermann, C., Sato, K. and Wickner, W. (1998) Nature 396, 543–548.
[21] Peters, C. and Mayer, A. (1998) Nature 396, 575–580.

THE JOURNAL OF BIOLOGICAL CHEMISTRY
Vol. 273, No. 51, Issue of December 18, pp. 34214–34221, 1998
Printed in U.S.A.

Assembly of a Ternary Complex by the Predicted Minimal Coiled-coil-forming Domains of Syntaxin, SNAP-25, and Synaptobrevin

A CIRCULAR DICHROISM STUDY*

(Received for publication, June 18, 1998, and in revised form, October 1, 1998)

Jaume M. Cànaves and Mauricio Montal‡

From the Department of Biology, University of California San Diego, La Jolla, California 92093-0366

The assembly of target (t-SNARE) and vesicle-associated SNAP receptor (v-SNARE) proteins is a critical step for the docking of synaptic vesicles to the plasma membrane. Syntaxin-1A, SNAP-25, and synaptobrevin-2 (also known as vesicle-associated membrane protein, or VAMP-2) bind to each other with high affinity, and their binding regions are predicted to form a trimeric coiled-coil. Here, we have designed three peptides, which correspond to sequences located in the syntaxin-1A H3 domain, the C-terminal domain of SNAP-25, and a conserved central domain of synaptobrevin-2, that exhibit a high propensity to form a minimal trimeric coiled-coil. The peptides were synthesized by solid phase methods, and their interactions were studied by CD spectroscopy. In aqueous solution, the peptides were unstructured and showed no interactions with each other. In contrast, upon the addition of moderate amounts of trifluoroethanol (30%), the peptides adopted an α-helical structure and displayed both homomeric and heteromeric interactions. The interactions observed in ternary mixtures induce a stabilization of peptide structure that is greater than that predicted from individual binary interactions, suggesting the formation of a higher order structure compatible with the assembly of a trimeric coiled-coil.

The assembly of the synaptic core complex is essential for Ca^{2+}-dependent neuroexocytosis. This early event in the secretory cascade is then followed by the priming and vesicle fusion steps (1–6). According to the SNARE[1] model, docking of synaptic vesicles to the plasma membrane is a critical step that involves the formation of a ternary complex by the v-SNARE synaptobrevin (also known as vesicle-associated membrane protein, or VAMP), and two t-SNAREs: SNAP-25 and syntaxin (7–9). Reconstitution of the v-SNARE synaptobrevin into lipid vesicles and the two t-SNAREs, SNAP-25 and syntaxin, into a distinct vesicle pool has provided evidence that the formation of a ternary complex is sufficient to join the independent vesicle pools and lead to fusion of the apposed bilayer membranes (10).

Understanding the interactions between the proteins of the trimeric complex in a simplified model may outline new ways to control its assembly and dissociation or to modulate the conformational changes that are presumably necessary for the progression from the docking step to the subsequent phases in the secretory process. The structural domains that appear to be implicated in the protein-protein interactions between SNAP-25, synaptobrevin, and syntaxin show a high propensity for the formation of α-helices (11–15). Secondary structure analysis shows that the periodic distribution of hydrophobic amino acids is consistent with a coiled-coil organization (2, 11, 12, 14, 15). Fluorescence energy transfer experiments (12) and electron microscopy (15) further indicate that synaptobrevin and syntaxin are aligned in parallel in the context of a ternary coiled-coil.

To investigate the postulated coiled-coil interactions between the proteins that constitute the docking complex in a minimal model, we have applied the principles involved in the formation of stable coiled-coils (16) to design three peptides corresponding to predicted coiled-coil-forming domains in SNAP-25, synaptobrevin-2, and syntaxin-1A. We have used CD spectroscopy to determine the secondary structure of these peptides and their interactions in binary and tertiary mixtures. Our findings are consistent with the assembly of the predicted ternary complex.

EXPERIMENTAL PROCEDURES

Reagents—HPLC grade trifluoroacetic acid, trifluoroethanol (TFE), ethanedithiol, thioanisol, phenol, and acetonitrile were purchased from Aldrich. Methyl *tert*-butyl ether was from Fisher. HPLC columns were from Vydac (Hesperia, CA). L-Amino acids and protected derivatives used for peptide synthesis were made by Calbiochem. Benzoic anhydride was obtained from Sigma. All other reagents for peptide synthesis and resins were from Applied Biosystems (Foster City, CA).

Peptide Synthesis and Purification—Peptides SN (human brain SNAP-25-(181–206)), SB (human brain synaptobrevin-2-(40–67)), ST (human brain syntaxin-1A-(191–218)), and SN_{RD} (scrambled SN peptide sequence: ESDNDTRAIKITQAGSMKRMGLNAKE) were produced using solid phase peptide synthesis. Synthesis started with a *p*-hydroxymethyl phenoxy methyl polysterene resin and was carried out using the Fastmoc® Fmoc strategy on an Applied Biosystems peptide synthesizer model 431A (Foster City, CA) according to a single coupling plus capping protocol. Cleavage from the resin and removal of all protecting groups was accomplished by using trifluoroacetic acid cleavage as described (17). Crude peptides were precipitated from the trifluoroacetic acid mixture in cold methyl *tert*-butyl ether and centrifuged, the supernatant was discarded, and the remaining methyl *tert*-butyl ether was removed under high vacuum at 0 °C for 3 h. Samples of crude peptide (10–20 mg) were dissolved in 0.1% trifluoroacetic acid, applied to a semipreparatory column (Vydac, C-18), and eluted at a flow rate of 3 ml/min with a linear gradient of 90% acetonitrile in 0.1% trifluoroacetic acid. Eluted peaks were monitored by absorbance measurements at 214 nm, pooled, and lyophilized. Peptide purity was assessed by RP-HPLC in an analytical column (Vydac, C-18).

Secondary and Tertiary Structure Predictions—Propensities of peptides to adopt a coiled-coil structure were estimated using two different

* This work was supported by U.S. Army Medical Research and Materiel Command Grants DAMD 17-93-C-3100 and DAMD 17-98-C-8040 (to M. M. and a grant from the Dystonia Medical Research Foundation (to J. M. C.). The costs of publication of this article were defrayed in part by the payment of page charges. This article must therefore be hereby marked "*advertisement*" in accordance with 18 U.S.C. Section 1734 solely to indicate this fact.

‡ To whom correspondence should be addressed: Dept. of Biology, University of California San Diego, 9500 Gilman Dr., La Jolla, CA 92093-0366. Tel./Fax: 619-534-0931; E-mail: montal@biomail.ucsd.edu.

[1] The abbreviations used are: SNARE, SNAP receptor; v-SNARE, vesicle SNARE; t-SNARE, target SNARE; BoNT, botulinum neurotoxin; SNAP-25, synaptosomal associated protein of 25 kDa; TFE, trifluoroethanol; HPLC, high pressure liquid chromatography.

programs: Coils and Paircoil. The Coils program uses the Lupas algorithm (18, 19). Sequences were compared with an unweighted MTIDK matrix (18) using 14- and 28-residue scanning windows. The second program uses the Berger algorithm (20), which is more stringent. Both methods are based on the relative frequency of occurrence of amino acids at each position (a–g) of the coiled-coil heptad repeat. Secondary structure predictions were performed using the SOPMA method (21, 22) and the AGADIR program (23).

CD Measurements—CD measurements were carried out on a modified Cary 61 (24) or an AVIV model 202 spectropolarimeter. The original Pockel cell and Cary linear polarizer in the Cary 61 were replaced with a 50-kHz photoelastic modulator (Hinds International, FS-5/PEM-80) and a MgF_2 linear polarizer (AVIV Inc.). The phase-detected output of the original end-on photomultiplier and preamplifier were integrated using an Egg Princeton Applied Research model 128A lock-in amplifier. System automation and multiple scan averaging were accomplished with an IBM PC-compatible computer interfaced directly to both the Cary 61 and the 128A amplifier. Constant N_2 flushing was employed. Spectra were measured at 195–250 nm using a 0.05-cm cell, a 1-nm bandwidth, a 0.3-ms time constant, and a cell temperature of 25 °C. All recordings were performed in 10 mM sodium phosphate buffer, pH 7.4, 100 mM NaCl, with or without TFE, unless otherwise indicated. Twenty scans were averaged for every spectrum. Base line subtraction, conversion of measured rotations to mean residue ellipticity $[\theta]$ ($deg \cdot cm^2 \cdot dmol^{-1}$) (25), and filtering of the spectra using a fast fourier transform filter were performed using the Microcal Origin 3.5 program. The percentage of α-helical content was estimated directly from the molar residue ellipticity at 222 nm as described by Chen *et al.* (26). Percentages of secondary structures were also estimated using the neural network-based K2 algorithm (27). To evaluate the spectral changes induced by peptide-peptide interactions in mixtures, the non-interacting spectra were calculated from the individual spectra using the equation,

$$[\theta]_{theo} = \Sigma(c_i \cdot n_i \cdot [\theta]_i)/\Sigma(c_i \cdot n_i) \quad \text{(Eq. 1)}$$

where c_i denotes the molar peptide concentrations, n_i represents the peptide lengths in number of residues, and $[\theta]_i$ values are observed mean residue ellipticities.

RESULTS AND DISCUSSION

Peptide Design

Basic Criteria for the Design of the Minimal Predicted Coiled-coil-forming Peptides—The sequences of the peptides synthesized from selected regions from human SNAP-25 (peptide SN), synaptobrevin-2 (peptide SB), and syntaxin-1A (peptide ST) are shown in Fig. 1*A*. Sequence selection was based on six criteria: 1) information about the minimal domains of SNAP-25, synaptobrevin, and syntaxin involved in protein-protein interactions in the core complex (1–5, 28); 2) botulinum neurotoxins (BoNTs) cleavage sites and their effects on neurotransmitter release (29–37); 3) sequence specificity of peptides inhibitors of neurotransmitter release (38–44); 4) effects of point mutations on the process of secretion and endocytosis (4, 11, 44–47); 5) predictions of secondary structure formation of coiled-coil structures; and 6) a minimum length for a stable parallel coil peptide of ~28 residues, or 4 heptad repeats (48, 49).

Design of the SN Peptide—The region of SNAP-25 interacting with synaptobrevin-2 has been localized between residue 41 and the C-terminal residue (2, 4). The segment from residue 181 to the C terminus is necessary for the SNAP-25-synaptobrevin interaction (3). Peptides corresponding to the 20 and 26 C-terminal residues, the latter analogous to the SNAP-25 segment released after cleavage by BoNT E, inhibit neurotransmitter release with IC_{50} values of 10 and 0.25 μM, presumably by preventing the docking of synaptic vesicles (40, 43).

The C-terminal region of SNAP-25 delimited by residues 169 and 206 displays a high propensity (99%) to form coiled-coil structures. Two distinct domains are predicted: one from position 166 to 187 (62%), and the second from position 189 to the C terminus (55%). Accordingly, the 26-residue peptide corresponding to the C-terminal segment of SNAP-25, hereafter designated as SN, was selected based on the fact that it is nearly 4 heptads long, it exhibits high propensity to form coiled-coils, and it is an efficient inhibitor of neurotransmitter release (Fig. 1*A*, *Peptide SN*).

Design of the ST Peptide—Similar considerations were used in the design of a potentially coiled-coil-forming peptide from syntaxin-1A. The region between positions 194 and 261 is necessary for the interaction with synaptobrevin-2 and SNAP-25 (2, 3, 5). The segment necessary for interaction with SNAP-25 has been located between residues 199 and 267 (1) and further delimited to residues 199–220 (4). All of these studies confine the SNAP-25 binding region on syntaxin to the N-terminal portion of the H3 domain (residues 191–266) (2, 4), and a putative minimal SNAP-25 binding domain (residues 189–220) has been identified (11, 44). Coiled-coil predictions using the sequence of human syntaxin revealed a region between positions 199 and 214 with high probability (78%) of coiled-coil formation.

Syntaxin-1A mutants containing point mutations (4, 11, 44) at the a and d repeats of a predicted coiled-coil show reduced SNAP-25 binding, supporting the involvement of this region in the interaction with SNAP-25 (Fig. 1*B*). Peptides corresponding to the predicted coiled-coil-forming region of syntaxin-1A have also been shown to inhibit neurotransmitter release (11, 42, 44). Given these considerations, the selected 4-heptad synthetic peptide corresponding to human syntaxin spanned from residue 191 to 218 (Fig. 1*A*, *Peptide ST*).

Design of the SB Peptide—The region of synaptobrevin-2 between positions 27 and 96 interacts with both SNAP-25 and syntaxin-1A in the core complex (3, 28). Synaptobrevin-2 contains a conserved domain between residues 57 and 88, with high propensity (95%) to form coiled-coils, and two distinct subdomains (28–42 and 52–72). Deletion of the region spanning from residue 41 to 50 abolishes endocytosis (45), and mutants lacking the segments 41–50 or 51–60 do not to bind to SNAP-25 and syntaxin-1A. The mutants with deletion of segment 31–38 show weak binding to t-SNAREs, whereas the deletion of segments 61–70 or 71–80 results in poor binding to syntaxin while maintaining the interactions with SNAP-25 (47). Moreover, a single mutation (M46A) inhibits endocytosis by 80% and reduces binding to syntaxin-1A and SNAP-25 (45, 46). Taken together, this information suggests that the region delimited by positions 40 and 60 is involved in the ternary interactions that result in the assembly of the docking complex; therefore, the peptide synthesized encompassed 4 heptads from position 40 (Fig. 1*A*, *Peptide ST*).

Design of the SN_{RD} Control Peptide—A control peptide corresponding to the scrambled sequence of the selected SNAP-25 peptide was also synthesized. Randomized sequences were generated, their secondary structures were predicted using the SOPMA method, and the sequences with an α-helical content similar to the original sequence were run against the Prosite data base. A peptide with the same functional sites but without the heptad periodicity was synthesized (sequence shown under "Experimental Procedures"), and it was shown to be pharmacologically inactive. The SN_{RD} peptide, at variance to SN, did not affect Ca^{2-}-dependent release in chromaffin cells.

Secondary structure predictions using the SOPMA method (21, 22) indicate that all three peptides may form stable α-helices in the context of a whole protein structure. Predicted helicities for SN, SB, and ST peptides were 62, 96, and 86%, respectively, when considered integrated in the protein, in contrast to 42, 57, and 67% as isolated peptides. The behavior of the isolated peptides in an aqueous environment was predicted by using the AGADIR algorithm (23). This program uses

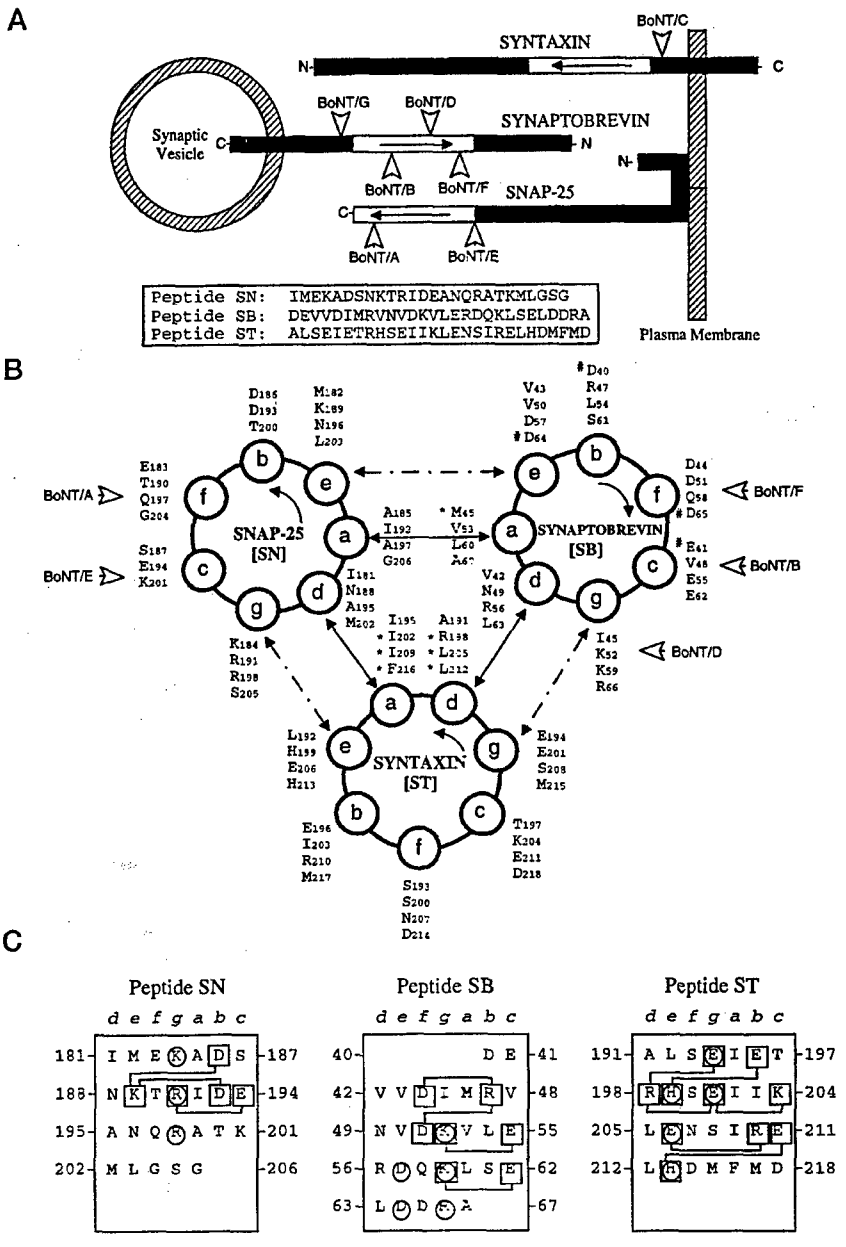

FIG. 1. **Model of a minimal trimeric coiled-coil using selected sequences from SNAP-25, synaptobrevin-2, and syntaxin-A.** *A*, schematic representation of the relative location of SNAP-25, synaptobrevin-2, and syntaxin-A in the synaptic terminal (*black boxes*). The *white boxes* represent the segments corresponding to the synthetic peptides SN, SB, and ST, respectively. The relative size of the proteins and synthetic peptides are not to scale. The amino acid sequences of the SN, SB, and ST peptides are given in the *box*. *B*, triple helical coiled-coil model of the segments of SNAP-25, synaptobrevin-2, and syntaxin-A represented by the synthetic peptides SN, SB, and ST, respectively. The sequences have a heptad pattern of residues (designated as *a–g*), where *a* and *d* are usually hydrophobic and *e* and *g* are frequently charged. *Solid arrows* denote hydrophobic interactions in the core of the complex, whereas *broken arrows* refer to potential ionic interactions, as described in detail in *C*. Mutations known to disrupt the interactions between proteins (*) are located in the hydrophobic core. Mutations known not to interfere in the assembly of the complex (#) are all located outside the hydrophobic core. Most of the charged residues are located in the outer shell of the complex (positions *b*, *c*, and *f*). *Hollow arrows* in *A* and *B* show the relative location of Botulinum neurotoxin cleavage sites, which are all accessible on the surface of the complex. *C*, potential interactions between charged residues of peptides SN, SB, and ST. Charged residues in positions *e* and *g* or at *i* + 3- or *i* + 4-positions can form intramolecular (*squares*) or intermolecular (*circles*) salt bridges that contribute to the overall stability of the trimeric complex.

statistical mechanics to consider short range interactions between residues at different pH and temperature. Given the size of our peptides, they are predicted to be unstructured (4% for SN, 3% for SB, and 2% for ST peptide, respectively) under aqueous conditions. Thus, considering both sets of data, we infer that these peptides can adopt α-helical structures only in the context of the intact protein and, therefore, that the presence of helicity-inducing conditions may be necessary to mimic the secondary structure of the peptides in the cytosol. TFE, a hydrophilic and hydrogen-bonding solvent, has been widely used to stabilize marginally stable α-helical structures in potentially α-helical peptides (48, 50–53). TFE is not limited to promoting helix formation, since it has also been shown to stabilize β-turns and even β-strands (54, 55). Notwithstanding, TFE-induced α-helical conformation in fragments of proteins known to be β-sheet in the native context has been documented (56–63). Therefore, caution must be exercised in inferring structure from CD data of peptides in the presence of TFE, particularly with regard to the extent that it represents the native structure in the context of the intact protein from which the peptide sequences were selected.

Trimeric Coiled-coil Model

Theoretical Considerations—A model of one of the trimeric conformers of the selected peptides forming a coiled-coil structure is shown in Fig. 1*B*. Given the helical wheel representation, residues at the *a*- and *d*-positions stabilize the structure by hydrophobic interchain interactions. According to this model, the synaptobrevin-2 residue Met[45], which upon mutation inhibits endocytosis, would be located in the hydrophobic core, where such a change would be predictably disruptive. The mutations in syntaxin that reduce its binding to SNAP-25 would also be located in positions *a* and *d* (residues denoted with an *asterisk* in Fig. 1*B*). Interestingly, the cleavage sites for

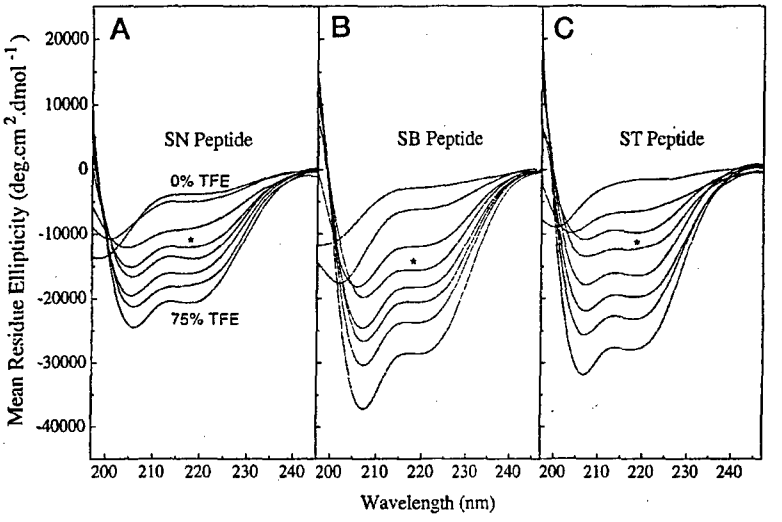

FIG. 2. **CD spectra of the synthetic peptides at different TFE concentrations.** *A*, SN peptide; *B*, SB peptide; *C*, ST peptide. Spectra were recorded in 10 mM sodium phosphate, pH 7.4, 100 mM NaCl, in the presence of increasing concentrations of TFE. Peptide concentration was 30 μM. TFE concentrations used were 10, 20, 30 (*), 40, 50, 65, and 75%.

five of the seven BoNT serotypes (BoNT A, B, D, E, and F) are found in the model peptides, and all are in surface locations potentially accessible to the BoNT proteases.

Interchain interactions of *e*- and *g*-positions mediated by charged residues also contribute to the stability of a coiled-coil (64). There are 12 charged residues in positions *e* and *g*; accordingly, inter- or intrahelical ionic interactions could synergistically contribute to the stability of the coil (Fig. 1*C*). Polar residues implanted in the hydrophobic core are potentially disruptive, although strategic placement can facilitate correct oligomerization arrangements (65). In the model, the core contains only two charged residues: Arg^{198} (peptide ST) could establish an intramolecular salt bridge with either Glu^{194} or Glu^{201} (Fig. 1*B*), and Arg^{56} (peptide SB) would be at a suitable distance to interact with the glutamate residues in position *g* of the ST peptide and form an intermolecular linkage (Fig. 1*B*).

In the outer layer (positions *b*, *c*, and *f*), 14 negatively and 3 positively charged residues would be exposed. This arrangement of negative charges mostly in the surface is consistent with observations by Regazzi *et al.* (47) that substitutions of negatively charged residues of synaptobrevin-2 do not alter function (66) (Fig. 1*B*).

Circular Dichroism Results—In aqueous media. all peptides (alone or in mixtures) were unstructured, and neither increasing peptide concentration nor changing pH, ionic strength, or divalent cation concentration increased the α-helical content. Typical single-stranded polypeptides generally do not form stable α-helices in aqueous solution and require the additional stabilization of less polar solvents (67, 68); therefore, we resorted to the use of the helix-promoting solvent TFE.

In the presence of increasing concentrations of TFE (Fig. 2, *A–C*), there was a significant increase in the α-helical content. The minimal concentration at which the peptides underwent a transition from mostly unstructured to partially structured was approximately 30%. At that concentration. the α-helical contents of the SNAP-25, synaptobrevin, and syntaxin peptides were 31. 44, and 32%, respectively. At the maximum concentration of TFE used (75%), the α-helical contents of the peptides were 59, 87, and 85%, respectively. TFE increases the α-helical content, while it disrupts tertiary and quaternary structures stabilized by hydrophobic interactions (69); therefore, it was imperative to use a concentration of TFE low enough to marginally stabilize the secondary structure of monomeric peptides while still allowing the expression of tertiary interactions. Notwithstanding the disrupting effects of TFE on the tertiary structure of oligomeric complexes, peptide-peptide interactions producing stable oligomers have been documented at concentrations of TFE as high as 50% (70). Interestingly, the TFE concentration used in our experiments (30%) has been reported to yield for numerous peptides secondary structures that compare favorably with those of the native systems (71–73).

Equimolar ternary mixtures SN/SB/ST in aqueous solution showed no interaction between the non-α-helical peptides (not shown). In the presence of TFE, the spectrum of the SN/SB/ST mixture (Fig. 3*E*, *solid line*) was significantly different from a noninteracting spectrum (Fig. 3*E*, *dashed line*) calculated from the three individual CD spectra (Fig. 3*A*). The expected α-helicity from the calculated spectrum was 35%, whereas the α-helicity from the experimental spectrum was 46%; *i.e.* a 31% net increase over the predicted value. The ratios between the intensities of the bands at 222 and 208 nm were 0.76 for the calculated and 0.80 for the experimental spectrum, respectively. This larger $\Theta_{222}/\Theta_{208}$ ratio is consistent with an increase in coiling.

The 31% net increase in helicity observed in the experimental ternary mixture spectrum with respect to the prediction could arise from the occurrence of distinct binary complexes in the mixture. Equimolar binary mixtures SN/SB, SN/ST, and SB/ST in aqueous solution showed no interaction between the peptides (not shown). In the presence of 30% TFE, the SN and SB peptides did not interact in binary mixtures (Fig. 3*B*). The helicity of the experimental spectrum was identical to that predicted by the noninteracting calculated spectrum (36%). In contrast, spectra from binary mixtures SB/ST (Fig. 3*C*) and SN/ST (Fig. 3*D*) indicated that both pairs of peptides interact under these experimental conditions. In each case, the α-helical content calculated from the experimental spectra was ~15% greater than expected for a noninteracting mixture. Predicted helicities were 34 and 33%, respectively, for the SB/ST and SN/ST mixtures, whereas the experimental values were 39 and 38%, *i.e.* 15% higher than expected for noninteracting mixtures.

Increasingly higher peptide concentration in equimolar mixtures of the SN, SB, and ST peptides in the presence of 30% TFE (Fig. 4*A*) also results in an increase in helicity and therefore a stabilization of the complex. Increasing the individual peptide concentrations from 10 to 30 μM results in an increase in helicity from 46 to 54%. It is noticeable that the three spectra define a unique isodichroic point, consistent with the occur-

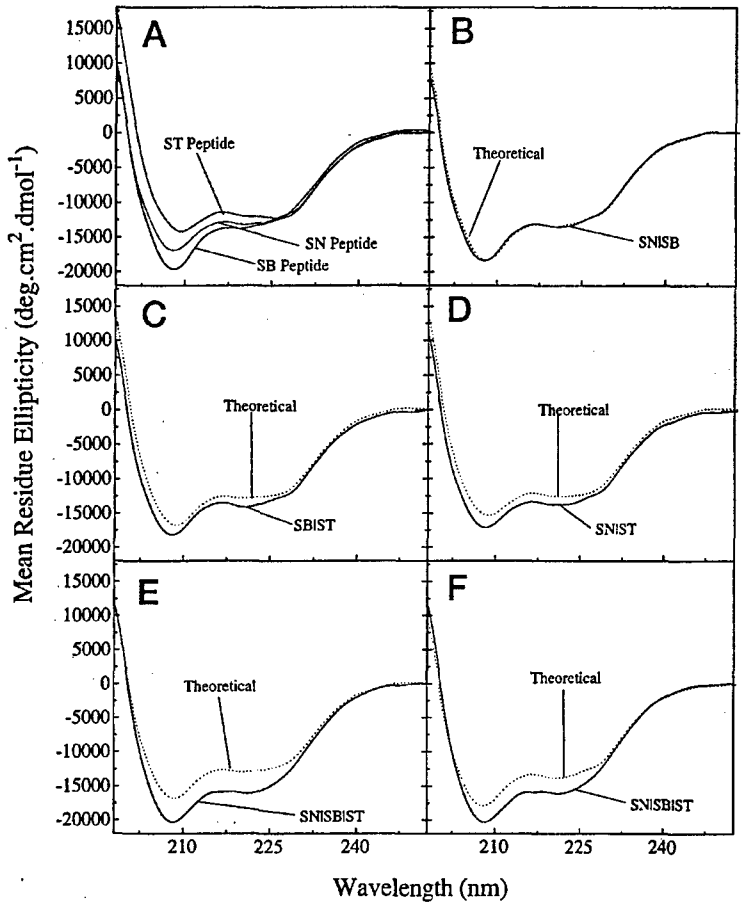

FIG. 3. **CD spectra of binary and ternary mixtures of synthetic peptides SN, SB, and ST.** Experimental (*solid line*) and calculated (*dashed line*) noninteracting spectra are shown for each mixture as well as recordings corresponding to the same peptide mixture after a 24-h incubation at 5 °C. *A*, individual spectra of SN, SB, and ST peptides used to determine the calculated noninteracting spectra; *B*, SN/SB mixture; *C*, SB/ST mixture; *D*, SN/ST mixture; *E*, SN/SB/ST ternary mixture; *F*, comparison between the spectrum of the ternary mixture after a 24-h incubation and the spectrum calculated from the summation of the binary spectra. Peptide concentration was 30 μM for each peptide. Spectra were recorded in 10 mM sodium phosphate, pH 7.4, 100 mM NaCl, with 30% TFE.

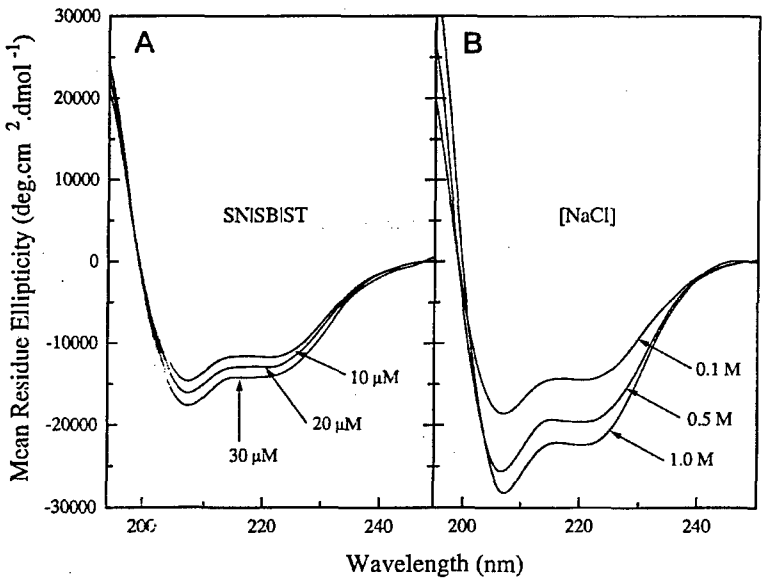

FIG. 4. **CD spectra of ternary mixtures of the SN, SB, and ST peptides as function of peptide concentration and ionic strength.** *A*, CD spectra of equimolar mixtures of SN, SB, and ST peptides, at individual peptide concentrations of 10, 20, and 30 μM. Spectra were recorded in 10 mM sodium phosphate, pH 7.4, 100 mM NaCl, with 30% TFE; *B*, effect of increasingly higher concentrations of NaCl on the secondary structure of equimolar ternary mixtures of SN, SB, and ST peptides at individual peptide concentrations of 30 μM. Spectra were recorded in 10 mM sodium phosphate, pH 7.4, 30% TFE. NaCl concentrations used were 0.1, 0.5, and 1 M.

rence of a single specific complex. When equimolar ternary mixtures are exposed to higher concentrations of NaCl in the presence of 30% TFE (Fig. 4*B*), there is a remarkable increase in the helicity (from 55% at 0.1 M NaCl to 72% at 0.5 M and 81% at 1 M). This feature is consistent with hydrophobic peptide-peptide interactions as suggested by the model (Fig. 1*B*). The increased α-helical content with increasing ionic strength is in accordance with data for coiled-coil peptides and can be explained by the increased strength of the hydrophobic interactions as the polarity of the medium is increased (69).

Whereas the spectra of all three peptides were independent of the peptide concentration in aqueous solution (Fig. 5, *A–C*),

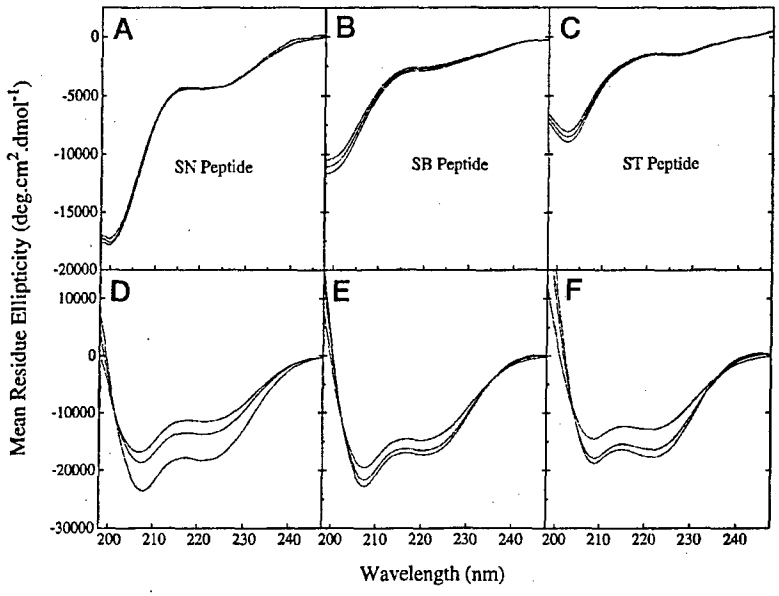

FIG. 5. **CD spectra of the synthetic peptides at increasingly higher concentrations in the absence or presence of TFE.** *A*, SN peptide; *B*, SB peptide; and *C*, ST peptide in aqueous solution. *D*, SN peptide; *E*, SB peptide; and *F*, ST peptide in 30% TFE. Peptide concentrations were 30, 60, and 90 μM, respectively. Spectra were recorded in 10 mM sodium phosphate, pH 7.4, 100 mM NaCl, with or without 30% TFE.

in the presence of 30% TFE the increase in peptide concentration resulted in a concomitant increase in the α-helical content, as indicated by the increase in negative ellipticity at 222 nm (Fig. 5, *D–F*). Helicity increased from 30 to 53% for SN, from 41 to 49% for SB, and from 35 to 51% for ST. This is consistent with the fact that peptides with α-helical structures that are dependent on dimerization or oligomerization show an augmentation of α-helical content as the peptide concentration is increased (74). This presumably arises because the equilibrium between monomeric peptide (in the form of random coil) and coiled-coil dimer is shifted toward the formation of the coiled-coil dimer, which increases the α-helical content of the peptide (65).

Higher peptide concentrations induced a moderate increase in the ratio between the peaks at 222 and 208 nm ($\Theta_{222}/\Theta_{208}$): from 0.68 to 0.78 for SN; from 0.75 to 0.77 for SB; and from 0.88 to 0.94 for ST. The ratio between the intensities of the bands at 222 and 208 nm may be regarded as a measure for the extent of coiling of α-helices around each other. The 222-nm CD band is mainly responsive to the α-helical content, whereas the band at 208 nm is sensitive to whether the α-helix is monomeric or is involved in tertiary contacts with other α-helices (75–77). Therefore, this is an additional criterion for the formation of stable coiled-coil structures. Each set of curves defined a unique isodichroic point, consistent with a single monomer-dimer equilibrium, which indicated that the oligomerization observed was sequence-specific and presumably stabilized by a concerted set of ion pairs in a defined spatial arrangement.

The ratio of the 222- to the 208-nm peak is an operational index to detect the presence of pure coiled-coils. For peptides stabilized at low TFE concentrations, an equilibrium between monomeric and multimeric states is anticipated, resulting in a profile intermediate between a pure coiled-coil and a predominantly monomeric situation. Given that the peptides exhibit a relatively low α-helical content and that there is a substantial fraction of peptide in monomeric form, the formation of homomeric or heteromeric arrays arising from interhelical interactions would result in an α-helical content of the mixtures larger than that expected from a spectrum calculated from the individual spectra (Fig. 3*A*).

To address the question of whether the increase in α-helicity observed in the ternary mixture could be accounted for by mere binary interactions between the SN, SB, and ST peptides, the calculated spectrum predicted from the sum of SN/ST and SB/ST interactions was calculated (Fig. 3*F*, *dashed line*). The experimental spectrum obtained from the ternary mixture (Fig. 3*F*, *solid line*) showed an α-helical content (46%) considerably higher than expected from a mixture of dimers (38%), suggesting the presence of ternary or higher order interactions.

The specificity of the interactions observed in binary mixtures was tested using mixtures of the SN, SB, and ST peptides with the SN_{RD} control peptide (Fig. 6). The SN_{RD} peptide was unstructured in aqueous solution, and in the presence of 30% TFE its α-helical content was similar to that of the SN peptide (spectrum not shown). Equimolar mixtures of SN_{RD} and SN (SN/SN_{RD}) showed no difference between the spectrum calculated for a noninteracting mixture and the experimental spectrum (Fig. 6*A*). Similarly, spectra obtained from SB/SN_{RD} and ST/SN_{RD} binary mixtures showed no difference with respect to the calculated noninteracting spectra (Fig. 6, *B* and *C*). The slight differences observed in the figure are not statistically significant as assessed using a Student's *t* test on the nonfiltered spectra. In the case of mixtures assayed in the presence of 30% TFE, the situation is the same: there is no interaction between SN, SB, or ST and the control peptide (Fig. 6, *D–F*). This indicates that the interactions observed upon increasing peptide concentration or mixing with other peptides, either in binary or ternary mixtures, is sequence-specific.

Conclusion

Our study identifies a minimal entity that opens a new perspective for the study of the molecular interactions between SNAP-25, synaptobrevin, and syntaxin. Three distinct synthetic peptides patterned after the sequences of the putative coiled-coil-forming domains of the main components of the docking and fusion complex self-assemble into a complex that exhibits spectral characteristics consistent with a coiled-coil structure. A synthetic coiled-coil ternary complex provides a basis for further developments: 1) the ternary complex appears suitable for both crystallization and NMR spectroscopy that, in due turn, may yield a high resolution structure of the fusion core complex; 2) it represents a conceptual framework to assist in the design and test of new peptide inhibitors of neurotransmitter release; 3) it provides leads for the design of small molecule peptidomimetic drugs; and 4) it may be valuable to generate specific antibodies to block neurotransmitter release.

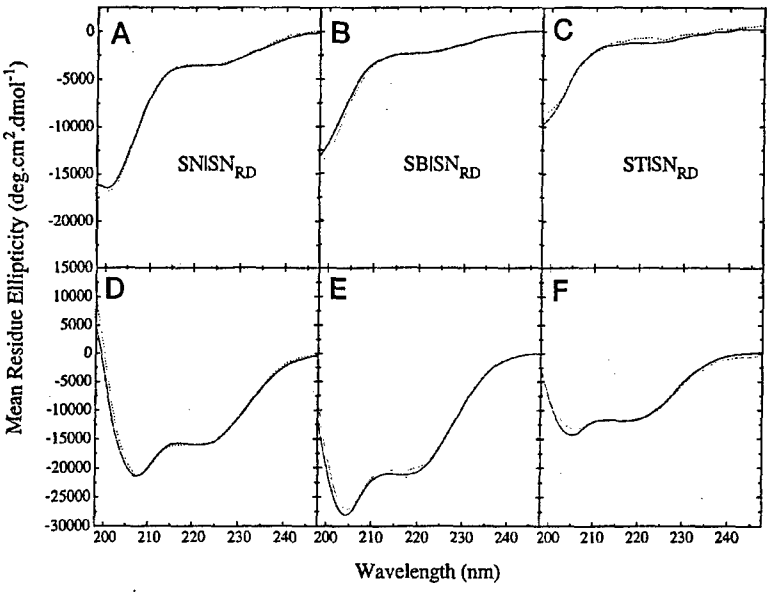

FIG. 6. **CD spectra of binary mixtures of synthetic peptides SN, SB, and ST and the control peptide SN_{RD}.** *A*, SN/SN_{RD} mixture; *B*, SB/SN_{RD} mixture; and *C*, ST/SN_{RD} mixture in aqueous solution. *D*, SN/SN_{RD} mixture; *E*, SB/SN_{RD}; and *F*, SB/SN_{RD} mixture in 30% TFE. Experimental (*solid line*) and calculated (*dashed line*) noninteracting spectra are shown for each binary mixture. Peptide concentration was 30 μM. Spectra were recorded in 10 mM sodium phosphate, pH 7.4, 100 mM NaCl, with or without 30% TFE.

Indeed, the synthetic peptides that, as shown here, participate in the assembly of the ternay complex in fact mimic the action of *Clostridial* neurotoxins (40, 43). Therefore, our findings may lead to the development of peptide-based agents that may be used as potential therapy in spastic neuromuscular disorders, substituting or complementing the current treatment with BoNTs.

Acknowledgments—We thank Professor Murray Goodman and Dr. Joseph Taulane for the use of the Cary 61 CD spectrometer and Dr. Susan S. Taylor for the use of the AVIV 202 CD spectrometer.

Note Added in Proof—After submission of this manuscript, two papers reported the structure of the SNARE complex as a parallel four-helix bundle determined by x-ray crystallography (Sutton R. B., Fasshauer, D., Jahn, R., and Brunger, A. T. (1998) *Nature* **395,** 347–353) and by electron paramagnetic resonance spectroscopy (Poirier, M. A., Xiao, W., Macosko, J. C., Chan, C., Shin, Y.-K., and Bennett, M. K. (1998) *Nat. Struct. Biol.* **5,** 765–769). The results of our study are consistent with the high resolution structure of the SNARE complex.

REFERENCES

1. Calakos, N., Bennet, M. K., Peterson, K. E., and Scheller, R. H. (1994) *Science* **263,** 1146–1149
2. Chapman, E. R., An, S., Barton, N., and Jahn, R. (1994) *J. Biol. Chem.* **269,** 27427–27432
3. Hayashi, T., McMahon, H., Yamasaki, S., Binz, T., Hata, Y., Sudhof, T. C., and Niemann, H. (1994) *EMBO J.* **13,** 5051–5061
4. Kee, Y., Lin. R. C., Hsu, S. C., and Scheller, R. H. (1995) *Neuron* **14,** 991–998
5. Hayashi, T., Yamasaki, S., Nauenburg, S., Binz. T., and Niemann, H. (1995) *EMBO J.* **14,** 2317–2325
6. Sudhof, T. C. (1995) *Nature* **375,** 645–653
7. Sollner, T., Whiteheart, S. W., Brunner, M., Erdjument-Bromage, H., Geromanos, S., Tempst, P., and Rothman, J. E. (1993) *Nature* **362,** 318–324
8. Sollner, T., Bennett, M. K., Whiteheart, S. W., Scheller, R. H., and Rothman, J. E. (1993) *Cell* **75,** 409–418
9. Rothman, J. E., and Sollner, T. (1997) *Science* **276,** 1212–1213
10. Weber, T., Zemeelman, B., McNew, J. A., Westermann, B., Gmachl. M., Parlati, F., Sollner, T., and Rothman, J. E. (1998) *Cell* **92,** 759–7772
11. Zhong, P., Chen, Y. A., Tam, D., Chung, D., Scheller, R. H., and Miljanich, G. P. (1997) *Biochemistry* **36,** 4317–4326
12. Lin, R. C., and Scheller, R. H. (1997) *Neuron* **19,** 1087–1094
13. Gerst, J. E. (1997) *J. Biol. Chem.* **272,** 16591–16598
14. Fasshauer, D., Bruns, D., Shen, B., Jahn, R., and Brunger, A. T. (1997) *J. Biol. Chem.* **272,** 4582–4590
15. Hanson, P. I., Roth, R., Morisaki, H., Jahn, R., and Heuser, J. E. (1997) *Cell* **90,** 523–535
16. O'Shea, E. K., Lumb, K. J., and Kim, P. S. (1993) *Curr. Biol.* **3,** 658–667
17. King, D. S., Fields, C. G., and Fields, G. B. (1990) *Int. J. Pept. Protein Res.* **36,** 255–266
18. Lupas, A., Van Dyke, M., and Stock, J. (1991) *Science* **252,** 1162–1164
19. Lupas, A. (1996) *Methods Enzymol.* **266,** 513–525
20. Berger, B., Wilson, D. B., Wolf, E., Tonchev, T., Milla, M., and Kim, P. S. (1995) *Proc. Natl. Acad. Sci. U. S. A.* **92,** 8259–8263
21. Geourjon, C., and Deleage, G. (1994) *Protein Eng.* **7,** 157–164
22. Geourjon, C., and Deleage, G. (1995) *Comp. Appl. Biosci.* **11,** 681–684
23. Munoz, V., and Serrano, L. (1997) *Biopolymers* **41,** 495–509
24. Feng, Y., Melacini, G., Taulane, J. P., and Goodman, M. (1996) *J. Am. Chem. Soc.* **118,** 10351–10358
25. Schmid, F. X. (1989) in *Protein Structure: A Practical Approach* (Creighton, T. E., ed) pp. 251–286, IRL Press, Oxford
26. Chen, Y. H., Yang, J. T., and Chau, K. H. (1974) *Biochemistry* **13,** 3350–3359
27. Andrade, M. A., Chacon, P., Merelo, J. J., and Moran, F. (1993) *Protein Eng.* **6,** 383–390
28. Archer, B. T., III, Ozcelik, T., Jahn, R., Francke, U., and Sudhof, T. (1990) *J. Biol. Chem.* **265,** 17267–17273
29. Binz, T., Blasi, J., Yamasaki, S., Baumeister, A., Link, E., Sudhof, T. C., Jahn, R., and Niemann, H. (1994) *J. Biol. Chem.* **269,** 1617–1620
30. Blasi, J., Chapman, E. R., Link, E., Binz, T., Yamasaki, S., De Camilli, P., Sudhof, T. C., Niemann, H., and Jahn, R. (1993) *Nature* **365,** 160–163
31. Foran, P., Lawrence, G. W., Shone, C. C., Foster, K. A., and Dolly, J. O. (1996) *Biochemistry* **35,** 2630–2636
32. Schiavo, G., Santucci, A., DasGupta, B. R., Mehta, P. P., Jontes, J., Benfenati, F., Wilson, M. C., and Montecucco, C. (1993) *FEBS Lett.* **335,** 99–103
33. Schiavo, G., Rosetto, O., Catsicas, S., Polverino de Laureto, P., DasGupta, B. R., Benfenati, F., and Montecucco, C. (1993) *J. Biol. Chem.* **268,** 23784–23787
34. Schiavo, G., Shone, C. C., Bennet, M. K., Scheller, R. H., and Montecucco, C. (1995) *J. Biol. Chem.* **270,** 10566–10570
35. Williamson, L. C., Halpern, J. L., Montecucco, C., Brown, J. E., and Neale, E. A. (1996) *J. Biol. Chem.* **271,** 7694–7699
36. Yamasaki, S., Baumeister, A., Binz, T., Blasi, J., Link, E., Cornille, F., Roques, B., Fykse, E. M., Sudhof, T. C., Jahn, R., and Niemann, H. (1994) *J. Biol. Chem.* **269,** 12764–12772
37. Yamasaki, S., Binz, T., Hayashi, T., Szabo. E., Yamasaki, N., Eklund, M., Jahn, R., and Niemann, H. (1994) *Biochem. Biophys. Res. Commun.* **200,** 829–835
38. Cornille, F., Deloye, F., Fournie-Zaluski, M. C., Roques, B. P., and Poulain, B. (1995) *J. Biol. Chem.* **270,** 16826–16832
39. Gutierrez, L. M., Canaves, J. M., Ferrer-Montiel, A. V., Reig, J. A., Montal, M., and Viniegra, S. (1995) *FEBS Lett.* **372,** 39–43
40. Gutierrez, L. M., Viniegra, S., Rueda, J., Ferrer-Montiel, A. V., Canaves, J. M., and Montal, M. (1996) *J. Biol. Chem.* **272,** 2634–2639
41. Hunt. J. M., Bommert, K., Charlton, M. P., Kistner, A., Haberman, E., Augustine, G. J., and Betz, H. (1994) *Neuron* **12,** 1269–1279
42. Martin. F., Salinas, E., Vazquez, J., Soria, B., and Reig, J. A. (1996) *Biochem. J.* **320,** 201–205
43. Ferrer-Montiel, A. V., Gutierrez, L. M., Apland. J. P., Canaves, J. M., Gil, A., Viniegra, S., Adler, M., and Montal, M. (1998) *FEBS Lett.* **435,** 84–88
44. Kee. Y., and Scheller, R. H. (1996) *J. Neurosci.* **16,** 1975–1981
45. Grote. E., and Kelly R. B. (1996) *J. Cell Biol.* **132,** 537–547
46. Hao. J. C., Salem, N., Peng, X. R., Kelly, R. B., and Bennet, M. K. (1997) *J. Neurosci.* **17,** 1596–1603
47. Regazzi. R., Sadoul, K., Meda, P., Kelly, R. B., Halban, P. A., and Wollheim, C. B. (1996) *EMBO J.* **15,** 6951–6959
48. Hodges, R. S., Zhou, N. E., Kay, C. M., and Semchuk, P. D. (1990) *Peptide Res.* **3,** 123–137
49. Marmorstein, R., Carey, M., Ptashne, M., and Harrison, S. C. (1992) *Nature* **356,** 408–414
50. Nelson. J. W., and Kallenbach, N. R. (1986) *Proteins* **1,** 211–217
51. Nelson. J. W., and Kallenbach, N. R. (1990) *Biochemistry* **28,** 5256–5261
52. Dyson. H. J., Merutka, G., Waltho, J. P., Lerner. R. A., and Wright, P. E. (1992) *J. Mol. Biol.* **226,** 795–818
53. Dyson. H. J., Sayre, J. R., Merutka, G., Shin. H. C., Lerner, R. A., and Wright,

P. E. (1992) *J. Mol. Biol.* **226,** 819–835
54. Blanco, J. F., and Serrano, L. (1995) *Eur. J. Biochem.* **230,** 634–649
55. Narayanan, U., Keiderling, T. A., Bonora, G. M., and Toniolo, C. (1986) *J. Am. Chem. Soc.* **108,** 2431–2437
56. Dong, A., Matsuura, J., Manning, M. C., and Carpenter, J. F. (1998) *Arch. Biochem. Biophys.* **355,** 275–281
57. Arunkumar, A. I., Kumar, T. K. S., and Yu, C. (1997) *Biochim. Biophys. Acta* **1338,** 69–76
58. Jayaraman, G., Kumar, T. K. S., Arunkumar, A. I., and Yu, C. (1996) *Biochem. Biophys. Res. Commun.* **222,** 33–37
59. Luidens, M. K., Figge, J., Breese, K., and Vajda, S. (1996) *Biopolymers* **39,** 367–376
60. Schonbrunner, N., Wey, J., Engels, J., Georg, H., and Kiefhaber, T. (1996) *J. Mol. Biol.* **260,** 432–445
61. Hamada, D., and Goto, Y. (1997) *J. Mol. Biol.* **269,** 479–487
62. Najbar, L. V., Craik, D. J., Wade, J. D., Salvatore, D., and McLeish, M. J. (1997) *Biochemistry* **36,** 11525–11533
63. MacPhee, C. E., Perugini, M. A., Sawyer, W. H., and Howlett, G. J. (1997) *FEBS Lett.* **416,** 265–268
64. Zhou, N. E., Kay, C. M., and Hodges, R. S. (1994) *Protein Eng.* **7,** 1365–1372
65. Adamson, J. G., Zhou, N. E., and Hodges, R. S. (1993) *Curr. Opin. Biotechnol.* **4,** 428–437
66. Pellizzari, R., Rosetto, O., Lozzi, L., Giovedi, S., Johnson, E., Shone, C. C., and Montecucco, C. (1996) *J. Biol. Chem.* **271,** 20353–20358
67. Bierzynski, A., Kim, P. S., and Baldwin, R. L. (1982) *Proc. Natl. Acad. Sci. U. S. A.* **79,** 2470–2474
68. Brown, J. E., and Klee, W. A. (1971) *Biochemistry* **10,** 470–476
69. Lau, S. Y. M., Taneja, A. K., and Hodges, R. S. (1984) *J. Biol. Chem.* **259,** 13253–13261
70. Vinogradov, A. A., Mari, F., Humphreys, R. E., and Wright G. E. (1996) *Int. J. Pept. Protein Res.* **47,** 467–476
71. Munoz, V., Serrano, L., Jimenez, M. A., and Rico, M. (1995) *J. Mol. Biol.* **247,** 648–669
72. Blanco, F. J., Ortiz, A. R., and Serrano, L. (1997) *Folding Design* **2,** 123–133
73. Ramirez-Alvarado, M., Serrano, L., and Blanco, F. J. (1997) *Protein Sci.* **6,** 162–174
74. Zhou, N. E., Kay, C. M., and Hodges, R. S. (1992) *J. Biol. Chem.* **267,** 2664–2670
75. Zhou, N. E., Zhu, B. Y., Kay, C. M., and Hodges, R. S. (1992) *Biopolymers* **32,** 419–426
76. Cooper, T. M., and Woody, R. W. (1990) *Biopolymers* **30,** 657–676
77. Greenfield, N. J., and Hitchcock-DeGregori, S. E. (1995) *Biochemistry* **34,** 16797–16805

ABSTRACTS

SOCIETY FOR NEUROSCIENCE

28TH ANNUAL MEETING • LOS ANGELES, CALIF. • NOVEMBER 7–12, 1998

24

Part 1

PART 1 OF 2

34.13

APPLICATION OF COMBINED FLUORESCENT IN SITU HYBRIDIZATION AND IMMUNOCYTOCHEMISTRY TO DETERMINE EFFICIENCY OF GENE TRANSFER MEDIATED BY A HERPES SIMPLEX VIRUS AMPLICON VECTOR. D.J. Tsai,[1] C.R. Ozawa[2] and R.M. Sapolsky[1,2]. [1]Department of Biological Sciences, Stanford University and [2]Neurosciences Program, Stanford University Medical School, Stanford, CA 94305

We have adapted fluorescent *in situ* hybridization (FISH) and immunocytochemistry (ICC) for co-detection of transgenes and their products transferred by a defective herpes Simplex Virus (HSV) amplicon vector into a host cell. Utilizing separate fluorescent labels (i.e. rhodamine, fluorescein, and 4'-6-diamidino-2-phenylindole [DAPI]) and confocal microscopy, we were able to simultaneously detect transgenes, their products, and their locations relative to the nuclear compartment of a single cell. Detection of reporter genes (i.e. *lacZ*) and their encoded proteins (i.e. β-galactosidase) was accomplished in both mixed rat hippocampal cultures and *in vivo* experiments of the dentate gyrus of rats. This method provides an alternative to current titering protocols based solely on immunocytochemistry, which cannot be applied to inducible systems in which transgene expression is normally quiescent and does not account for infected cells that fail to express protein. By using FISH to titer, we are able to obtain a more comprehensive assessment of the efficiency of gene transfer into cells.

In gene therapy applications employing HSV amplicon vectors a prevailing problem is downregulation of transgene expression over time. Past studies have suggested that although protein and RNA levels rapidly decline, vector DNA levels within tissue remain constant. We have applied FISH and ICC to examine if downregulation of transgene expression in a single cell correlates with loss of vector DNA from the host cell nucleus or to nuclear localization of a transgene. In addition, we look at the relationship between multiple infections of the viral vector and the stability of transgene expression within a cell. These studies may offer insight into the mechanisms by which genes transferred by viral vectors lose their stability over time.

Support via Howard Hughes Predoctoral Fellowship to CRO and NIH RO1 NS32848.

34.14

INSULT-INDUCIBLE GENE EXPRESSION CONFERRED BY A HERPES SIMPLEX VIRUS AMPLICON VECTOR CONTAINING A SYNTHETIC GLUCOCORTICOID-RESPONSIVE PROMOTER. C.R. Ozawa[1], D.Y. Ho[2] and R.M. Sapolsky[1,2]. Neurosciences Program[1] Stanford University Medical School, and Department of Biological Sciences[2], Stanford University, Stanford, CA 94305.

Herpes Simplex Virus (HSV) amplicon vectors encoding various transgenes (i.e. glucose transporter-1, bcl2) have previously been shown to significantly attenuate neuron death caused by necrotic insults such as ischemia, hypoglycemia, and seizure in rat hippocampus. A limitation to the utility of such vectors as a gene therapy strategy for intervention of necrotic death, however, is that transcription of transgenes is currently under constitutive rather than inducible control. A novel approach to regulating transgene expression is to use stress-inducible promoters, so that the signal for induction is the insult itself.

The ability of a synthetic promoter containing glucocorticoid responsive elements upstream of a minimal promoter to respond to stress signals was assessed in rat hippocampal primary cultures. A reporter gene (*luc*) was placed under direction of the promoter, and the time course and extent of luciferase expression induced by physiologically-relevant steroid levels was measured. Maximal induction (approx. 30-45 fold above control) was achieved two hours after addition of steroid concentrations equivalent to those triggered *in vivo* by necrotic insult (10^{-6} M). Induction was demonstrated to be tightly dose-responsive and steroid specific (responsive to natural and synthetic glucocorticoids, but not to estradiol, testosterone or progesterone). Preliminary results *in vivo* in rat hippocampus suggest that this vector may be induced by high circulating concentrations of glucocorticoids or by kainic acid-induced seizure. The neuroprotective potential of these inducible vectors against necrotic insults is being examined when glucose transporter-1 is added as the induced transgene. These studies will hopefully provide insight towards clinically applicable treatments for reduction of brain injury caused by necrotic insult.

Support via Howard Hughes Predoctoral Fellowship to CRO and NIH RO1 NS32848

34.15

CHARACTERIZATION OF TETRACYCLINE-SENSITIVE GFAP PROMOTER FOR AUTOREGULATORY GENE-EXPRESSION IN TRANSGENIC RAT ASTROCYTES. M. Barton, J. Kulik, L.J. DeGennaro, S.P. Kash. Dept. of Molecular Genetics, Wyeth-Ayerst Research, Princeton, NJ 08543

We evaluated alternate methods for tetracycline-inducible transgenic over expression in rat astrocytes. The native human GFAP promoter was modified to include 1 or 8 copies of the tet-operon in place of a native enhancer element, rendering it responsive to tetracycline regulation. These changes were aimed at reducing basal promoter activity and tTA transactivator toxicity while permitting a large induction of expression when the gene is released from tet-suppression.

The promoters were initially studied *in vitro* using a bicistronic reporter system (luciferase and tTA transactivator separated by an internal ribosome entry site). All 3 promoters showed preferential expression in glial cells under basal conditions in the 4 cell lines that were tested (C6-glioma, CHO-K1, SK-N-SH, and HT-1080). However, GFAPwt and GFAPtetO1 promoters retained glial cell specificity in the absence of doxycycline while GFAPtetO8 increased significantly in all cell lines. Basal promoter activities of GFAPO1 and GFAPO8 in C6-glioma five days after transfection were 1:546 and 1:250, respectively, when compared to native GFAP. These promoters auto-induced by 3-7 fold in the absence of DOX, reaching 1:146 and 1:35 the level of GFAPwt, respectively. In stably transfected C6-gliomas, GFAPtetO1 showed basal promoter activity of 1:2562 and autoinduced activity of 1:500 compared to the native GFAP promoter after 12 days of induction.

The results indicate that 1) basal GFAP promoter activity can be reduced without altering cell specificity by enhancer modification, 2) the modification made here confers regulation by doxycycline/tTA, and 3) there is a dose dependent relationship between the tet-operon and cell-specificity. We are currently evaluating GFAP and GFAPO1 promoters in transgenic rats for glial-specific expression and auto-induction.

PRESYNAPTIC MECHANISMS: RELEASE MACHINERY

35.1

PEPTIDES COMPOSED OF CARBOXY-TERMINAL DOMAINS OF SNAP-25 BLOCK ACETYLCHOLINE RELEASE AT AN *APLYSIA* SYNAPSE. J.P. Apland[1], L.A. Biser[1], M. Adler[1], A.V. Ferrer-Montiel[2], M. Montal[2], and M.G. Filbert[1]. [1]Neurotoxicology Branch, USAMRICD, Aberdeen Proving Ground, MD 21010-5425; [2]Dept. of Biology, UCSD, La Jolla, CA 92083-0366.

Botulinum neurotoxin serotypes A and E (BoNT-A and BoNT-E) block neurotransmitter release, presumably by cleaving SNAP-25. A 20-amino acid peptide called ESUP-A (excitation-secretion uncoupling peptide) spans the cleavage site for BoNT-A and mimics the carboxy-terminal domain of SNAP-25. Gutierrez *et al.* (FEBS Lett. 372:39, 1995) showed that this peptide inhibited transmitter release from permeabilized bovine chromaffin cells, apparently by blocking vesicle docking (Gutierrez *et al.*, J. Biol. Chem. 272:2634, 1997). Two similar peptides that span the cleavage site for BoNT-E, one with 20 amino acids (ESUP-E20) and one with 26 (ESUP-E26), have also been synthesized. ESUP-E26 is reported to be much more potent than is ESUP-E20 in chromaffin cells. These peptides were tested for effects on acetylcholine (ACh) release at an identified cholinergic synapse of *Aplysia* neurons.

Recordings were obtained from isolated buccal ganglia of *Aplysia*. The presynaptic neuron was stimulated electrically to elicit action potentials. The postsynaptic neuron was voltage-clamped, and evoked inhibitory postsynaptic currents (IPSCs) were recorded. ESUPs were pressure-injected into the presynaptic neuron, and their effects were studied. ACh release from presynaptic cells, as measured by IPSC amplitudes, was gradually inhibited by the peptides. ESUP-A, ESUP-E20 and ESUP-E26 all caused about 40% reduction in IPSC amplitude in 2 hr. Random-sequence peptides of the same amino acid composition as ESUP-A and ESUP-E26 had no effect. Injection of BoNT E, in contrast, caused about 50% reduction in IPSC amplitude in 30 min, and almost complete inhibition in 2 hr. These results suggest that ESUPs compete with intact SNAP-25 for binding with other fusion proteins, thus inhibiting exocytosis of neurotransmitter. Production of peptide fragments by BoNT-induced cleavage of synaptic proteins may indirectly contribute to inhibition of neurotransmitter release.

Supported by DoD.

35.2

INTERACTION BETWEEN SNAP-25 AND SYNTAXIN IN CULTURED CELLS CONTROLS THE EXPRESSION AND TARGETING OF SNARE PROTEINS INVOLVED IN EXOCYTOSIS. N.E. Lovrano, V. Cansino, and M.C. Wilson* *Dept. of Neurosciences, School of Medicine, Univ. of New Mexico, Albuquerque, NM 87131.*

The core 7S complex of the synaptic vesicle docking/fusion machinery that serves as the scaffolding to recruit accessory proteins necessary for regulated exocytosis is comprised of plasma membrane proteins SNAP-25, syntaxin and the vesicle protein VAMP. While SNAP-25 plays a principal role in the release of neurotransmitters and peptides from neurons and neuroendocrine cells, it has been also implicated in vesicular trafficking required for neurite extension. (These different roles of SNAP-25 may be played by developmentally regulated isoforms: SNAP-25b and SNAP-25a). Our studies were focused to determine whether interactions between SNAP-25 and syntaxin can regulate the expression and membrane targeting of these molecules. Steady-state levels of SNAP-25 and syntaxin were determined by immunoblotting and rates of synthesis and turnover by in vivo labeling of transfected non-neuronal cell lines. Our results show that the steady-state level of both SNAP-25 isoforms was greatly reduced by co-expression with syntaxin. Pulse labeling and chase experiments demonstrated that this was not due translational regulation, but suggest that the decrease was in part due to rapid turnover of SNAP-25 in presence of syntaxin. When expressed independently, the half-life of these proteins was 11-14 hr; however when co-expressed a large component showed an increased turnover rate of 1-2 hr. In contrast to the integral membrane protein syntaxin, intrinsic membrane association of SNAP-25 requires post-translational fatty acylation. Mutations that either eliminate cysteine residues that serve as sites of palmitoylation in SNAP-25, or the transmembrane region of syntaxin, largely eliminated the decreased expression seen in co-transfections. Nevertheless, intact syntaxin was able to effectively recruit the cysteine-less SNAP-25 mutants to membrane fractions. These results show that cellular interaction between SNAP-25 and syntaxin requires both proteins to be independently targeted to the membrane which is likely to be an important step in governing the assembly of the docking and fusion machinery required for neurotransmitter release. (Funded by NIH MH-39989).

ABSTRACTS

SOCIETY FOR NEUROSCIENCE

28TH ANNUAL MEETING • LOS ANGELES, CALIF. • NOVEMBER 7–12, 1998

24

Part 2

Includes:
Key Word Index
Author Index

PART 2 OF 2

812.1

A NOVEL PROTEIN REQUIRED FOR STRORE-OPERATED CALCIUM ENTRY

Chaoxian Geng*, Hung-Tat Leung, Young-Seok Hong, Chenjian Li, Lydia L. R. Strong, and William L. Pak, Department of Biological Sciences, Purdue University, West Lafayette, IN 47907

The TRP protein of Drosophila is a founding member of a family of store-operated calcium channels. Several proteins, including INAD, PLCβ, TRPL, calmodulin and probably rhodopsin, have been found to form a multi-molecular complex with TRP, and the complex seems necessary for effective signal transduction in the fly photoreceptors.

We isolated a new Drosophila mutant, *inaF*, by P-element-mediated mutagenesis. Molecular cloning of the *inaF* gene showed that it encodes a novel, soluble protein. The null *inaF* mutants, isolated by imprecise excision of the P element, exhibited electrophysiological phenotypes indistinguishable from null trp mutants in all parameters of photoreceptor potential examined. The results suggest that in the absence of the INAF protein, the TRP channel cannot function. We carried out biochemical analyses to examine possible interactions between the INAF protein and other known protein components of the phototransduction cascade. The null *inaF* mutation seems to cause a drastic and specific reduction in the amount of TRP protein but does not eliminate the protein. Our results suggest that INAF protein is required for the store-operated calcium entry (SOCE) probably by either directly interacting with the TRP protein or regulating the amount of TRP protein at the transcription and translation levels. (Supported by NIH Grant EY00033 to WLP)

812.2

MOLECULAR CLONING AND FUNCTIONAL EXPRESSION OF RAT STORE-OPERATED Ca^{2+} CHANNELS.

N. Mizuno,[1]* S.Kitayama,[2] Y. Saishin,[2] S. Shimada,[2] K. Morita,[2] C. Mitsuhata,[3] H.Kurihara,[1] T. Dohi.[3] [1]Dept. of Endodontology and Periodontology, Hiroshima University School of Dentistry; [2]Dept. of Anatomy, Nagoya City University Medical School; [3]Dept. of Pharmacology, Hiroshima University School of Dentistry; Hiroshima, 734-8553, Japan.

Capacitative calcium entry (CCE) demonstrated in various cell types plays an important role in cell signaling. Depletion of intracellular Ca^{2+} store activates Ca^{2+} influx from extracellular space through plasma membrane channel, called store-operated channel (SOC). Identification of *trp* (transient receptor potential) gene from *Drosophila* photoreceptor and the subsequent molecular cloning of human homologues suggested that *trp* or its related gene may participate in CCE or SOC. In the present study, we have identified five different *trp*-related amplifications by reverse-transcription-polymerase chain reaction (RT-PCR) from rat various tissues, and designated rtrp1,3,4,5,6. From rat brain cDNA library, we isolated two novel homologous, rtrp3 and rtrp6. By RT-PCR and *in situ* hybridization, mRNAs of rtrp3 and rtrp6 were found to be expressed differently in brain and other various tissues. Ca^{2+} entry in response to thapsigargin-induced store depletion was demonstrated in COS cells expressed rat TRP3 and TRP6, suggesting that trps function as SOC.

812.3

STORE-DEPENDENT CALCIUM INFLUX IN CULTURED MAMMALIAN CENTRAL NEURONS.

V. Pinelis[1], D. Fayuk[2], T. Storozhevykh[1], N. Andreeva[3], L. Khaspekov[3], O. Vergun[2], A. Lyzhin[3], N. Grigortsevich[2], N. Vinskaya[1], B. Khodorov[2] [1]Institute of Pediatrics, [2] Institute of General Pathology and Pathophysiology, [3] Brain Research Institute; Moscow, 117963, Russia.

The plasma membrane of nonexcitable cells is known to be endowed with so-called store-operated Ca^{2+} selective channels. The aim of the present work was to clarify whether these channels also exist in mammalian central neurons. Experiments were performed on cultural cortical, hippocampal neurons and cerebellar granule cells loaded with fura-2. Blockade of the endoplasmic reticulum (ER) Ca^{2+} pump was achieved by cyclopiazonic acid (CPA, 10-30 μM) or thapsigargin (TG, 1-5 μM). Applications of these inhibitors to the cortical neurons in the Ca^{2+}-free medium induced a transient increase in the $[Ca^{2+}]_i$ determined by Ca^{2+} leakage from ER stores. In the Ca^{2+} containing medium CPA or TG applications induced a steady $[Ca^{2+}]_i$ increase which could be reversibly abolished by removal of external Ca^{2+}. Similar Ca^{2+} dependent increase in $[Ca^{2+}]_i$ during the action of CPA was observed in almost all the cortical and hippocampal neurons and in about of 50% of cerebellar granule cells. In order to clarify whether the TG or CPA-induced Ca^{2+} influx was resulted from depletion of Ca^{2+} stores but not due to an initial increase in $[Ca^{2+}]_i$, we treated nerve cells for 5-10 min by TG or CPA in Ca^{2+}- free medium. After such a treatment inducing depletion of Ca^{2+} stores, readmission of Ca^{2+} produced a stable increase in $[Ca^{2+}]_i$ which could be reversibly abolished by removal of external Ca^{2+}. These results strongly suggested that the plasma membrane of mammalian central neurons like the that of a wide variety of other cells endowed with Ca^{2+} channels activated by depletion of intracellular Ca^{2+} stores Ca^{2+} influx via this pathway, modulated by the activity of intracellular Ca^{2+} pump, may contribute to regulation of the neuronal $[Ca^{2+}]_i$ homeostasis under various physiological and pathophysiological conditions. Supported by RFBR.

812.4

BOTULINUM NEUROTOXIN A INHIBITS CAPACITATIVE Ca^{2+} INFLUX BUT NOT Ca^{2+} RELEASE IN *XENOPUS* OOCYTES.

Yong Yao*, Antonio V. Ferrer-Montiel[2], Mauricio Montal[2] and Roger Y. Tsien[1] [1]Dept. Pharmacology and [2]Dept. Biology, University of California, San Diego, La Jolla, CA 92093-0647

Depletion of Ca^{2+} stores by various means ($InsP_3$, Ca^{2+}-ATPase inhibitors, Ca^{2+} ionophores, Ca^{2+} buffers etc.) induces plasma membrane Ca^{2+} influx in most non-excitable cells, but the coupling mechanism remains one of the major controversies in Ca^{2+} signaling. Here we report that botulinum neurotoxins (BoNTs) injection into *Xenopus* oocytes inhibit capacitative Ca^{2+} influx (quantified as the Ca^{2+} current I_{soc}) without reducing Ca^{2+} release induced by $InsP_3$ or ionomycin. I_{soc} was maximally inhibited by about 50% by BoNT A at 100 nM (K_i = 13 ± 9 nM), whereas 100 nM BoNT B, E, and tetanus toxin inhibited I_{soc} at most 20%. BoNT A inhibition of I_{soc} was noncompetitive with respect to stores depletion and developed with a time constant of 1.1 hr. Subsequent recovery from BoNT A was slow, with about 24% inhibition remaining 48 hrs after injection. Because botulinum neurotoxins are well known to inhibit exocytosis potently and specifically by cleaving SNARE proteins, these results suggest that components of the exocytic apparatus may play a crucial role in the mechanism by which Ca^{2+}-depleted endoplasmic reticulum signals to the plasma membrane.

812.5

MUSCARINIC ACETYLCHOLINE RECEPTORS (AChR) IN PC12D CELLS REGULATE Ca^{2+} INFLUX BY ACTIVATING BOTH NOT STORE-OPERATED AND RECEPTOR-OPERATED Ca^{2+} CHANNELS.

D. Saffen, T. Ebihara, F.-F. Guo. Department of Neurochemistry, Faculty of Medicine, Tokyo University, Tokyo 113, Japan.

We have previously shown that activation of the mAChR in PC12D cells, a rapidly differentiating subline of the rat pheochromocytoma-derived cell line PC12, induces the discharge of Ca^{2+} from intracellular stores and a subsequent sustained influx of extracellular Ca^{2+} (Ebihara and Saffen, J. Neurochem. 1997). In the present study we used PC12D cells loaded with the Ca^{2+}-sensitive fluorescent dye fura2 to examine pathways of mAChR-stimulated Ca^{2+} influx. These studies revealed that the mAChR agonist carbachol stimulates Ca^{2+} influx by activating two distinct kinds of Ca^{2+} channels: i) store-operated Ca^{2+} channels (SOCC) that are also activated when intracellular Ca^{2+} stores are discharged by exposure to thapsigargin, ii) permeable to Mn^{2+} but largely impermeable to Ba^{2+}, iii) insensitive to phorbol esters, iv) slow to close following the addition of the mAChR antagonist atropine, and 2. receptor-activated Ca^{2+} channels (ROCC) that are i) not activated by thapsigargin, ii) highly permeable to Ba^{2+} and Na^+ (in the absence of Ca^{2+}), iii) blocked by phorbol esters, iv) rapidly inactivated following inhibition of mAChR by atropine. The carbachol-activated ROCC are distinct from nicotinic acetylcholine receptors and L- and N-type Ca^{2+} channels since they are not blocked by tubocurarine, verapamil or ω-conotoxin. Supported by Grants from the Japanese Ministry of Education (# 07279107 and #08278178).

812.6

THE MUSCARINIC Ca^{2+} RESPONSE, POSITIVE FEEDBACK INVOLVING NO, cGMP AND CNG CHANNELS.

C. Mathes[1]*, A.A. Alousi and S.H. Thompson[1] [1]Dept. Biol. Sci./Hopkins Marine Station, Stanford Univ., Pacific Grove, CA 93950. [2]Axon Instruments, Inc.

We are studying the dynamics of signaling in response to M1 receptor activation in N1E-115 mouse neuroblastoma cells. Stimulation of IP_3 production by carbachol causes both intracellular Ca^{2+} release and activation of a voltage independent Ca^{2+} current. These two processes are coupled via the NO/cGMP pathway. Carbachol promotes 16-20 fold increase in cGMP within 30 sec due entirely to Ca^{2+} dependent activation of NOS and subsequent activation of guanylyl cyclase. cGMP directly activates a 47 pS channel in inside-out patches with properties similar to channels in sensory cells. The relationship between cGMP conc. and channel opening is fit by the Hill equation assuming K_D = 10 μM and Hill coeff. = 2. cAMP fails to activate. The Ca^{2+} current turns on more slowly than Ca^{2+} release, lagging behind the measured depletion of the IP_3 releasable Ca^{2+} pool, but it activates in parallel with cGMP production, measured in individual cells with a patch cramming method, and nitrite accumulation which was used as a measure of NO production in plate assays. Ca^{2+} influx is responsible for 60% of cGMP production but makes little contribution to the volume averaged Ca^{2+} signal, indicating that CNG channels and NOS may be co-localized. The activation of CNG channels by this route is necessary to refill the IP_3 sensitive Ca^{2+} pool during repetitive stimulation, demonstrating that the NO→cGMP→CNG channel pathway plays a critical role in Ca^{2+} homeostasis. Because Ca^{2+} entry effectively promotes further cGMP production, the system is prone to positive feedback. This positive feedback mechanism may explain the large and rapid increases in cGMP that occur in neurons in the cerebellum, the basal forebrain and in sympathetic ganglia. (Supported by NSF and AHA).

PERGAMON

Neuropharmacology 37 (1998) 139–147

NEURO PHARMACOLOGY

Structural determinants of the blocker binding site in glutamate and NMDA receptor channels

Antonio V. Ferrer-Montiel [a], Jaime M. Merino [a], Rosa Planells-Cases [b], William Sun [1,a], Mauricio Montal [a,*]

[a] *Department of Biology, University of California San Diego, 950 Gilman Dr., La Jolla, CA 92093-0366, USA*
[b] *Department of Neurosciences, University of California San Diego, 9500 Gilman Dr., La Jolla, CA 92093-0366, USA*

Accepted 4 December 1997

Abstract

Glutamate receptor channels of the NMDA-type (*N*-methyl-D-aspartate) and non-NMDA-type (GluR) differ in their pore properties. The N-site in the M2 transmembrane segment of NMDA receptors (NMDAR), or the corresponding Q/R-site in GluRs, is a pivotal structural determinant of their permeation and blockade characteristics. Substitutions at a second site in M2, the L-site (L577) in GluR1, drastically alter the receptor selectivity to divalent cations. Here we report that M2 mutants carrying an asparagine or a threonine residue at the Q-site of GluR1, along with a tryptophan residue at the L-site, form homomeric GluR1 channels that are highly sensitive to structurally diverse, uncompetitive NMDA antagonists such as arylcyclohexylamines, dibenzocycloheptenimines, and to morphinian and adamantane derivatives. Analysis of the voltage dependence of channel blockade locates the blocker binding site ~ 0.65 partway into the transmembrane electric field in both GluR1 mutants and NMDAR channels. Our results suggest that the homomeric GluR1 double mutants, L577W/Q582N and L577W/Q582T, fairly approximate the pore properties of the heteromeric NMDA receptor and support the structural kinship of their permeation pathways.

Keywords: Adamantane derivatives; Arylcyclohexylamines; Dibenzocycloheptenimines; Morphinian derivatives; Neuroprotectants

1. Introduction

Glutamate-gated channels, also known as ionotropic glutamate receptors mediate excitatory neurotransmission in the central nervous system (CNS) (Collingridge and Lester, 1989; Nakanishi, 1992; Choi, 1992). Glutamate receptors are subclassified into *N*-methyl-D-aspartate (NMDA), α-amino-3-hydroxy-5-methyl-4-isoxazole propionate (AMPA) and kainate (KA) receptors according to their pharmacology (Hollmann and Heinemann, 1994; Nakanishi and Masu, 1994). These receptors are oligomeric proteins and the existence of several subunits of a given GluR subtype expands the structural and functional diversity of this receptor family. AMPA receptors may be either homomeric or heteromeric proteins composed of GluR1–4 subunits, while KA receptors are formed by GluR5–7 subunits (Hollmann and Heinemann, 1994; Nakanishi and Masu, 1994). NMDA receptors, in contrast, are heteroligomers formed by the co-assembly of the ubiquitous NR1 subunit and one or more of the NR2 subunits (NR2A–D) (Hollmann and Heinemann, 1994; Nakanishi and Masu, 1994). Recently, it was reported that homomeric GluRs and heteromeric NMDA-gated channels have pentameric subunit stoichiometry (Ferrer-Montiel and Montal, 1996; Premkumar and Auerbach 1996a).

At variance with AMPA and KA receptors, the NMDA receptor is highly selective to Ca^{2+} and blocked by external Mg^{2+} in a voltage dependent manner (Mayer et al., 1984; Mayer and Westbrook, 1987; Ascher and Nowak, 1988; Iino et al., 1990; Jahr and Stevens, 1993; Kawajiri and Dingledine, 1993; Zarei and Dani, 1994). The remarkable Ca^{2+}-permeability of the NMDA receptor underlies its pivotal

* Corresponding author. Tel.: +1 619 5340931, fax: +1 619 5340931; e-mail: montal@biomail.ucsd.edu

[1] Present address: Neurosciences Program, University of Southern California, Los Angeles, CA 90089-2520, USA.

0028-3908/98/$19.00
PII: S0028-3908(98)00007-0

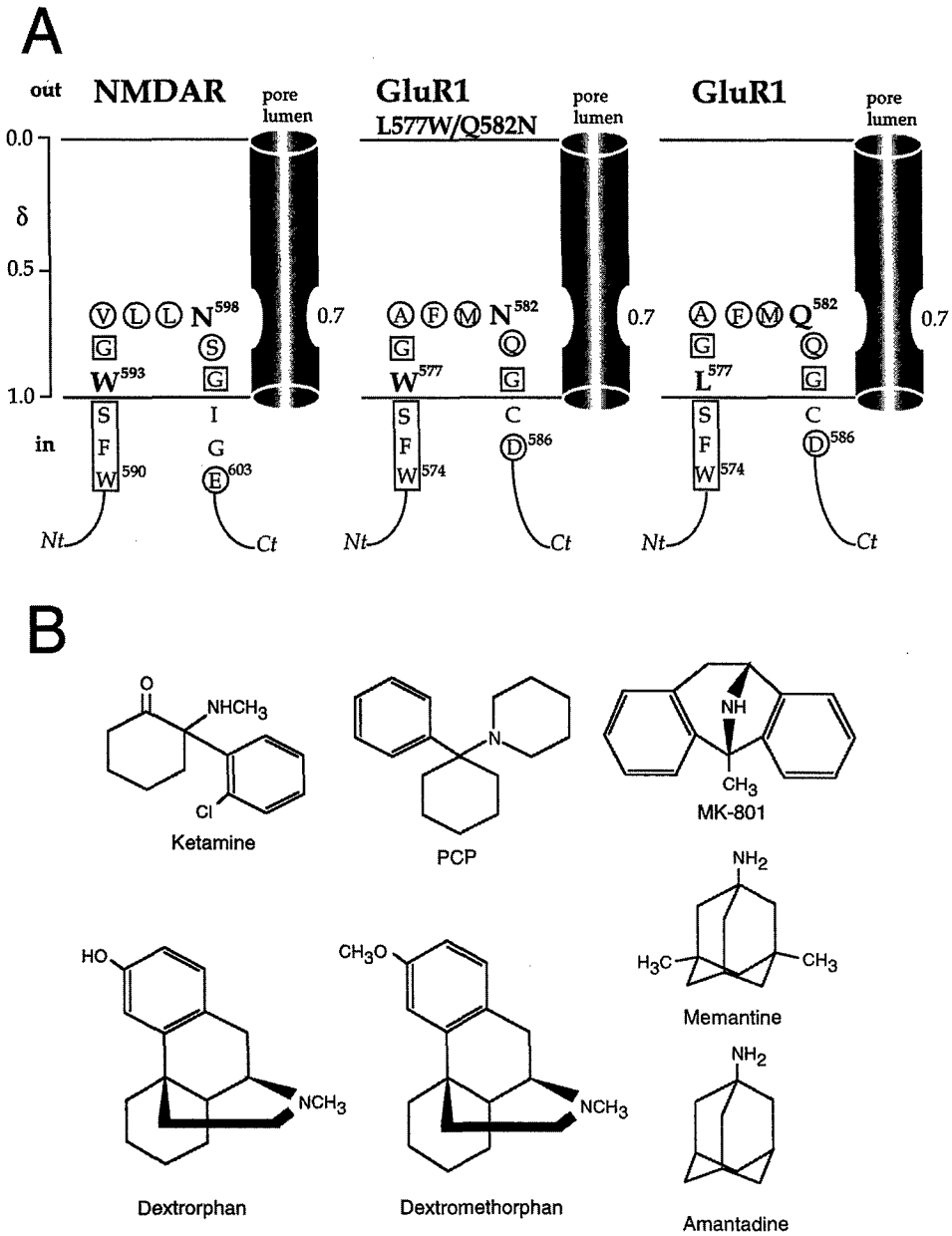

Fig. 1. (A) Schematic representation of the presumed locations of the N/Q-site and the W/L-site in the putative membrane embedded stretch of M2 for NMDAR (left) (Kuner et al., 1996) GluR1 (right) and the GluR1 L577W/Q582N mutant (center). Assignment of the blocker binding site corresponds to the constriction of the pore lumen and is calibrated according to δ, the electrical distance from the entryway (out) to the binding site (Fig. 4, Eq. (3)). Amino acids within circles highlight similarity; residues within boxes are identical. Single letter code used; numbers indicate the position of the residue in the deduced amino acid sequence. Nt and Ct denote N- and C-terminals. (B) Uncompetitive NMDA antagonists acting as open channel blockers. Structural representation of the arylcyclohexylamines PCP and ketamine, the dibenzocycloheptenimine MK-801, the morphinian derivatives dextrorphan and dextromethorphan, and the adamantane derivatives amantadine and memantine.

involvement in both the physiology and pathology of the CNS. NMDA receptors have been implicated in induction of long term potentiation, a process associated with learning and memory (Collingridge and Lester, 1989; Jessell and Kandel, 1993; Stevens, 1993). Prolonged stimulation of these receptors, however, overloads neurons with Ca^{2+} leading to neuronal death, a process that may contribute to the etiology of several acute and chronic brain disorders (Collingridge and Lester, 1989; Olney, 1990; Choi and Rothmann, 1990; Herrling, 1994). Therefore, the NMDA receptor is a key target for pharmacological intervention in glutamate excitotoxicity processes (Schinder et al., 1996) and uncompetitive NMDA antagonists acting as open channel blockers are considered candidates for drug development (Huettner and Bean, 1988; Chen et al., 1992; Parsons et al., 1993, Iversen and Kemp, 1994; Parsons et al., 1995; Bresink et al., 1996; Koroshetz and

Moskowitz, 1996; Blanpied et al., 1997; McBurney, 1997) (Fig. 1).

The structural determinants that specify the different pore properties exhibited by GluRs and NMDA receptors are beginning to be defined. The M2 segment appears to be the major component of the pore-lining structure (Dingledine et al., 1992; Mori et al., 1992; Burnashev et al., 1992a,b; Sakurada et al., 1993; Ferrer-Montiel et al., 1995, 1996; Montal, 1995) (Fig. 1(A)). Site specific mutagenesis of asparagine at position N598 in M2 of NMDAR subunits, known as the N-site, demonstrates its participation in Ca^{2+}-permeability, Mg^{2+}-blockade, and drug binding (Mori et al., 1992; Burnashev et al., 1992b; Sakurada et al., 1993; Ferrer-Montiel et al., 1995; Sharma and Stevens, 1996; Wollmuth et al., 1996). Likewise, mutation of the cor-responding Q582 in M2 of GluR (Q/R-site) modulates the ionic permeability and blockade properties (Hume et al., 1991; Mishina et al., 1991; Verdoorn et al., 1991; Dingledine et al., 1992; Jonas and Burnashev, 1995; Burnashev et al., 1996). Substitutions of L577 in M2 of GluR1 (L-site) markedly modify the selectivity to divalent cations (Ferrer-Montiel et al., 1996). Furthermore, GluR1 mutant channels carrying a tryptophan in the L-site and an asparagine or theronine at the Q-site exhibited sensitivity to block by phencyclidine (PCP) and dizolcipine (MK-801), two uncompetitive NMDA antagonists (Ferrer-Montiel et al., 1995). The sensitivity to NMDA receptor channel blockers and the high Ca^{2+}-selectivity suggest that the GluR1 double mutants L577W/Q582N and L577W/Q582T may mimic the pore lining of the NMDA receptor. In this paper, we pursue the characterization of this GluR1 mutant channels, hereafter denoted as the GluR1 L577W/Q582N and L577W/Q582T channels, and show that these are blocked by an array of structurally diverse open channel blockers of the NMDA receptor in a voltage dependent manner. Collectively, our results substantiate the structural kinship between the permeation pathways of homomeric GluR1 L577W/Q582N or GluR1 L577W/Q582T and heteromeric NMDAR channels.

2. Materials and methods

All the drugs used were purchased from Research Biochemicals International (RBI, Natick, MA).

All the procedures have been described in detail elsewhere (Ferrer-Montiel and Montal, 1994; Ferrer-Montiel et al., 1995; Ferrer-Montiel and Montal, 1996; Ferrer-Montiel et al., 1996) and are followed accordingly, unless otherwise indicated.

2.1. Site-directed mutagenesis, cRNA preparation and microinjection into Xenopus oocytes

GluR1 is a cDNA clone encoding a functional AMPA receptor from human brain (Sun et al., 1992). NR1 (Planells-Cases et al., 1993) and NR2A (Le

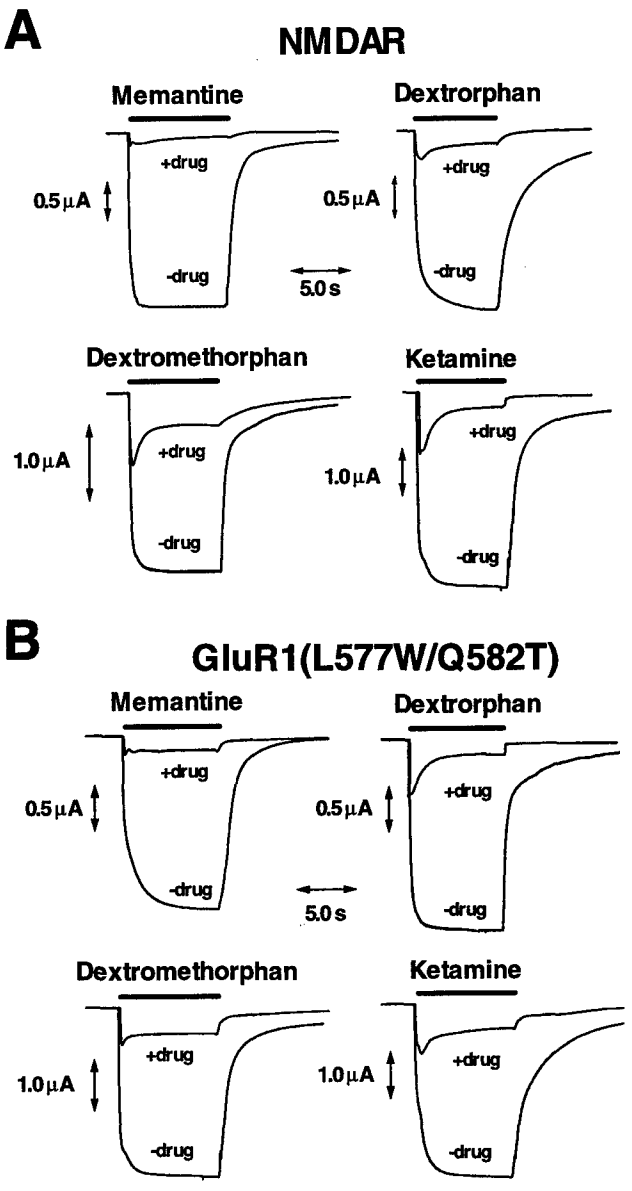

Fig. 2. The channel activity of the GluR1 L577W/Q582T receptor is inhibited by NMDAR channel blockers. Blockade of the NMDA receptor (A) and the GluR1 L577W/Q582T double mutant (B) by the uncompetitive NMDA antagonists memantine, dextrorphan, dextromethorphan and ketamine. NMDA receptors were activated by 100 μM L-glu/20 μM gly and GluR1 channels by 500 μM KA in Ba^{2+}-Ringer's supplemented with 100 μM niflumic and flufenamic acids. Evoked currents, indicated as downward deflections, were recorded at $V_h = -80$ mV in the absence (−drug) and presence (+drug) of the inhibitors. GluR1 L577W/Q582T double mutant and NMDA receptors were blocked by 100 and 10 μM blocker, respectively. Agonist was applied for the duration indicated by the horizontal bars.

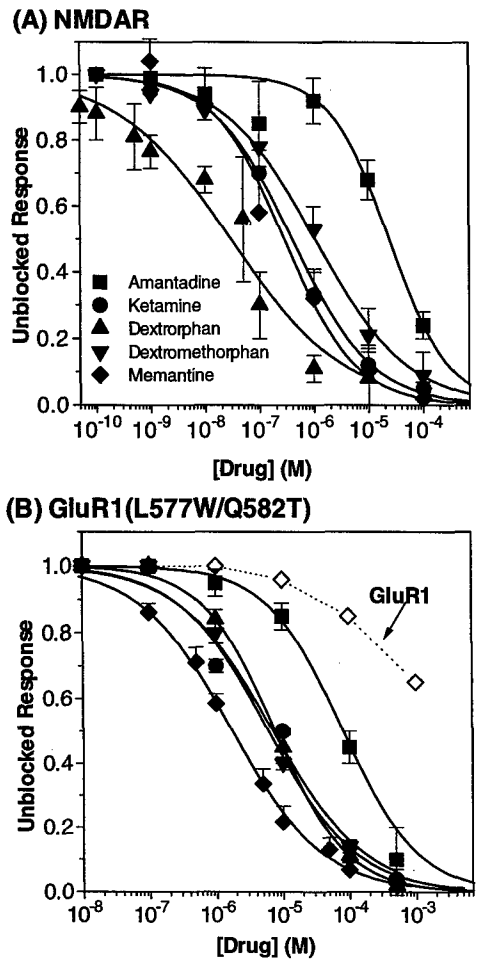

Fig. 3. Open channel blockers of the NMDA receptor block the GluR1 L577W/Q582T channel with high affinity. Dose–response curves for blockade of NMDAR (A) or GluR1 mutant receptor (B) by uncompetitive NMDA antagonists. Agonist-elicited responses, measured at the end of a 8 s pulse, were normalized with respect to those obtained in the absence of channel blocker. Current responses from the NMDAR were evoked by 100 μM L-glu/20 μM gly and from the GluR1 L577W/Q582T channel by 500 μM KA. Ionic currents were recorded at $V_h = -80$ mV in Ba^{2+}-Ringer's (supplemented with 100 μM niflumic and flufenamic acids). Solid lines depict the best fit to a Hill equation (Eq. (1)). Open symbols joined by dotted line are corresponding values for wild type GluR1 channels blocked by memantine. The IC_{50} values and Hill coefficients are listed in Table 1. Values are given as mean ± S.E.M. with $n = 4$.

Bourdelles et al., 1994) (kindly provided by Dr Paul Whiting) are cDNA clones encoding two subunits of an NMDA receptor from human brain. cRNA (5–10 ng) microinjection into oocytes, and site-directed mutagenesis were as described (Ferrer-Montiel and Montal, 1994; Ferrer-Montiel et al., 1995). GluR1 and NR1 mutants were generated as described (Ferrer-Montiel et al., 1995). Recombinant NMDA receptors were obtained by co-injection of NR1 or NR1(N598Q) or NR1(W593L/N598Q) and NR2A subunits at a ratio 1:3 (w/w).

2.2. Electrophysiological characterization of receptor mutants in Xenopus oocytes

Whole-cell currents were recorded with a conventional two-microelectrode voltage-clamp amplifier at 20°C (Ferrer-Montiel and Montal, 1994). All electrophysiological studies were performed in Ba^{2+}-Ringer's solution (in mM: 10 *N*-tris[hydroxymethyl]methyl-2-aminoethanesulfonic acid pH 7.4, 115 NaCl, 2.8 KCl, 1.8 $BaCl_2$, 0.1 flufenamic acid, 0.1 niflumic acid). GluR1 channels were activated by application of 500 μM KA in absence or presence of increasing concentrations of channel blockers at a holding potential (V_h) of −80 mV. NMDAR channels were activated with 100 μM L-glutamate (L-glu) supplemented with 20 μM glycine. Responses were normalized with respect to that evoked in absence of channel blockers. Dose-response curves were fitted to a Hill equation (Ferrer-Montiel et al., 1995):

$$\frac{I}{I_{max}} = \frac{1}{1 + \left(\frac{[\text{blocker}]}{IC_{50}}\right)^{n_H}} \quad (1)$$

where IC_{50} denotes the channel blocker concentration that inhibits half of the response obtained in its absence (I_{max}) and, n_H denotes the Hill coefficient which is an estimate of the number of drug binding sites (Levitzki, 1984). Experimental data were fitted to the Hill equation with a nonlinear least-squares regression algorithm using MicroCal ORIGIN version 2.8 (Microcal, Amherst).

I–V characteristics were recorded using a ramp protocol (pClamp 5.5 (Foster City, CA)): oocytes were depolarized from −80 mV to 40 mV (NMDAR) or from −100 mV to 20 mV (GluR1 L577W/Q582N and L577W/Q582T) in 2 s (60 mV/s). Leak currents were measured in the absence of agonist in the external bath medium and subtracted from the ionic current recorded in the presence of the ligand. To study the voltage dependence of channel block, the IC_{50} values for most of the blockers were determined at different potentials (-90 mV $\leq V \leq -40$ mV in increments of 5 mV) and plotted as a function of the applied voltage. For dextrorphan, which showed slow dissociation kinetics, IC_{50} values were obtained using a stepwise voltage protocol.

3. Results

3.1. GluR1 channels incorporating a tryptophan at the L-site and an asparagine or a threonine at the Q-site emulate the sensitivity profile of the NMDA receptor to open channel blockers

GluR1 L577W/Q582N and L577W/Q582T channels display high sensitivity to PCP and MK-801 blockade suggesting the presence of a binding site for NMDAR

Table 1
Channel blockade of GluR and NMDAR channels by uncompetitive NMDA antagonists

Species	Memantine		Ketamine		Amantadine		Dextro-methorphan		Dextrorphan	
	IC_{50} (μM)	n_H	IC_{50} (μM)	n_H	IC_{50} (μM)	n_H	IC_{50} (μM)	n_H	IC_{50} (μM)	n_H
NMDAR	0.3 ± 0.1	0.6 ± 0.1	0.4 ± 0.1	0.7 ± 0.1	24 ± 5	0.8 ± 0.1	1.0 ± 0.4	0.7 ± 0.1	0.03 ± 0.01	0.4 ± 0.1
N598Q	6.5 ± 2.0	0.7 ± 0.1	12 ± 4	0.8 ± 0.1	>250	—	34 ± 20	0.6 ± 0.1	26 ± 5	0.6 ± 0.1
W593L/N598Q	10 ± 2	0.7 ± 0.1	35 ± 20	0.7 ± 0.1	>250	—	43 ± 18	0.7 ± 0.1	18 ± 7	0.5 ± 0.2
GluR1	>250	—	>250	—	NB	—	NB	—	NB	—
L577W/Q582N	13 ± 2	0.6 ± 0.1	29 ± 1	1.0 ± 0.1	260 ± 80	0.7 ± 0.1	19 ± 1	0.8 ± 0.1	14 ± 1	0.7 ± 0.1
L577W/Q582T	1.3 ± 0.1	0.7 ± 0.1	7 ± 1	0.6 ± 0.1	50 ± 10	0.6 ± 0.1	8 ± 1	0.7 ± 0.1	8 ± 2	0.6 ± 0.1

IC_{50} is the concentration of drug necessary to block half of the maximal response elicited by 100 μM L-glu/20 μM gly (NMDAR) or 500 μM kainate (GluR1) at −80 mV. IC_{50} and n_H were determined from the best fit of the experimental data to a Hill equation (Eq. (1)). Values are given as mean ± S.E.M., with $n = 4$.
NB: not blocked.

open channel blockers (Ferrer-Montiel et al., 1995). To define the properties of this blocker binding site, we examined the sensitivity of both GluR1 L577W/Q582N and L577W/Q582T channels to an array of structurally diverse NMDAR open channel blockers (Fig. 1(B)). At 10 μM, memantine, dextrorphan, dextromethorphan and ketamine blocked ≥ 90% of agonist-evoked current in NMDAR and GluR1 L577W/Q582T channels (Fig. 2). Dose-response curves show that the array of drugs assayed blocked NMDAR channels with IC_{50} values ranging from 0.03 to 24 μM (Fig. 3 and Table 1), and GluR1 L577W/Q582T (Fig. 3 and Table 1) and GluR1 L577W/Q582N (Table 1) channels with efficacies ranging from 1.0 to 265 μM. The Hill coefficient for either GluR1 L577W/Q582N or GluR1 L577W/Q582T and for NMDAR channels was ≤ 1.0, consistent with the occurrence of a single binding site (Table 1). Noteworthy, the GluR1 double mutant bearing an asparagine in place of a threonine at the Q-site, L577W/Q582N, exhibited 2–10-fold lower sensitivity to open channel blockers (Table 1). This finding suggests that blocker binding involves hydrogen bond formation between the n_H-group of the drug and the polar side chain at the Q-site. Thus, an aromatic residue at position 577 and a hydroxyl-containing amino acid at position 582 in M2 appear to be sufficient to create GluR1 channels that are sensitive to blockade by chemically diverse, uncompetitive NMDA antagonists, with apparent affinities approaching those characteristic of the NMDA receptor.

To further examine the involvement of these two positions on M2 in drug binding, we analyzed the consequences of the corresponding mutations in the M2 segment of the NR1 subunit (Table 1). Mutations at N598 reduced the affinity by ≥ 40-fold indicating that the N-site is critical for drug binding, while the W-site, W593, modulates blocker sensitivity. Note that both positions contributed to form the binding pocket for ketamine (Table 1), which is structurally related to PCP (Fig. 1(B)) (Ferrer-Montiel et al., 1995). These data indicate that the N-site is a structural determinant of channel blockade by the wide array of drugs tested.

3.2. The voltage-dependent blockade of GluR1 L577W/Q582N, GluR1 L577W/Q582T and NMDAR channels locates the blocker binding site at a similar 'electrical depth' across the transmembrane pore

Open channel blockers of the NMDA receptor exert their action in a voltage-dependent manner (Huettner and Bean, 1988; Chen et al., 1992). This property, together with their interaction with residue at the N-site (and Q-site), make these drugs valuable probes to determine the position of the receptor site within the membrane electrostatic field. Thus, we next compared the voltage-dependent drug blockade of NMDAR and GluR1 L577W/Q582T channels (Fig. 4). To illustrate this set of experiments, we focus on the voltage-dependent blockade exerted by memantine. As shown, the drug reduced the glutamate or kainate-activated currents only at negative membrane potential (Fig. 4(A) and (B)). This is evidenced in Fig. 4(C) and (D), where IC_{50} of memantine binding is plotted as a function of the membrane potential. As the oocyte membrane is hyperpolarized, the blocker affinity increases, indicating that the blocker moves into the pore electric field. Under these conditions, the fraction of unblocked response, $f(V_m) = I_{blocker}/I_{control}$, is a function of the concentration of blocking drug, [blocker], and the applied transmembrane voltage, V_m:

$$f(V_m) = \frac{IC_{50}(V_m)}{[\text{blocker}] + IC_{50}(V_m)} \quad (2)$$

where IC_{50} (V_m) is the blocker's half-maximal blockade at the transmembrane voltage V_m. According to the Woodhull model (Woodhull, 1973), the IC_{50} of a molecule with valence z binding to a site within the membrane electric field is described by the relation (Woodhull, 1973; Ascher and Nowak, 1988; Zarei and Dani, 1995; Kuner and Schoepfer, 1996; Premkumar and Auerbach, 1996b):

$$IC_{50}(V_m) = IC_{50}(0\ mV) \times \exp\left(\frac{z\delta V_m F}{RT}\right) \quad (3)$$

where IC_{50} (0 mV) is the half-maximal block at $V_m = 0$ mV, δ is the location of the energy barrier for block (i.e. the blocker binding site) expressed as a fraction of the electrostatic field gradient sensed by the blocking site (Woodhull, 1973). RT/F is a constant of value 25.3 mV at 20°C. Considering the occurrence of a single binding site within the pore electric field and a negligible multiple ion occupancy of this site, Eq. (3) may be used to estimate the electrical distance of the drug binding site from the mouth of the channel (Woodhull, 1973; Mayer et al., 1984; Ascher and Nowak, 1988; Zarei and Dani, 1995; Kuner and Schoepfer, 1996; Kupper et al., 1996; Premkumar and Auerbach, 1996b). Occurrence of a single binding site is supported experimentally by a Hill coefficient, $n_H \leq 1$ (Table 1), and the absence of significant multiple ion occupancy at negative membrane potentials is evidenced by the insensitivity of the apparent blocker affinity to increments in the extracellular concentration of permeant divalent cations (data not shown). As illustrated for NMDAR channels (Fig. 4(C)), the voltage dependence of IC_{50} for the memantine block, in the voltage range of −80 to −40 mV, is well described by Eq. (3), with $\delta \sim 0.77$ and IC_{50} (0 mV) ~3.1 μM (Fig. 4(C), Table 2). The electrical distance for memantine binding is consistent with that estimated for Mg^{2+}, which also binds to the N-site (Ascher and Nowak, 1988; Burnashev et al., 1992b; Kuner and Schoepfer, 1996; Kupper et al., 1996; Premkumar and Auerbach, 1996b; Sharma and Stevens, 1996). Hence, this analysis indicates that memantine traverses partway through the membrane electrostatic field to reach its binding site.

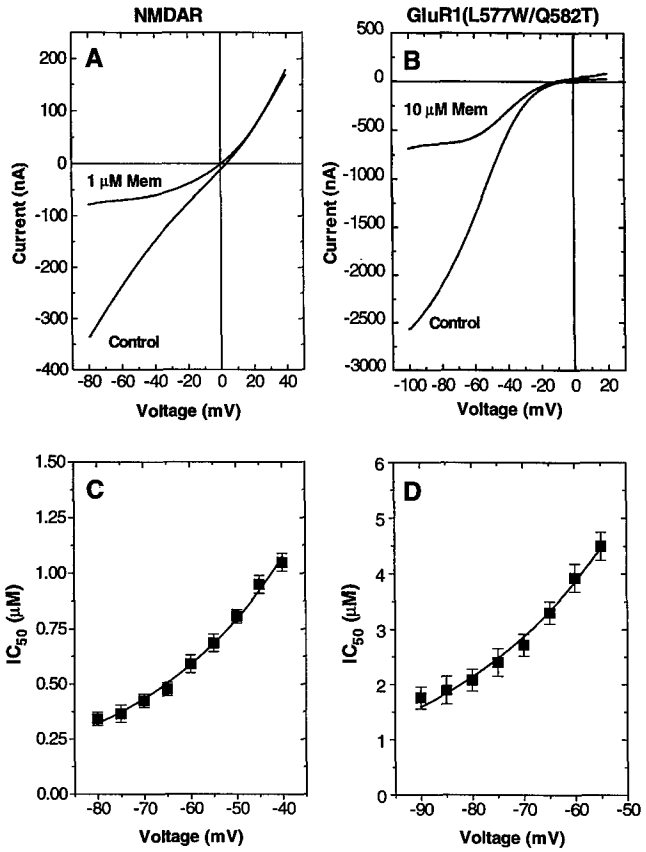

Fig. 4. GluR1 mutant channels mimic the voltage-dependence of the memantine block on NMDAR. Voltage dependent blockade by memantine of the NMDA receptor (A) and the GluR1 L577W/Q582T double mutant (B). Current–voltage characteristics of responses elicited by 100 μM L-glu/20 μM gly (NMDA receptor) or 500 μM KA (GluR1 mutant) in the absence (control) or presence (Mem) of 1 μM or 10 μM memantine, respectively. Oocytes were held at −80 mV (or −100 mV for the GluR1 L577W/Q582T mutant) and depolarized to 40 mV (or 20 mV for the GluR1 L577W/Q582T mutant) in 2 s using a computer-controlled ramp protocol (Pclamp5.5). Leak currents were obtained in the absence of agonist and subtracted from the elicited ionic currents. Traces are representative of a minimum of three oocytes. (C and D) IC_{50} values of memantine blockade plotted as a function of the applied transmembrane voltage. Solid lines depict the theoretical fit to the Woodhull model with a single-site, Eq. (3). The parameters of the best fit are reported in Table 2.

The GluR1 L577W/Q582T channel (Fig. 4(B) and (D)) and GluR1 L577W/Q582N (data not shown) fairly reproduced the voltage-dependent blockade exerted by memantine on NMDA receptors (Fig. 4(A) and (C)): memantine blocked the KA-evoked current exclusively at negative membrane potentials. As illustrated in Fig. 4(D), the voltage dependence of IC_{50} in the voltage range of −90 to −50 mV was well-fitted by the Woodhull relation with $\delta \sim 0.75$ and IC_{50} (0 mV) ~15.4 mM (Table 2). More depolarized potentials produced a significant deviation of the experimental data from the Woodhull model, presumably arising from the strong inward rectification exhibited by this GluR1 mutant channel. The similarity of the voltage-dependent blockade of GluR1 L577W/Q582T and NMDAR channels was substantiated by the data obtained for dextrorphan, and dextromethorphan (Table 2). Intriguingly, ketamine blockade of the GluR1 L577W/Q582T channel displayed weaker voltage dependence than that exhibited by the NMDAR suggesting the involvement of other NMDAR residues and/or subunits in ketamine binding. Taken together, these data suggest that GluR1 mutant receptor fairly approximates the voltage-dependent properties of open channel blockers on NMDA receptors. Because these drugs presumably hydrogen bond with residues at the N-site and Q-site, these results imply that this key structural determinant is located deep into the pore electrostatic field.

Table 2
Electrical distances (δ) of the blockade of NMDAR and GluR1 577W/Q582T channels by uncompetitive NMDA antagonists

Drug	NMDAR		GluR1 (L577W/Q582T)	
	δ	IC_{50} (0 mV) (μM)	δ	IC_{50} (0 mV) (μM)
Memantine	0.77 ± 0.14	3.1 ± 1.6	0.75 ± 0.02	15.4 ± 4.6
Dextrorphan	0.51 ± 0.06	0.46 ± 0.07	0.68 ± 0.05	47.9 ± 11.9
Dextromethorphan	0.60 ± 0.09	4.8 ± 3.7	0.56 ± 0.06	22.7 ± 5.6
Ketamine	0.77 ± 0.13	4.9 ± 1.7	0.24 ± 0.02	46.9 ± 10.9

Electrical distance (δ) was obtained using the Woodhull model to describe the voltage-dependent drug blockade. IC_{50} (0 mV) is the half-maximal block at $V_m = 0$ mV (Eq. (3)).

4. Discussion

4.1. The GluR1 L577W/Q582N and L577W/Q582T channels emulate the pore properties of the heteromeric NMDA receptor

Our findings indicate that two sites in the M2 of GluR1 are critical to create channels that resemble the pore properties of the NMDA receptor. As summarized in Table 3, the GluR1 L577W/Q582N and L577W/Q582T channels are blocked by PCP, MK-801, memantine, ketamine, amantadine, dextromethorphan, and dextrorphan with apparent affinities that approximate those exhibited by the heteromeric NMDA receptor. The voltage-dependence of drug blockade is also recapitulated by the GluR1 L577W/Q582T channel (Fig. 4, Table 2). The structural diversity of these drugs, in conjunction with their similar blockade properties on GluR1 mutant and NMDAR channels, suggest that the permeation pathways of both receptors may be similar with just two mutations in M2 required to create GluR1 receptors exhibiting NMDA receptor-like pore properties.

The overall topology of the membrane domain of glutamate receptors, inferred from accessibility analysis of *N*-glycosylation- or protease-sites used as specific tags, suggests that M2 is a re-entrant loop surrounded by the transmembrane segments M1, M3 and M4 (Hollmann et al., 1994; Taverna et al., 1994; Bennett and Dingledine, 1995; Wo and Oswald, 1995; Wo et al., 1995; Sutcliffe et al., 1996). A proposed secondary structure of M2 of NR1 and NR2A, consists of an ascending α-helix at the N-terminal half and a descending extended structure at the C-terminal half (Kuner et

Table 3
Pore properties of NMDAR, GluR1 L577W/Q582N and L577W/Q582T channels

	NMDAR	GluR1 (L577W/Q582N)	GluR1 (L577W/Q582T)
(a) Permeation[a]			
Monovalent cations	1.2	1.3	1.1
Divalent cations	7.0	5.0	4.5
(b) $I-V$ relationship	Linear	Linear	Inwardly rectifying
(c) Channel blockade[b]			
Phencyclidine (PCP)	$2.3 \cdot 10^{-8}$ M	$3.4 \cdot 10^{-6}$ M	$2.5 \cdot 10^{-6}$ M
MK-801	$1.8 \cdot 10^{-8}$ M	$3.8 \cdot 10^{-5}$ M	$1.6 \cdot 10^{-5}$ M
Memantine	$0.3 \cdot 10^{-6}$ M	$1.3 \cdot 10^{-5}$ M	$1.3 \cdot 10^{-6}$ M
Amantadine	$2.4 \cdot 10^{-5}$ M	$26.0 \cdot 10^{-5}$ M	$5.0 \cdot 10^{-5}$ M
Ketamine	$0.4 \cdot 10^{-6}$ M	$29.0 \cdot 10^{-6}$ M	$7.0 \cdot 10^{-6}$ M
Dextrorphan	$3.0 \cdot 10^{-8}$ M	$14.0 \cdot 10^{-6}$ M	$8.0 \cdot 10^{-6}$ M
Dextromethorphan	$1.0 \cdot 10^{-6}$ M	$19.0 \cdot 10^{-6}$ M	$8.0 \cdot 10^{-6}$ M
Extracellular Ca^{2+}	$1.7 \cdot 10^{-4}$ M	$1.5 \cdot 10^{-3}$ M	$>1 \cdot 10^{-2}$ M
Extracellular Mg^{2+}	$1.5 \cdot 10^{-5}$ M	$1.0 \cdot 10^{-3}$ M	$2.0 \cdot 10^{-3}$ M
(d) Blocker binding site[c]	~0.65	~0.65	~0.65
(e) Subunit stoichiometry	Pentameric[d]	Pentameric[e]	Pentameric[e]
(f) Oligomeric structure	Heteromeric	Homomeric	Homomeric

[a] Relative permeabilities to monovalent (P_K/P_{Na}) and divalent (P_{Ca}/P_{Na}) cations, taken from Ferrer-Montiel et al. (1996).
[b] Concentration at which the drug and/or cations inhibited half of the maximal agonist-activated current.
[c] Fraction of the electrostatic field gradient across the ionic pore (Table 2).
[d] Value taken from Premkumar and Auerbach (1996a).
[e] Value taken from Ferrer-Montiel and Montal (1996).

al., 1996). The N-site is positioned at the middle of the turn connecting both M2 stretches, a key location to control the permeation properties in accord with the narrowest region of the pore (Wollmuth et al., 1996). This location appears consistent with results showing that the N-site of NR1 is a key determinant of the high Ca^{2+}-permeability and drug sensitivity of the NMDA receptor (Mori et al., 1992; Burnashev et al., 1992b; Sakurada et al., 1993). The identification of the Mg^{2+}-binding site with a $\delta \sim 0.6–0.7$, locates the N-site deep into the pore suggesting that the M2 loops around halfway through the lipid bilayer (Mayer et al., 1984; Mayer and Westbrook, 1987; Ascher and Nowak, 1988; Kuner and Schoepfer, 1996; Kupper et al., 1996; Premkumar and Auerbach, 1996b). Our results are compatible with a deep location of the N-site in NMDA receptors and the Q-site in GluR1, as evidenced by the comparable $\delta \sim 0.65$ of the open channel blocker binding site, which is specified by the residue at this position (Table 1).

The role of the L-site appears more difficult to reconcile with current models of the pore lining (Fig. 1(A)). The involvement of the L-site in pore blockade by uncompetitive NMDA antagonists and its contribution to specify Ca^{2+}-selectivity on the GluR1 mutant channels suggest that this position points into the channel lumen. Topological models place the L-site at the loop of M2, consistent with its role in pore properties (Sutcliffe et al., 1996). This site, however, was not accessible to the sulphydryl-specific probes used in the SCAM analysis, implying a location on the hydrophobic surface of the proposed α-helix, rather than exposed to the pore lumen (Kuner et al., 1996). It may be argued that the L-site exerts its functional effects via an steric mechanism: An aromatic residue at this position may expand the pore size. Such a mechanism could account for the loss of sensitivity to blockade by external divalent cations and the increased Ca^{2+}-permeability of mutant channels bearing an aromatic residue at this site (Ferrer-Montiel et al., 1996). Although the SCAM approach may be useful to identify residues exposed to the luminal face of the channel, the inferred secondary structures should be interpreted with caution due to technical limitations, especially in the absence of protein structure.

Acknowledgements

A.V.F.M. and J.M.M. contributed equally to this work. We thank Paul Whiting for providing the NR2A subunit cDNA. This work was supported by grants from the US Army Medical Research and Materiel Command (DAMD 17-93-C-3100) and from the National Institutes of Health (GM-49711) (to M.M.), and a Postdoctoral Fellowship from the Ministerio de Educacion y Ciencia, Spain (to J.M.M.).

References

Ascher, P., Nowak, L., 1988. The role of divalent cations in the N-methyl-D-aspartate responses of mouse central neurons in culture. J. Physiol. 399, 247–266.

Bennett, J.A., Dingledine, R., 1995. Topology profile for a glutamate receptor: three transmembrane domains and a channel-lining reentrant membrane loop. Neuron 14, 373–384.

Blanpied, T.A., Boeckman, F.A., Aizenman, E., Johnson, J.W., 1997. Trapping channel block of NMDA-activated responses by amantadine and memantine. J. Neurophysiol. 77, 309–323.

Bresink, I., Benke, T.A., Collett, V.J., et al., 1996. Effects of memantine on recombinant rat NMDA receptors expressed in HEK293 cells. Br. J. Pharmacol. 119, 195–204.

Burnashev, N., Monyer, H., Seeburg, P.H., Sakmann, B., 1992a. Divalent ion permeability of AMPA receptor channels is dominated by the edited form of a single subunit. Neuron 8, 189–198.

Burnashev, N., Schoepfer, R., Monyer, H., et al., 1992b. Control by asparagine residues of calcium permeability and magnesium blockade in the NMDA receptor. Science 257, 1415–1419.

Burnashev, N., Villarroel, A., Sakmann, B., 1996. Dimensions and ion selectivity of recombinant AMPA and kainate receptor channels and their dependence on Q/R site residues. J. Physiol. 496.1, 165–173.

Chen, H.-S.V., Pellegrine, J.W., Aggarwal, S.K., et al., 1992. Open channel block of N-methyl-D-aspartate (NMDA) responses by memantine: therapeutic advantages against NMDA receptor-mediated neurotoxicity. J. Neurosci. 12, 4427–4436.

Choi, D.W., Rothmann, S.M., 1990. The role of glutamate neurotoxicity in hypoxic ischemic neuronal death. Annu. Rev. Neurosci. 13, 171–182.

Choi, D.W., 1992. Bench to bedside the glutamate connection. Science 258, 241–243.

Collingridge, G.L., Lester, R.A.J., 1989. Excitatory amino acid receptors in the vertebrate central nervous system. Pharmacol. Rev. 40, 143–210.

Dingledine, R., Hume, R.I., Heinemann, S.F., 1992. Structural determinants of barium permeation and rectification in non-NMDA receptor channels. J. Neurosci. 12, 4080–4087.

Ferrer-Montiel, A.V., Montal, M., 1994. Structure-function relations in ligand–gated ion channels: Reconstitution in lipid bilayers and heterologous expression in Xenopus oocytes. Methods: A Companion to Methods in Enzymology 6, 60–69.

Ferrer-Montiel, A.V., Sun, W., Montal, M., 1995. Molecular design of the N-methyl-D-aspartate receptor binding site for phencyclidine and dizolcipine. Proc. Natl. Acad. Sci. USA 92, 8021–8025.

Ferrer-Montiel, A.V., Montal, M., 1996. Pentameric subunit stoichiometry of a neuronal glutamate receptor. Proc. Natl. Acad. Sci. USA 93, 2741–2744.

Ferrer-Montiel, A.V., Sun, W., Montal, M., 1996. A single tryptophan on M2 of glutamate receptor channels confers high permeability to divalent cations. Biophys J. 71, 749–758.

Herrling, P.L., 1994. Clinical implications of NMDA receptors. In: Collingridge, G.L. (Ed.), The NMDA Receptor. IRL Press at Oxford, University Press, Oxford, pp. 376–394.

Hollmann, M., Heinemann, S.F., 1994. Cloned glutamate receptors. Annu. Rev. Neurosci. 17, 31–108.

Hollmann, M., Maron, C., Heinemann, S.F., 1994. *N*-glycosylation site tagging suggests a three transmembrane domain topology for the glutamate receptor GluR1. Neuron 13, 1331–1343.

Huettner, J.E., Bean, B.P., 1988. Block of N-methyl-D-aspartate-activated current by the anticonvulsant MK-801: selective binding to open channels. Proc. Natl. Acad. Sci. USA 85, 1307–1311.

Hume, R.I., Dingledine, R., Heinemann, S.F., 1991. Identification of a site in glutamate receptor subunits that controls calcium permeability. Science 253, 1028–1031.

Iino, M., Ozawa, S., Tsuzuki, K., 1990. Permeation of calcium through excitatory amino acid receptor channels in cultured rat hippocampal neurons. J. Physiol. 424, 151–165.

Iversen, L.L., Kemp, J.A., 1994. Non-competitive NMDA antagonists as drugs. In: Collingridge, G.L. (Ed.), The NMDA Receptor. IRL Press at Oxford, University Press, Oxford, pp. 468–486.

Jahr, C.E., Stevens, C.F., 1993. Calcium permeability of the N-methyl-D-aspartate receptor channel in hippocampal neurons in culture. Proc. Natl. Acad. Sci. USA 90, 11573–11577.

Jessell, T.M., Kandel, E.R., 1993. Synaptic transmission: a bidirectional and self-modifiable form of cell–cell communication. Cell 72/Neuron 10 (Suppl), 1–30.

Jonas, P., Burnashev, N., 1995. Molecular mechanisms controlling calcium entry through AMPA-type glutamate receptor channels. Neuron 15, 987–990.

Kawajiri, S., Dingledine, R., 1993. Multiple structural determinants of voltage-dependent magnesium block in recombinant NMDA receptors. Neuropharmacol. 32, 1203–1211.

Koroshetz, W.J., Moskowitz, M.A., 1996. Emerging treatments for stroke in humans. Trends Pharmacol. Sci. 17, 227–233.

Kuner, T., Wollmuth, L.P., Karlin, A., Seeburg, P.H., Sakmann, B., 1996. Structure of the NMDA receptor channel M2 segment inferred from the accessibility of substituted cysteines. Neuron 17, 343–352.

Kuner, T., Schoepfer, R., 1996. Multiple structural elements determine subunit specificity of Mg^{2+}-block in NMDA receptor channels. J. Neurosci. 16, 3549–3558.

Kupper, J., Ascher, P., Neyton, J., 1996. Probing the pore region of recombinant N-methyl-D-aspartate using external and internal magnesium block. Proc. Natl. Acad. Sci. USA 93, 8648–8653.

Le Bourdelles, B., Wafford, K.A., Kemp, J.A., et al., 1994. Cloning functional expression and pharmacological characterisation of human cDNAs encoding NMDA receptor NR1 and NR2A subunits. J. Neurochem. 62, 2091–2098.

Levitzki, A., 1984. Receptors: A Quantitative Approach. Benjamin Cummings, Menlo Park, CA, pp. 1–142.

Mayer, M.L., Westbrook, G.L., Guthrie, P.B., 1984. Voltage-dependent block by Mg^{2+} of NMDA responses in spinal cord neurons. Nature 309, 261–263.

Mayer, M.L., Westbrook, G.L., 1987. Permeation and block of N-methyl-D-aspartic acid receptor channels by divalent cations in mouse cultured central neurons. J. Physiol. 394, 501–527.

McBurney, R.W., 1997. Development of the NMDA ion-channel blocker, aptiganel hydrochloride as a neuroprotective agent for acute CNS injury. Int. Rev. Neurobiol. 40, 173–195.

Mishina, M., Sakimura, K., Mori, H., et al., 1991. A single amino acid residue determines the Ca^{2+}-permeability of AMPA-selective glutamate receptor channels. Biochem. Biophys. Res. Commun. 180, 813–821.

Montal, M., 1995. Design of molecular function: Channels of communication. Annu. Rev. Biophys. Biomol. Struct. 24, 31–57.

Mori, H., Masaki, H., Yamakura, T., Mishina, M., 1992. Identification by mutagenesis of a Mg^{2+}-block site of the NMDA receptor channel. Nature 358, 673–675.

Nakanishi, S., 1992. Molecular diversity of glutamate receptors and implications for brain function. Science 258, 597–603.

Nakanishi, S., Masu, M., 1994. Molecular diversity and functions of glutamate receptors. Annu. Rev. Biophys. Biomol. Struct. 23, 319–348.

Olney, J.W., 1990. Excitotoxic amino acid and neuropsychiatric disorders. Annu. Rev. Pharmacol. Toxicol. 30, 47–71.

Parsons, C.G., Gruner, R., Rozental, J., Millar, J., Lodge, D., 1993. Patch clamp studies on the kinetics and selectivity of *N*-methyl-D-aspartate receptor antagonism by memantine (1-amino-3-5-dimethyladamantan). Neuropharmacology 32, 1337–1350.

Parsons, C.G., Quack, G., Bresink, I., et al., 1995. Comparison of the potency kinetics and voltage-dependency of a series of uncompetitive NMDA receptor antagonists in vitro with anticonvulsive and motor impairment activity in vivo. Neuropharmacology 34, 1239–1258.

Planells-Cases, R., Sun, W., Ferrer-Montiel, A.V., Montal, M., 1993. Molecular cloning, functional expression and pharmacological characterization of an N-methyl-d-aspartate receptor subunit from human brain. Proc. Natl. Acad. Sci. USA 90, 5057–5061.

Premkumar, L.S., Auerbach, A., 1996. Stoichiometry of recombinant NMDA receptor channels. Abstract Soc. Neurosci. 22, 593, Abs # 237.8.

Premkumar, L.S., Auerbach, A., 1996b. Identification of a high affinity divalent cation binding site near the entrance of the NMDA receptor channel. Neuron 16, 869–880.

Sakurada, K., Masu, M., Nakanishi, S., 1993. Alteration of Ca^{2+}-permeability and sensitivity to Mg^{2+} and channel blockers by a single amino acid substitution in the N-methyl-D-aspartate receptor. J. Biol. Chem. 268, 410–415.

Schinder, A.F., Olson, E.C., Spitzer, N.C., Montal, M., 1996. Mitochondrial dysfunction is a primary event in glutamate excitotoxicity. J. Neurosci. 16, 6125–6133.

Sharma, G., Stevens, C.F., 1996. A mutation that alters magnesium block of N-methyl-D-aspartate receptor channels. Proc. Natl. Acad. Sci. USA 93, 14170–14175.

Stevens, C.F., 1993. Quantal release of neurotransmitter and long-term potentiation. Cell 72/Neuron 10 (Suppl), 55–63.

Sun, W., Ferrer-Montiel, A.V., Schinder, A.F., McPherson, J.P., Evans, G.A., Montal, M., 1992. Molecular cloning, chromosomal mapping and functional expression of human brain glutamate receptors. Proc. Natl. Acad. Sci. USA 89, 1443–1447.

Sutcliffe, M.J., Wo, G.Z., Oswald, R.E., 1996. Three-dimensional models of non-NMDA glutamate receptors. Biophys. J. 70, 1575–1589.

Taverna, F.A., Wang, L., McDonald, J.F., Hampson, D.R., 1994. A transmembrane model for an ionotropic glutamate receptor predicted on the basis of the location of asparagine-linked oligosaccharides. J. Biol. Chem. 269, 14159–14164.

Verdoorn, T.A., Burnashev, N., Monyer, H., Seeburg, P.H., Sakmann, B., 1991. Structural determinants of ion flow through recombinant glutamate receptor channels. Science 252, 1715–1718.

Wo, Z.G., Oswald, R.E., 1995. Unraveling the modular design of glutamate-gated ion channels. Trends in Neurosci. 18, 161–168.

Wo, Z.G., Bian, Z.C., Oswald, R.E., 1995. ASN-265 of frog kainate binding protein is a functional glycosylation site. Implications for the transmembrane topology of glutamate receptors. FEBS Lett. 368, 230–234.

Wollmuth, L.P., Kuner, T., Seeburg, P.H., Sakmann, B., 1996. Differential contribution of the NR1 NR2A-subunits to the selectivity filter of recombinant NMDA receptor channels. J. Physiol 491, 779–797.

Woodhull, A.M., 1973. Ionic blockage of sodium channels in nerve. J. Gen. Physiol. 61, 687–708.

Zarei, M.M., Dani, J.A., 1994. Ionic permeability characteristics of the N-methyl-D-aspartate receptor channel. J. Gen. Physiol. 103, 231–248.

Zarei, M.M., Dani, J.A., 1995. Structural basis for explaining open-channel blockade of the NMDA receptor. J. Neurosci. 15, 1446–1454.

FEBS Letters 429 (1998) 78–82 FEBS 20336

Structural stabilization of botulinum neurotoxins by tyrosine phosphorylation

José A. Encinar[a], Asia Fernández[a], José A. Ferragut[a], José M. González-Ros[a], Bibhuti R. DasGupta[b], Mauricio Montal[c], Antonio Ferrer-Montiel[c,*]

[a]*Department of Neurochemistry, University Miguel Hernández, Cl Monóvar s/n (Polígono de Carrús), E-03206 Elche (Alicante), Spain*
[b]*University of Wisconsin, Madison, WI 53706, USA*
[c]*Department of Biology, University of California at San Diego, La Jolla, CA 92093-0366, USA*

Received 20 March 1998; revised version received 28 April 1998

Abstract Tyrosine phosphorylation of botulinum neurotoxins augments their proteolytic activity and thermal stability, suggesting a substantial modification of the global protein conformation. We used Fourier-transform infrared (FTIR) spectroscopy to study changes of secondary structure and thermostability of tyrosine phosphorylated botulinum neurotoxins A (BoNT A) and E (BoNT E). Changes in the conformationally-sensitive amide I band upon phosphorylation indicated an increase of the α-helical content with a concomitant decrease of less ordered structures such as turns and random coils, and without changes in β-sheet content. These changes in secondary structure were accompanied by an increase in the residual amide II absorbance band remaining upon H-D exchange, consistent with a tighter packing of the phosphorylated proteins. FTIR and differential scanning calorimetry (DSC) analyses of the denaturation process show that phosphorylated neurotoxins denature at temperatures higher than those required by non-phosphorylated species. These findings indicate that tyrosine phosphorylation induced a transition to higher order and that the more compact structure presumably imparts to the phosphorylated neurotoxins the higher catalytic activity and thermostability.

Key words: Protein structure; Protein folding; Metalloprotease; Fourier transform infrared; Exocytosis

1. Introduction

Botulinum neurotoxin (BoNT), considered the most potent neurotoxin and the sole cause of the neuroparalytic disease botulism, blocks acetylcholine release at the neuromuscular junction and thus produces flaccid paralysis in skeletal muscles [1,2]. Because of the extremely selective mode of action, inhibition of neurotransmitter release, BoNT is now an important therapeutic agent in the treatment of several neurological disorders associated with uncontrolled muscular contractions or spasms [3].

BoNT (serotypes A–G) is produced by the bacterium *Clostridium botulinum* as a single chain of 150 kDa which undergoes proteolytic cleavage yielding a fully active dichain protein composed of a 100-kDa heavy chain (HC) and a 50-kDa light chain (LC), linked by a disulfide bond. The neurotoxin first binds to a specific neuronal surface receptor, is internalized by receptor-mediated endocytosis, and the LC is then translocated to the cytosol, where it acts [1,4]. The LCs are Zn^{2+}-dependent metalloproteases that selectively cleave proteins involved in targeting and fusion of presynaptic vesicles with the plasma membrane [1,4–6]. The result is induction of nerve dysfunction by inhibiting Ca^{2+}-evoked neurotransmitter release.

The long lasting paralytic effects exerted by BoNT in botulism or in its therapeutic application suggest that these proteins are highly stable inside neurons at 37°C. This stability contrasts with the in vitro thermolability of pure BoNT implying structural difference(s) between the in vivo and in vitro forms [7,8]. Our discovery that tyrosine phosphorylation of BoNTs increases both their catalytic activity and thermal stability [7], suggests that significant changes in protein conformation may ensue, as reported for the phosphorylation of other proteins [9]. We examined this question by FTIR spectroscopy to monitor structural changes produced by phosphorylation of two neurotoxin serotypes, BoNT A and BoNT E, and differential scanning calorimetry to investigate the effect on their thermal denaturation process. Tyrosine phosphorylation of BoNT A and E increased their α-helix content, as evidenced from the conformationally-sensitive amide I bands [10]. The increment in structural order was accompanied by an increase in the absorbance of the amide II band remaining upon H-D exchange, suggesting that the phosphorylated neurotoxins are structurally more compact and less accessible to the solvent than the non-phosphorylated forms. Furthermore, the phosphorylation-induced structural change promoted a stabilization of the folded proteins that was reflected in an increase in the temperature at which the phosphorylated neurotoxins denature.

2. Materials and methods

Deuterium oxide (D_2O, 99.9% by atom) was purchased from Sigma. Centrifugal filter device Biomax-50K was from Millipore, Bedford, MA, USA. Recombinant Src kinase (specific activity 900 000 U/mg) was from Upstate Biotechnology, Lake Placid, NY, USA.

2.1. Phosphorylation of BoNT A and E

BoNT A and E were purified and tyrosine phosphorylated as described [7,11,12]. Briefly, 1 mg of neurotoxins in 500 μl of 20 mM HEPES (pH 7.4), 20 mM $MgCl_2$, 1 mM EGTA, 2 mM dithiothreitol, 0.5 mM ATP were incubated with 30 units of Src kinase for 90 min at 30°C. Non-phosphorylated and phosphorylated neurotoxins were kept at −80°C until used. Non-phosphorylated neurotoxin refers to samples in which ATP was omitted. Tyrosine phosphorylation was monitored by Western immunoblotting using a anti-phosphotyrosine monoclonal antibody (clone 4G10, UBI) as described [7]. To quantify tyrosine phosphorylation as mol Pi/mol neurotoxin a 40-μl aliquot of the phosphorylation reaction was supplemented with 5 μCi [γ-^{32}P]ATP (3000 Ci/mmol). Phosphorylated neurotoxins were bound to phosphocellulose filters (SpinZyme, Pierce) and washed with 0.75

*Corresponding author. Fax: (34) 6) 665 86 80.
E-mail: aferrer@umh.es

PII S0014-5793(98)00571-7

phosphoric acid. Phosphocellulose filters were immersed and equilibrated in scintillation fluid and the radioactivity was counted.

2.2. Infrared spectroscopy

BoNTs aqueous buffer was exchanged for deuterated buffer by subjecting the samples to two centrifugation cycles in a Biomax-50K filter, followed by incubation in D_2O-based buffer (10 mM HEPES buffer, pH 7.0, 130 mM KCl, 30 mM NaCl) for 2 h at ~20°C and, thereafter, another round of centrifugation cycles. Each sample of BoNTs (20 μl, at 8 mg/ml) was placed between a pair of CaF_2 windows separated by a 50-μm thick mylar spacer in a Harrick Ossining demountable cell. Spectra were recorded on a Nicolet 520 instrument equipped with a DTGS detector and the sample chamber was continuously purged with dry air. A minimum of 600 scans per sample were taken, averaged, apodized with a Happ-Genzel function and Fourier-transformed to give a nominal resolution of 2 cm^{-1} [13]. Three spectra at 20°C of each BoNT sample were recorded. Temperature was kept constant with a circulating water bath. Contribution of buffer spectra was subtracted and the resulting spectra used for analysis.

2.3. Determination of secondary structure components

Protein secondary structure components were quantified from curve-fitting analysis by band decomposition of the original amide I band after spectra smoothing [14,15]. Spectrum smoothing was carried out applying the maximum entropy method, assuming that noise and bandshape follow a normal distribution [14]. The minimum bandwidth was set to 12 cm^{-1} [14]. The resulting spectra possess a signal/noise ratio better than 4500:1. Derivation of IR spectra was performed using a power of 3, breakpoint of 0.3, and Fourier self-deconvolution was performed using a Lorenztian bandwidth of 18 cm^{-1} and a resolution enhancement factor (k) of 2.0 [16,17]. To quantify the secondary structure, the number and position of the absorbance band components were taken from the deconvoluted spectra, the bandwidth was estimated from the derived spectra, and the absorbance height from the original spectra [14]. The iterative curve-fitting process was performed in CURVEFIT running under SpectraCalc (Galactic Industries Corp., Salem, NH, USA). The number, position and bandshape were kept fixed during the first 200 iterations. The fittings were further refined by allowing the band positions to vary for 50 additional iterations. The goodness of fit between experimental and theoretical spectra was assessed from the χ^2 values (1×10^{-5}–4.5×10^{-5}). The area of the fitted absorbance band components was used to calculate the percent of secondary structure [13–18].

2.4. Differential scanning calorimetry

Differential scanning calorimetry (DSC) was performed on a Microcal MC-2 microcalorimeter, as described [19]. The difference in the heat capacities between 1-ml aliquots of BoNTs at 1 mg/ml (contained in the 'sample' cell of the instrument) and buffer alone ('reference' cell) were recorded by raising the temperature at a constant rate of 90°C/h.

3. Results and discussion

3.1. The helical content of BoNTs increases upon phosphorylation

The conformationally-sensitive amide I infrared absorbance band of BoNT A and E after tyrosine-specific phosphorylation (~0.5 mol Pi/mol toxin) were compared with non-phosphorylated neurotoxins. At this phosphorylation stoichiometry, both the LC and HC are similarly phosphorylated, and the activity and stability of the neurotoxins is augmented [7]. The original and the deconvoluted spectra of control and phosphorylated BoNTs samples are shown in Fig. 1. Tyrosine phosphorylation of BoNT A and E notably affected the spectral shape of the amide I band (Fig. 1, dashed lines). Although phosphorylated neurotoxins show the maxima observed in non-phosphorylated samples, the relative intensities of specific bands appear altered, suggesting that tyrosine phosphorylation modulates the relative content of secondary structural components. The individual components may be discerned upon application of resolution-enhancement and band-narrowing techniques [14,15]. Band-narrowing deconvolution of the amide I band showed that BoNT A and BoNT E exhibit maxima at approximately 1690, 1680, 1668, 1652, 1640, 1630 and 1615 cm^{-1}. Whereas the 1615-cm^{-1} component corresponds to amino acid side chain vibration, all the other maxima are assigned to vibration of the carbonyl group in peptide bonds within different secondary structural motifs [10]. The 1630-cm^{-1} component is assigned to β-structure, the 16[illegible]-cm^{-1} component to random structure, the 1652-cm^{-1} component to α-helix, the 1690- and 1668-cm^{-1} components to turns, and the 1680-cm^{-1} band includes contributions from

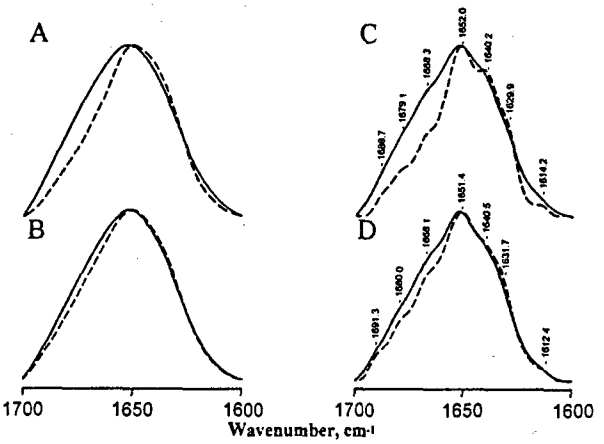

Fig. 1. Tyrosine phosphorylation modulates the secondary structure content of BoNT A and E. Infrared amide I band region of the original (A,B) and deconvoluted spectra (C,D) of BoNTA (A,C) and BoNT E (B,D) from control (solid line) and tyrosine phosphorylated samples (dashed line). Neurotoxins (8 mg/ml) were in D_2O medium prepared from 10 mM HEPES, pH 7.0, 130 mM KCl and 30 mM NaCl. Spectra were taken at 20°C and corrected from the buffer contribution by subtracting the spectrum characteristic of the buffer. Three spectra were acquired for each BoNT sample. Fourier self-deconvolution was carried out with a Lorentzian band of 18 cm^{-1} half-width, and a resolution enhancement factor of 2.0.

Table 1
Denaturation temperatures of non-phosphorylated and phosphorylated BoNTs

	BoNT A		BoNT E	
	Control	Phosphorylated	Control	Phosphorylated
T_m (°C) DSC	51.1	53.	50.5	53.2
T_m (°C) FT-IR	50.5	53.5	51.3	55.1

Denaturation temperatures were obtained from the DSC thermograms as the temperature at which the transition endotherm peaks [27]. Because of the need of large amounts of protein for DSC analysis, measures correspond to a single experiment.

Denaturation temperatures correspond to the inflexion point of the sigmoidal curve obtained when the changes in the width at half-height of the amide I absorbance band are plotted as a function of the temperature (Fig. 4). Values correspond to three independent measurements. Experimental error is ≤ 1°C.

turns as well as from the (0,π) β-sheet vibration band [10,20–22]. The secondary structures of non-phosphorylated and phosphorylated BoNTs were quantified using a maximum entropy method that reduces spectral noise providing a more accurate estimate of secondary structure [14,15]. Fig. 2 illustrates band-fitting analysis of the original amide I band of non-phosphorylated BoNT A (Fig. 2A) and BoNT E (Fig. 2B) and the corresponding phosphorylated species (Fig. 2C,D). Note that BoNT A shows a higher content of α-helix than BoNT E (Fig. 2E), consistent with other reports [23]. Upon phosphorylation, the α-helix content of BoNT A increased from 36% to 50% (Fig. 2E), and for BoNT E it augmented from 26% to 43% (Fig. 2E). This increment in α-helical structure was concomitant with a ≈40% decrease in less ordered structures such as turns (1668 cm^{-1}) and/or random coils (1640 cm^{-1}), without altering the β-sheet content (Fig. 2E). Therefore, these findings indicate that tyrosine phosphorylation promotes a disorder-to-order transition in the neurotoxin structure.

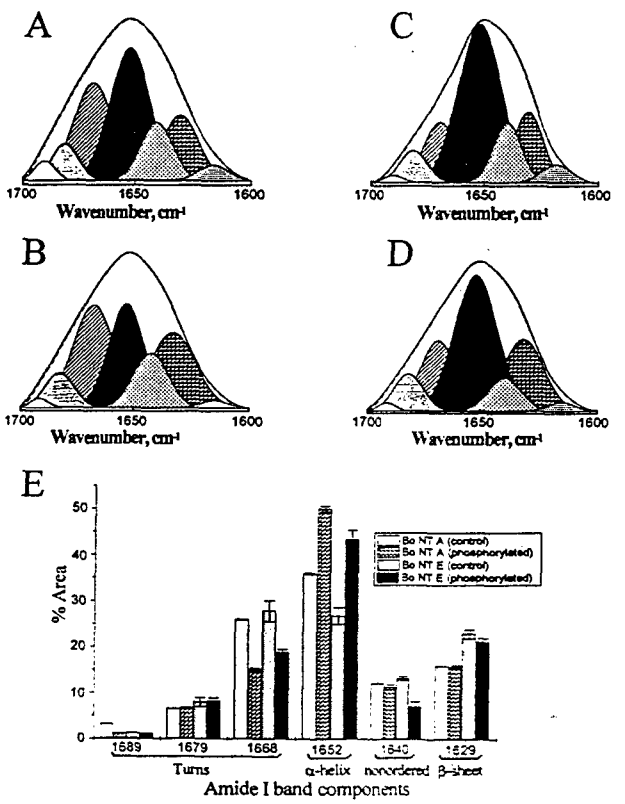

Fig. 2. Tyrosine phosphorylation increases the percent of α-helix secondary structure. Band-fitting analysis of the infrared amide I band of BoNT A (A,C) and BoNT E (B,D) from control (A,B) and phosphorylated samples (C,D). Each panel shows representative results from band-fitting analysis of BoNTs secondary structure. The discontinuous trace, superimposed on the original spectra, denotes the theoretical curve resulting from the contribution of all individual components, which are displayed as gaussian distributions under the spectra. E: Calculated percentages of all different components of the secondary structure of control and tyrosine phosphorylated BoNT A and BoNT E. Secondary structure elements were calculated by band decomposition and curve-fitting of the original amide I band after spectra smoothing [14,15]. Other conditions were as in legend to Fig. 1.

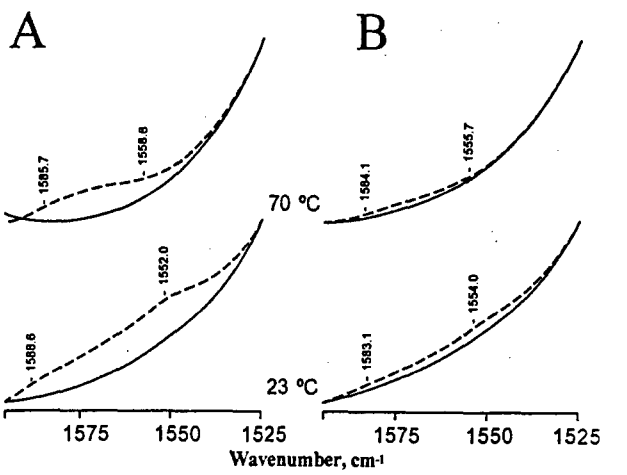

Fig. 3. Tyrosine phosphorylation of BoNT A and E promotes tighter packing. Phosphorylation-dependent changes in the amide II (1595–1525 cm^{-1} region) band of BoNT A (A) and BoNT E (B) remaining upon H-D exchange. Solid lines denote non-phosphorylated samples, and dashed lines indicate tyrosine-phosphorylated proteins. H-D exchange was carried out by 2-h incubation of samples in D_2O-based buffer followed by two washes with Biomax-50K centrifugal filters. The IR spectra were recorded in D_2O medium at the indicated temperatures during a heating cycle of 2.5 h. Protein concentration was 8 mg/ml. Contribution of buffer spectrum was subtracted.

3.2. The compactness of the BoNTs increases upon phosphorylation

The amide II band in proteins originates primarily from N-H bending in the peptide backbone [24,25]. Its residual intensity remaining after D_2O exchange arises from those NH groups unable to undergo H-D exchange and, therefore, it reports on the inaccessibility of the protein core to the solvent which, in turn, indicates the compactness of the protein [24,25]. Replacement of H_2O by D_2O from the non-phosphorylated neurotoxin resulted in the virtual disappearance of the amide II absorbance band centered at 1550 cm^{-1} (Fig. 3, lower panels, solid lines). Phosphorylated species, however, exhibited a substantial residual amide II band absorbance (Fig. 3, lower panels, dashed lines), which partly remained even after heating at 70°C (Fig. 3, upper panels). These results indicate a hindrance of H-D exchange in phosphorylated BoNTs, presumably because of the increased compactness of the structure. Taken together, the spectral changes in the amide I and the amide II upon phosphorylation suggest that the non-exchangeable hydrogens correspond to those involved in the newly generated α-helical structure.

3.3. The thermal stability of BoNTs increases upon phosphorylation

Non-phosphorylated neurotoxins displayed minor alterations on the spectral shape of the amide I band upon increasing the temperature up to 70°C (Fig. 4, solid lines). In contrast, for tyrosine-phosphorylated BoNTs the appearance of two components at 1618 and 1685 cm^{-1} (Fig. 4, dashed lines) which correspond to interactions between extended chains was detected. This observation has been interpreted as a consequence of aggregation of thermally unfolded proteins [13,25–27]. The heat-induced denaturation process was irreversible as evidenced by the lack of recovery of the initial

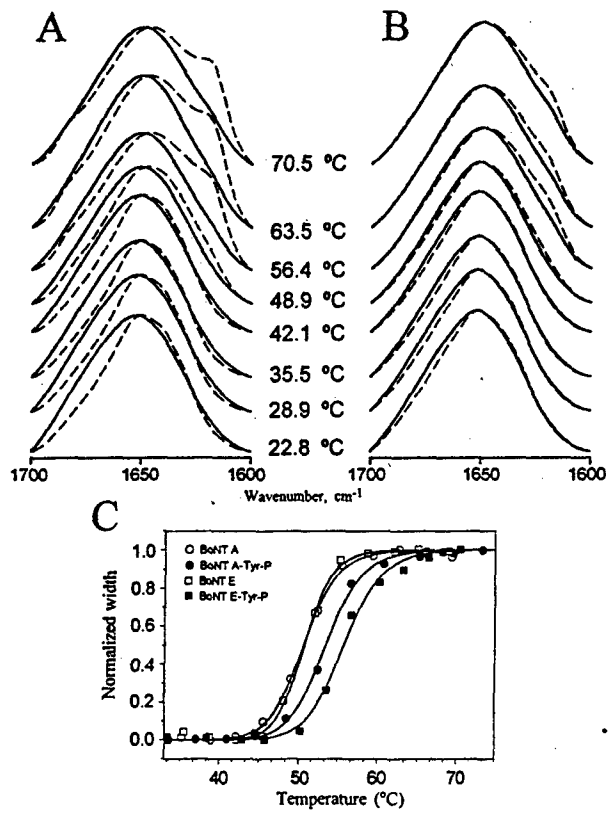

Fig. 4. Tyrosine phosphorylation increases the thermostability of BoNT A and BoNT E. Temperature dependence of the amide I band of BoNT A (A) and BoNT E (B) for control (solid line) and phosphorylated (dashed line) proteins. IR spectra were recorded in D_2O medium at the indicated temperatures during a heating cycle of 2.5 h. C: To determine the denaturing temperature, changes in the width at half-height of the amide I band were measured, normalized and plotted as a function of the temperature at which the spectrum was recorded. The data were described by the logistic equation:

$$\frac{w}{w_{max}} = \frac{1}{1+\left(\frac{T}{T_d}\right)^n}$$

where w denotes the width at half-height of the amide I band, w_{max} the maximal width at half-height, n the slope of the sigmoid, T the temperature, and T_d the denaturing temperature which corresponds to the inflexion point of the sigmoidal curve. Experimental data were fitted to the logistic equation with a non-linear least-squares regression algorithm using MicroCal ORIGIN version 2.8 (Microcal, Amherst). Solid lines depict the best fit to a sigmoidal curve. Denaturing temperatures are listed in Table 1.

spectral shape upon cooling the heated samples back to 20°C (data not shown).

The temperature-dependent changes in the width at half-height of the amide I IR band, plotted as a function of the temperature, display a sigmoidal shape with an inflexion point that corresponds to the denaturation temperature (Fig. 4C) [27]. Accordingly, BoNT A was found to denaturate at 50.5°C and BoNT E at 51.1°C, while phosphorylated BoNT A denatured at 53.5°C, and BoNT E at 55.1°C, i.e. 3–5°C higher than non-phosphorylated neurotoxins (Fig. 4C). The increased thermal stability was also detected by DSC, which measures directly the energetics of the heat-induced denaturation [28]. DSC demonstrated that phosphorylation induced a thermal stabilization, which was manifested as an increase of 2–3°C of the melting temperature (Table 1). These findings indicate that tyrosine phosphorylation of botulinum neurotoxins induces a conformation characterized by higher thermostability.

3.4. Structural basis of the functional modulation of BoNTs by tyrosine phosphorylation

Our findings show that tyrosine phosphorylation induces a disorder-to-order structural transition characterized by a significant increase in α-helical content with a decrease in less ordered structures. Consequently, phosphorylated BoNTs exhibit tighter packing than the non-phosphorylated species and denature at temperatures higher than those required for non-phosphorylated neurotoxins. The induction of structural order favors side chain interactions by hydrogen bond formation, an enthalpic gain. Higher order also augments the compactness of the protein, which presumably decreases the number of cavities, an entropic gain [9,29]. This mechanism to increase protein stability resembles that proposed to account for the extreme stability of thermophile enzymes, which are highly ordered and tightly packed structures [30]. We suggest that the more compact structure may account for the augmentation of the LC catalytic activity produced by tyrosine phosphorylation [7]. However, we cannot exclude a contribution of the HC to the structural changes observed in this study. Hence, additional studies are needed to determine the structural modulation of each neurotoxin chain by tyrosine phosphorylation.

Acknowledgements: This work was supported by grants from the Spanish DGICYT 95PM-0108 to (J.M.G.-R.) and PB93-0934 (to J.A.F.), the DAMD 17-93-C-3100 from the US Army Medical Research and Material Command (to M.M.), and an unrestricted generous gift from Athena Neurosciences (to B.R.D.G.). J.A.E. is recipient of a predoctoral fellowship from the Ministerio de Educación y Ciencia of Spain.

References

[1] Montecucco, C. and Schiavo, G. (1994) Molec. Microbiol. 13, 1–8.
[2] Ahnert-Hilger, G. and Bigalke, H. (1995) Prog. Neurobiol. 46, 83–96.
[3] Jankovic, J. and Hallett, M. (Eds.) (1994) Therapy with Botulinum Toxin, Marcel Dekker, New York, NY.
[4] Montecucco, C., Papini, E. and Schiavo, G. (1994) FEBS Lett. 346, 92–95.
[5] Jahn, R. and Südhof, T.C. (1994) Annu. Rev. Neurosci. 17, 219–246.
[6] Südhof, T.C. (1995) Nature 375, 645–653.
[7] Ferrer-Montiel, A.-V., Canaves, J.M., DasGupta, B.R., Wilson, M.C. and Montal, M. (1996) J. Biol. Chem. 271, 18322–18325.
[8] Kitamura, M., Sakaguchi, S. and Sakaguchi, G. (1969) J. Bacteriol. 98, 1173–1178.
[9] Johnson, L.N. and Barford, D. (1993) Annu. Rev. Biophys. Biomol. Struct. 22, 199–232.
[10] Braiman, M.S. and Rothschild, K.J. (1988) Annu. Rev. Biophys. Biophys. Chem. 17, 541–570.
[11] Sathyamoorthy, V. and DasGupta, B.R. (1985) J. Biol. Chem. 260, 10461–10466.
[12] Ferrer-Montiel, A.V., Montal, M.S., Diaz-Muñoz, M. and Montal, M. (1991) Proc. Natl. Acad. Sci. USA 88, 6418–6422.
[13] Fernández-Ballester, G., Castresana, J., Arrondo, J.L.R., Ferragut, J.A. and González-Ros, J.M. (1992) Biochem. J. 288, 421–426.
[14] Echabe, I., Encinar, J.A. and Arrondo, J.L.R. (1997) Biospectroscopy 3, 469–475.

[15] Bañuelos, S., Arrondo, J.L.R., Goñi, F.M. and Pifat, G. (1995) J. Biol. Chem. 270, 9192–9196.
[16] Moffatt, D.J., Kaupinnen, J.K., Cameron, D.G., Mantsch, H.H. and Jones, R.N. (1986) Computer Programs for Infrared Spectroscopy, NHCC Bulletin 18, National Research Council of Canada, Ottawa.
[17] Moffat, D.J. and Mantsch, H.H. (1992) Methods Enzymol. 210, 192–200.
[18] Surewicz, W.K., Mantsch, H.H. and Chapman, D. (1993) Biochemistry 32, 389–394.
[19] Artigues, A., Villar, M.T., Ferragut, J.A. and González-Ros, J.M. (1987) Arch. Biochem. Biophys. 258, 33–41.
[20] Arrondo, J.L.R., Mantsch, H.H., Mullner, N., Pikula, S. and Martonosi, A. (1987) J. Biol. Chem. 262, 9037–9043.
[21] Krimm, S. and Bandekar, J. (1986) Adv. Prot. Chem. 38, 181–364.
[22] Byler, D.M. and Susi, H. (1986) Biopolymers 25, 469–487.
[23] Singh, B.R., Wasacz, F.M., Strand, S., Jakobsen, R.J. and Das-Gupta, B.R. (1990) J. Protein Chem. 9, 705–713.
[24] Zhang, Y.P., Lewis, R.N.A.H., Hodges, R.S. and McEllaney, R.N. (1992) Biochemistry 31, 11572–11578.
[25] Baezinger, I.E. and Méthot, N. (1985) J. Biol. Chem. 270, 29129–29137.
[26] Surewicz, W.K., Leddy, J.J. and Mantsch, H.H. (1990) Biochemistry 29, 8106–8111.
[27] Castresana, J., Fernández-Ballester, G., Fernándes, A.M., Laynez, J.L., Arrondo, J.L.R., Ferragut, J.A. and González-Ros, J.M. (1992) FEBS Lett. 314, 171–175.
[28] Freire, E., Osdol, W.W., Mayorga, O.L. and Sanchez-Ruiz A. J.M. (1990) Annu. Rev. Biophys. Biophys. Chem. 19, 159–188.
[29] Shaw, A. and Bot, R. (1996) Curr. Opin. Struct. Biol. 6, 546–550.
[30] Szilagyi, A. and Zavodszky, P. (1995) Protein Eng. 8, 779–789.

STRUCTURE, DYNAMICS AND CONFORMATIONAL CHANGE

361-T

Conformational Changes of a Channel-Forming Peptide from the Translocation Domain of Botulinum Neurotoxin as Detected by Circular Dichroism Michael P. Byrne, Mauricio Montal, Jaume Canaves, and Frank J. Lebeda. USAMRIID

A channel-forming peptide from the translocation domain of botulinum neurotoxin serotype A (residues 659-681) (Montal et al., 1992 FEBS, 313:12-18) was investigated by circular dichroism. When the peptide was titrated with the helix-stabilizing reagent 2,2,2-trifluoroethanol (TFE) from 10-60% at pH 7.0, the secondary structure changed from primarily random coil with some beta-sheet to a mixture of beta-sheet and helix. The resulting set of titration spectra revealed a lack of an isodichroic point, suggesting this peptide may be obeying a multistate folding mechanism. However, at pH 3.3, the peptide adopted primarily a beta-sheet conformation at TFE concentrations below 30%, but at 40% TFE an abrupt conformational change occurred revealing the peptide had adopted a primarily helical structure. To determine the effect of pH on conformational change of this peptide, a pH titration was perfomed. Results showed the peptide changed conformation from primarily random coil to primarily beta-sheet at approximately pH 6.0. This set of spectra revealed an isodichroic point at 211 nm suggesting that under these conditions the peptide is following a two-state transition from coil to beta-sheet. The charged residues present in the peptide are two glutamates whose pKas as free amino acids in aqueous solutions are 3.5-4. Since the transition occurred at pH 6, the glutamate residues may reside in a hydrophobic environment. Because this peptide is only 23 amino acids long, it can be reasoned that the beta-sheet structure formed was caused by intermolecular interactions due to peptide association.

362-S

CRYSTALLIZATION AND MAD-PHASING OF THE FUNCTIONAL DOMAINS OF APOLIPOPROTEIN E M.Forstner, C.Peters-Libeu, B.Segelke, S.Trakhanov, M.Knapp, Y.Newhouse, K.Weisgraber, B.Rupp. Lawrence Livermore Laboratory and Gladstone Inst. for Cardiovascular Disease

Apolipoprotein E (apoE) plays a key role in cholesterol metabolism serving as a ligand for members of the low-density lipoprotein (LDL) receptor family. Genetic variants of apoE are associated with both atherosclerosis and Alzheimer's disease. Thus, two of the most prominent causes of death in Western society are linked to this molecule. We have investigated the structures of the wild-type apolipoprotein (apoE3) and fragments of the protein, corresponding to the N- and the C-terminal structural domains (22k and 10k, respectively). The 22k domain contains the LDL receptor-binding domain, whereas the 10k domain contains the major lipid-binding elements and is responsible for the oligomerisation of apoE, which exists as a tetramer in the lipid-free state. All proteins were obtained as recombinant native and seleno-methionine containing proteins for use in MAD-phasing. Crystallization trials routinely employed the hanging drop vapor diffusion method at room temperature or 4°C. Thus far, we have obtained diffraction quality crystals of the 22k domain of the three common isoforms (apoE2, E3 and E4), improving on the resolution of existing data sets, and several mutants that display LDL receptor-binding defects. The structures of apoE3 and apoE2(D154A) have been solved and the other structures are currently in different stages of refinement. Two different variants of the 10k C-terminal fragment have also been crystallized and diffraction quality crystals have been obtained.

363-M

NMR STRUCTURE AND BACKBONE DYNAMICS OF THE CX_3C CHEMOKINE DOMAIN OF FRACTALKINE
Laura S. Mizoue, J. Fernando Bazan, and Tracy M. Handel. U. C. Berkeley, Berkeley, CA 94720

Chemokines (chemoattractant cytokines) help direct the migration of leukocytes in the immune response and are believed to play key roles in both normal host defense and the pathogenesis of a variety of diseases including cancer, atherosclerosis, abnormal inflammation, and AIDS. Most chemokines are small (8-12 kDa), secreted proteins that belong to one of 3 classes (CXC, CC, or C) depending on the number and arrangement of N-terminal cysteines. Recently, a fourth type of human chemokine was identified. The protein, called fractalkine has a unique CX_3C spacing of the characteristic motif and is membrane-bound with a chemokine module attached to the membrane via an extended mucin-like stalk. We have determined the solution structure and backbone dynamics of the N-terminal chemokine domain (residues 1-76) of fractalkine using multidimensional, heteronuclear NMR spectroscopy. We show that the protein is monomeric and compare its structure to those from both CXC and CC families. Our results show that the small difference in cysteine spacing leads to distinct structural differences for this chemokine family.

364-T

PROTEOLYTIC STUDIES INDICATE NOVEL TOPOLOGY FOR THE GLYCINE RECEPTOR. John Leite, Andrew Amoscato and Michael Cascio. University of Pittsburgh School of Medicine, Pittsburgh, Pa 15219

The glycine receptor (GlyR), an inhibitory neurotransmitter receptor, is a member of the ligand-gated channel superfamily. The current topological model for GlyR postulates a large extracellular N-terminal domain and four transmembrane α-helices. Recent circular dichroism analysis (Cascio *et al.*, submitted) estimates the α-helical content of GlyR to be significantly lower than that required by this model. This study tests the current topological model by limited proteolysis. Homomeric channels composed of GlyR α subunits were overexpressed using a baculovirus system, purified and reconstituted into lipid vesicles of defined composition. Proteolytic enzymes were used to probe GlyR for regions susceptible to cleavage, followed by ultracentrifugation to separate soluble from membrane-associated peptides. Digests were analyzed by a combination of mass spectrometry (MS) techniques including MALDI-TOF, capillary reverse-phase HPLC on-line with electrospray ionization MS and tandem MS. The analysis has yielded a wealth of peptides which were assigned to the GlyR amino acid sequence by molecular mass. Assignments were confirmed by fragmentation spectra analysis and/or chemical modification. We have identified membrane-associated domains within the GlyR sequence, previously thought to be soluble. In addition, proteolytic cleavages have been detected within the postulated transmembrane domains. These results suggest a new topological model characterized by the presence of membrane-associated peptides too short to be membrane-spanning α-helices.

365-S

Probing the Structure of Rhodopsin by Cysteine Scanning Mutagenesis and Disulfide Cross-linking Mary Struthers, Hongbo Yu, Masahiro Kono, Daniel Oprian. Department of Biochemistry and the Volen Center for Complex Systems. Brandeis University. Waltham MA. 02254

Rhodopsin is a well-studied member of the superfamily of G-protein coupled receptors (GPCR), which are integral membrane proteins consisting of seven transmembrane spanning (TM) segments. Cysteine scanning mutagenesis and disulfide cross-linking have been used to probe the structure of rhodopsin in the fifth and sixth transmembrane segments. Mutations were performed in a split receptor (SR1-5 6-7) consisting of non-covalently associated N-terminal (TM 1-5) and C-terminal (TM 6-7) fragments, which enabled facile detection of disulfide bond formation in a mobility shift assay using non-reducing SDS-PAGE. A mild oxidation strategy involving treatment of dark state split-rhodopsins at pH 8.0 was employed to promote cross-linking. A series of cysteine substitutions in TM5 were evaluated for the ability to cross-link with cysteine mutations in TM6. A single cysteine mutation in TM6 selectively cross-links with cysteines introduced at positions spaced at i and $i+4$ in TM5, indicating tertiary interactions between these sites. This helical pattern of cross-links for TM5 is not maintained by mutants containing cysteine replacements in the proposed extracellular loop region between TM4 and TM5. At least one cross-linked rhodopsin activates the G-protein transducin at a rate similar to that of the wild type split receptor, indicating that cross-linking of TM5 and TM6 in this region does not restrict the light-induced conformational changes required for receptor activation.

366-M

Structural study of copper-oxidized low density lipoprotein
G. Steve Huang. Pig Research Institute Taiwan

Porcine plasma low density lipoprotein has been oxidized in vitro at different copper concentrations and analysed by 1H NMR spectroscopy and by circular dichroism. We found that: 1) there was structural alternation of protein moities: 2) this alternation could be characterized by NMR and CD; Results indicated that conformational change could contribute to the atherogenic property of oxidized LDL.

United States Army Medical Research & Materiel Command

Program Book

Bioscience Review

"Research for the Warfighter"

31 May - 4 June

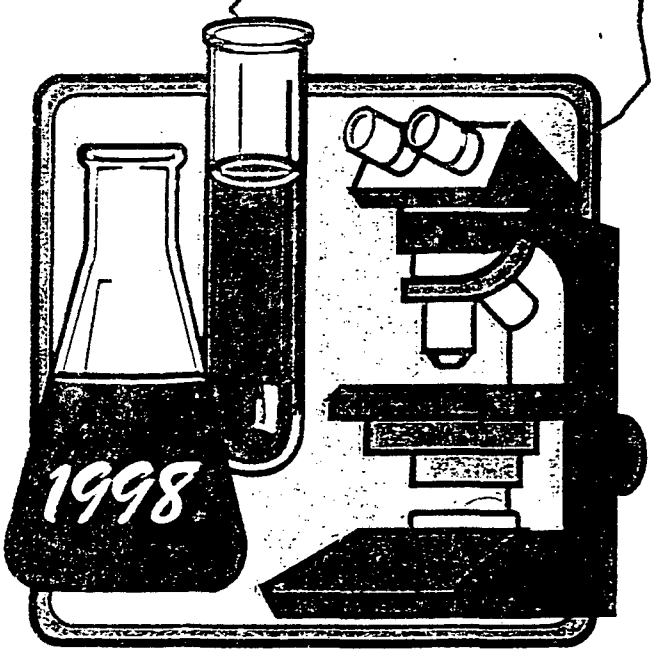

PEPTIDES THAT MIMIC THE CARBOXY-TERMINAL DOMAIN OF SNAP-25 BLOCK ACETYLCHOLINE RELEASE AT AN *APLYSIA* SYNAPSE

J.P. Apland*[1], J.A. Biser[1], M. Adler[1], A.V. Ferrer-Montiel[2], M. Montal[2], and M.G. Filbert[1]

[1]Neurotoxicology Branch, USAMRICD, Aberdeen Proving Ground, MD 21010-5425, and
[2]Dept. of Biology, UCSD, La Jolla, CA 92083-0366

ABSTRACT

Botulinum neurotoxin serotypes A and E (BoNT-A and BoNT-E) block neurotransmitter release, presumably by cleaving SNAP-25. A 20-amino acid peptide called ESUP-A (for excitation-secretion uncoupling peptide) spans the cleavage site for BoNT-A and mimics the carboxy-terminal domain of SNAP-25. Gutierrez *et al.* (FEBS Lett. 372:39, 1995) showed that this peptide inhibited transmitter release from permeabilized bovine chromaffin cells, apparently by blocking vesicle docking (Gutierrez *et al.*, J. Biol. Chem. 272:2634, 1997). Two similar peptides that span the cleavage site for BoNT-E, one with 20 amino acids and one with 26 (named ESUP-E20 and ESUP-E26, respectively), have also been synthesized. ESUP-E26 is reported to be much more potent than is ESUP-E20 in chromaffin cells. These three peptides were tested for effects on acetylcholine (ACh) release at an identified cholinergic synapse of *Aplysia* neurons.

Recordings were obtained from isolated buccal ganglia of *Aplysia.* The presynaptic neuron was current-clamped and stimulated electrically at 0.1 Hz to elicit action potentials. The postsynaptic neuron was voltage-clamped, and evoked inhibitory postsynaptic currents (IPSCs) were recorded. ESUPs were pressure-injected into the presynaptic neuron, and their effects on the amplitude of the IPSCs were studied. ACh release from presynaptic cells, as measured by the amplitudes of IPSCs, was gradually inhibited by the peptides. ESUP-A, ESUP-E20 and ESUP-E26 were about equally effective in reducing evoked responses. All peptides caused about 40% reduction in IPSC amplitude in 2 hr. Random-sequence peptides of the same amino acid composition as ESUP-A and ESUP-E26 had no effect. These results suggest that ESUPs compete with the intact SNAP-25 for binding with other fusion proteins, thus inhibiting exocytosis of neurotransmitter. Production of peptide fragments by BoNT-induced cleavage of synaptic proteins may therefore indirectly contribute to inhibition of neurotransmitter release.

United States Army Medical Research & Materiel Command

Program Book

Bioscience Review

"Research for the Warfighter"

31 May - 4 June

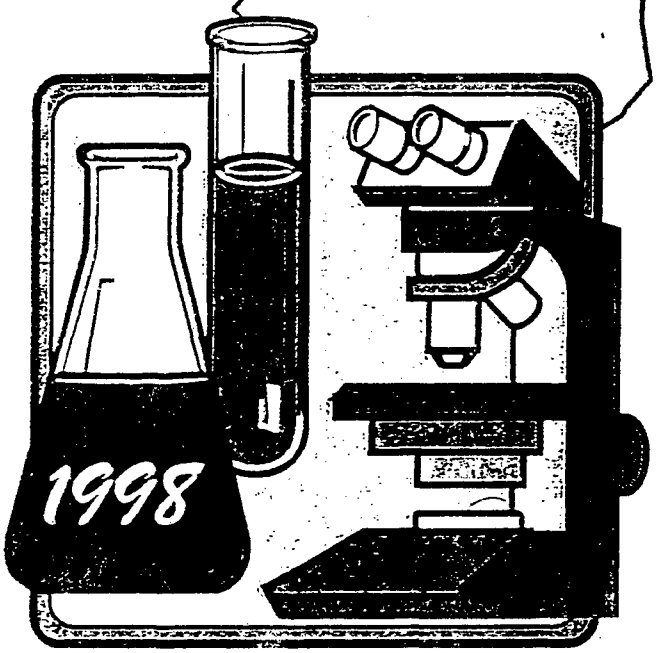

BOTULINUM NEUROTOXINS: MODULATION OF PROTEASE AND CHANNEL ACTIVITIES BY TYROSINE PHOSPHORYLATION

A.V. Ferrer-Montiel, M. Oblatt-Montal, J. Canaves, and M. Montal

Department of Biology, University of California San Diego,
La Jolla, California 92093-0366

ABSTRACT

Clostridial neurotoxins metalloprotease domain selectively cleaves proteins implicated in the process of synaptic vesicle fusion with the plasma membrane and, accordingly, blocks neurotransmitter release into the synaptic cleft. However, protease activity alone cannot explain the *in vivo* long term effects of botulinum neurotoxins nor the potentiation of its neuroparalytic action by elevations of intracellular calcium and nerve stimulation. This discrepancy between *in vitro* and *in vivo* effects could be resolved if once internalized, the neurotoxins were subjected to modulation by intracellular cascades triggered by environmental signals which in turn may alter its activity on target substrates. We discovered that the nonreceptor tyrosine kinase Src phosphorylates botulinum neurotoxins A, B and E [1]. Specific protein tyrosine phosphorylation of serotypes A and E dramatically increases both their catalytic activity and thermal stability, while dephosphorylation reverses the effect. This suggests that the biologically significant form of the neurotoxins inside neurons is phosphorylated. Indeed, in PC12 cells in which tyrosine kinases such as Src and PYK2 are highly abundant, stimulation by membrane depolarization in presence of extracellular calcium induces rapid and selective tyrosine phosphorylation of internalized light chain, the metalloprotease domain, of botulinum toxin A. Tyrosine phosphorylation of botulinum toxin A heavy chain, the channel-forming domain [2], appears to stabilize the conductive state of the channel with minor modifications of the single channel conductance. These findings provide a conceptual framework to connect intracellular signaling pathways involving tyrosine kinases, G-proteins, phosphoinositides and calcium with the action of botulinum neurotoxins in abrogating vesicle fusion and neurosecretion.

1. Ferrer-Montiel, et al. *J. Biol.Chem.* 271:18322-18325, 1996.
2. Oblatt-Montal, M., et al. *Protein Sci.* 4:1490-1497, 1995.

The collaboration of Bibhuti R. DasGupta is acknowledged.

This work was supported by the U.S. Army Medical Research and Materiel Command under Grant DAMD 17-93-C-3100.

FEBS Letters 435 (1998) 84–88 FEBS 20774

The 26-mer peptide released from SNAP-25 cleavage by botulinum neurotoxin E inhibits vesicle docking

Antonio V. Ferrer-Montiel[1,2,a], Luis M. Gutiérrez[b], James P. Apland[c], Jaume M. Canaves[a], Anabel Gil[b], Salvador Viniegra[b], Jennifer A. Biser[c], Michael Adler[c], Mauricio Montal[a,*]

[a]*Department of Biology, University of California San Diego, 9500 Gilman Dr, La Jolla, CA 92093-0366, USA*
[b]*Departamento de Neuroquímica, Instituto de Neurociencias and Facultad de Medicina, Universidad Miguel Hernández, San Juan, Spain*
[c]*Neurotoxicology Branch, U.S. Army Medical Research Institute of Chemical Defense, 3100 Ricketts Point Road, Aberdeen Proving Ground, MD 21010-5425, USA*

Received 3 August 1998

Abstract Botulinum neurotoxin E (BoNT E) cleaves SNAP-25 at the C-terminal domain releasing a 26-mer peptide. This peptide product may act as an excitation-secretion uncoupling peptide (ESUP) to inhibit vesicle fusion and thus contribute to the efficacy of BoNT E in disabling neurosecretion. We have addressed this question using a synthetic 26-mer peptide which mimics the amino acid sequence of the naturally released peptide, and is hereafter denoted as ESUP E. This synthetic peptide is a potent inhibitor of Ca^{2+}-evoked exocytosis in permeabilized chromaffin cells and reduces neurotransmitter release from identified cholinergic synapses in in vitro buccal ganglia of *Aplysia californica*. In chromaffin cells, both ESUP E and BoNT E abrogate the slow component of secretion without affecting the fast, Ca^{2+}-mediated fusion event. Analysis of immunoprecipitates of the synaptic ternary complex involving SNAP-25, VAMP and syntaxin demonstrates that ESUP E interferes with the assembly of the docking complex. Thus, the efficacy of BoNTs as inhibitors of neurosecretion may arise from the synergistic action of cleaving the substrate and releasing peptide products that disable the fusion process by blocking specific steps of the exocytotic cascade.

Key words: SNARE hypothesis; Neurosecretion; Exocytosis; Synaptic transmission; Protein-protein interaction

1. Introduction

A widely held view considers that the process of vesicle fusion with the plasma membrane which occurs during neuronal exocytosis is mediated by SNARE proteins [1–5]. This family of membrane proteins provides a specific means of pairing vesicles (v-SNAREs) with target (t-SNAREs) membranes [1–5]. *Clostridial* neurotoxins are metalloproteases that cleave specific components of the v-SNARE and t-SNARE and abolish neurotransmitter release. Botulinum neurotoxins (BoNT) B, D, F, and G, and the structurally related tetanus toxin specifically cleave VAMP at different sites [6,7]; BoNT A and E cleave SNAP-25 at the C-terminus [8,9], and BoNT C cuts syntaxin and SNAP-25 [10,11]. Proteolysis of each of these substrates produces a truncated protein and releases a peptide product [6–11]. It has been proposed that these peptide products may also prevent the formation of the core complex and thereby abrogate Ca^{2+}-triggered exocytosis [12,13]. This hypothesis is supported by the finding that truncated fusion proteins and synthetic peptides that mimic the amino acid sequence of segments from synaptotagmin [14,15], SNAPs [16], synaptobrevin [17], syntaxin [18], Ca^{2+} channels [19], and SNAP-25 [12,13,20] are specific inhibitors of neurosecretion. In particular, a 20-mer peptide encompassing the C-terminal domain of SNAP-25 blocked exocytosis by inhibiting vesicle docking in permeabilized chromaffin cells [12,13]. The term ESUP (excitation-secretion uncoupling peptide) was coined to highlight this inhibitory activity [12]. Although these results suggest that peptide products resulting from substrate cleavage by BoNTs may block vesicle fusion, experimental support to substantiate this notion is still limited.

Here, we show that a 26-mer peptide corresponding to the amino acid sequence of the peptide product released by BoNT E cleavage of SNAP-25, referred to as ESUP E, efficiently and selectively blocks Ca^{2+}-evoked exocytosis in chromaffin cells and neurotransmitter release in *Aplysia* cholinergic synapses. Our results are consistent with the notion that ESUP E prevents vesicle docking by interfering with the assembly of the synaptic ternary complex formed by SNAP-25, VAMP and syntaxin.

2. Material and methods

2.1. Reagents

[^{3}H]Noradrenaline was from DuPont-NEN (Boston, MA). t-Boc and Fmoc amino acids, with standard side chain protecting groups, were obtained from Applied Biosystems (Foster City, CA), NovaBiochem (La Jolla, CA) or Peninsula Laboratories (Belmont, CA). Solvents, reagents and resins for peptide synthesis were obtained from Applied Biosystems (Foster City, CA), Percoll from Pharmacia, collagenase (EC 3.4.24.3) from Boehringer Mannheim (Germany), anti-SNAP-25 mAb (clone SM81) from Sternberger (Baltimore, MD), anti-syntaxin mAb (clone HPC1) from Sigma (St. Louis, MO) and anti-VAMP Ab from Stressgen (Canada). Agarose-conjugated protein G was from Pierce (Rockford, IL). BoNTs were kindly provided by Drs. B.R. DasGupta and M. Goodnough (University of Wisconsin). All other reagents were of analytical grade from Sigma.

*Corresponding author. Fax: (1) (619) 534-0931.
E-mail: montal@biomail.ucsd.edu

[1]A.V.F.-M. and L.M.G. contributed equally to this work.

[2]Present address: Centro de Biología Molecular y Celular, Universidad Miguel Hernández, C/ Monóvar s/n, 03206 Elche, Spain.

Abbreviations: BoNT, botulinum neurotoxin; SNAP-25, synaptosomal associated protein of 25 kDa; ESUP, excitation-secretion uncoupling peptide; VAMP, vesicle associated membrane protein; SNARE, SNAP receptor; v-SNARE, vesicle-SNARE; t-SNARE, target-SNARE; NSF, *N*-ethylmaleimide-sensitive fusion protein; SNAP, soluble NSF attachment protein; IPSC, inhibitory postsynaptic current; ACh, acetylcholine

PII: S0014-5793(98)01012-6

2.2. Peptide synthesis and purification

ESUP E (SNAP-25 [181–206]: IMEKADSNKTRIDEANQRATKMLGSG) and ESUP E^{RDM} (ESDNDTRAIKITQAGSMKRMGLNAKE) were synthesized by Fastmoc Fmoc chemistries in an Applied Biosystems 431A automated solid-phase peptide synthesizer, cleaved and purified as described [12,13].

2.3. Activation of BoNT E

The single chain BoNT E in 25 mM HEPES was converted to the 'nicked' di-chain form by treatment with 0.3 mg/ml trypsin XI for 30 min at 37°C, followed by incubation with 0.5 mg/ml soybean trypsin inhibitor for 15 min at room temperature. Aliquots of the nicked toxin were frozen at −80°C, then thawed and treated with 1 mM dithiothreitol (DTT) immediately before use to expose the active site of the light chain protease.

2.4. Chromaffin cell cultures and secretion assays

Chromaffin cell cultures were prepared from bovine adrenal glands by collagenase digestion and further separated from debris and erythrocytes by centrifugation on Percoll gradients as described [12,13]. Cells were maintained in monolayer cultures at a density of 625 000 cells/cm^2 and were used 3–6 days after plating. All the experiments were performed at 37°C. Secreted [^{3}H]noradrenaline was assayed in digitonin-permeabilized cells as described [12,13]. The CPM released from control cells under basal conditions was ~3000, and increased to ~11 000 when stimulated with 10 μM Ca^{2+}. The total number of counts obtained from detergent-permeabilized cells was ~110 000. Thus, the normalized basal release represents 3.5% of the total secretion, and the Ca^{2+}-evoked component accounts for ~10% of the total. Statistical significance was calculated using Student's *t*-test with data from ≥4 independent experiments.

2.5. Immunoprecipitation of the ternary complex SNAP-25/VAMP/syntaxin from solubilized rat brain synaptosomes

Rat brain synaptosomes were prepared from brain cortices as described [21]. Synaptosomes (100 μg) were solubilized in radioimmunoprecipitation assay buffer (50 mM Tris-HCl pH 7.4, 150 mM NaCl, 1% Nonidet P-40, 0.25% deoxycholate, 1 mM EGTA, 1 mM NaF, 1 mM Na_3VO_4, 1 mM phenylmethylsulfonyl fluoride and 5 mM iodoacetamide), incubated with or without 100 μM ESUPs for 2 h at 4°C, unless otherwise indicated. Insoluble material was removed by centrifugation at 10 000×*g* for 30 min at 4°C. Immunopurification of the ternary complex SNAP-25/VAMP/syntaxin from the soluble material was achieved by using an overnight incubation with anti-SNAP-25 monoclonal antibody (1 μg mAb/100 μg protein). Immunocomplexes were captured with agarose-conjugated protein G (100 μl, 50% slurry), and washed six times with 500 μl of radioimmunoprecipitation buffer at 4°C. Immunoprecipitates were dissolved with 50 μl of SDS-PAGE buffer, boiled 5 min, separated by SDS-PAGE and analyzed by immunoblotting. Blots were probed with the anti-SNAP-25 mAb, an anti-syntaxin mAb and an anti-VAMP Ab. Bands were visualized using the ECL system, and quantified using the public domain NIH Image program version 1.57 [13]. Data are given as mean ± S.E.M., with *n* (number of experiments) = 3.

2.6. Inhibition of neurotransmitter release in Aplysia synapses

Experiments were performed with neuronal preparations from the marine mollusc *Aplysia californica*. Intraneuronal inhibition of nerve-evoked release of acetylcholine (ACh) was measured at identified cholinergic synapses of *Aplysia* buccal ganglia [22,23]. The ganglia were surgically removed and pinned to the Sylgard lined bottom of an acrylic chamber, and the connective tissue capsule was excised. The soma of identified pre- and postsynaptic cholinergic neurons were impaled with glass microelectrodes (2–4 MΩ) filled with 2 M potassium acetate. Action potentials were evoked in presynaptic neurons by suprathreshold depolarizing stimuli applied at 0.1 Hz. Neurotransmitter release was assessed by measuring the amplitudes of inhibitory postsynaptic currents (IPSCs) in voltage-clamped follower neurons. Presynaptic potentials and postsynaptic currents were digitized and stored on a personal computer using pClamp software (Axon Instruments, Foster City, CA). Only responses that were not accompanied by spontaneous activity were analyzed. The preparation was superfused continuously at a rate of 1 ml/min with artificial sea water containing in mM: NaCl 480; KCl 10; $CaCl_2$ 10; $MgCl_2$ 20; $MgSO_4$ 30; $NaHCO_3$ 2.5; HEPES 10, at pH 7.8, maintained at room temperature. ESUP E and ESUP E^{RDM} (5 mM) were dissolved in 600 mM NaCl containing 1% (w/v) fast green FCF dye to aid in visualizing the volume injected. The solution was air pressure-injected into the presynaptic cell by micropipette. A maximum pressure of 60 psi was used to introduce an adequate volume of solution into the presynaptic cell as indicated by the appearance of intracellular dye. The volume of solution injected was ≤10% of the estimated cell volume, yielding a final intracellular peptide concentration ≤100 μM. BoNT E concentration in the micropipette was 3.3 μM.

3. Results and discussion

3.1. A peptide mimicking the 26-aa peptide fragment released by BoNT E cleavage of SNAP-25 blocks exocytosis

Cleavage of the C-terminus of SNAP-25 by BoNT E releases a 26-mer peptide that may block neurosecretion [12,13]. To test this hypothesis, we synthesized this 26-mer peptide (ESUP E) and assayed the presumed inhibitory activity on Ca^{2+}-evoked catecholamine release from digitonin-permeabilized chromaffin cells. ESUP E blocked noradrenaline

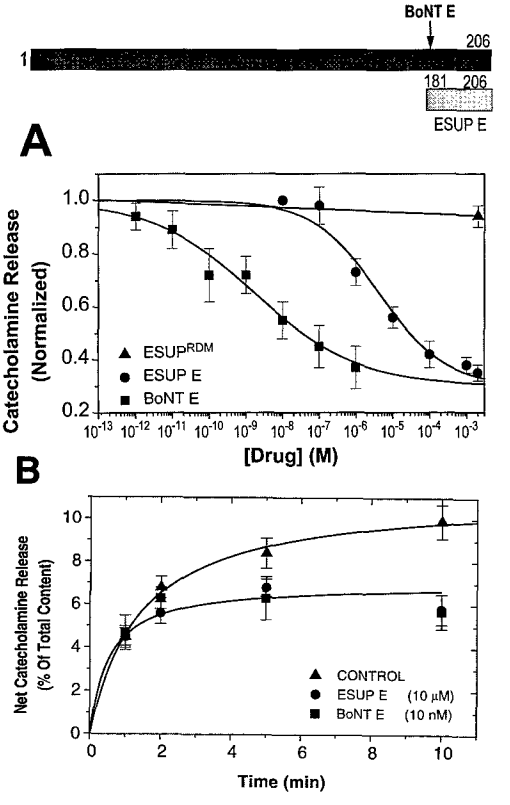

Fig. 1. ESUP E blocks Ca^{2+}-dependent catecholamine secretion from permeabilized chromaffin cells. Top: Schematic representation of SNAP-25 with the cleavage site for BoNT E. ESUP E represent the peptide product (aa 181–206) released by BoNT E cleavage of SNAP-25. Bottom: A: Concentration-dependent inhibition of Ca^{2+}-evoked catecholamine release from pemeabilized chromaffin cells by BoNT E, ESUP E and ESUP E^{RDM}. Net release is given as mean ± S.E.M. with *n* (number of experiments performed in triplicate) = 4. Solid lines depict the best fit to the logistic equation: $B/B_{max} = 1/(1+([blocker]/IC_{50})^n)$, where B denotes the extent of block, B_{max} represents the maximal block; IC_{50} denotes the concentration of blocker (BoNT E or ESUP E) that produces half-maximal block, and n is the Hill coefficient of the blocking activity. For BoNT E the values were $IC_{50} = 1.8 \pm 1.3$ nM, n = 0.5; and for ESUP E, $IC_{50} = 250 \pm 75$ nM, n = 0.6. B: Time course of the net noradrenaline release (Ca^{2+}-stimulated minus basal) obtained in presence or absence of 100 μM ESUP E or 10 nM BoNT E.

release with an IC_{50}=250±75 nM, and a maximal inhibition of ~70% (Fig. 1A). The ESUP inhibitory activity was similar to that elicited by BoNT E with respect to maximal inhibition (~70%) but was ~140-fold less efficient (BoNT E IC_{50}=1.8±1.3 nM). The sequence specificity of ESUP activity was assessed by synthesizing a randomized version of the peptide (ESUP E^{RDM}), which was proven inert in blocking catecholamine release at concentrations up to 100 μM (Fig. 1A).

To identify the step of the exocytotic cascade blocked by ESUP E, we investigated its activity on the kinetics of the secretory process and compared it with that produced by BoNT E (Fig. 1B). Permeabilized cells were incubated with ESUP E or DTT-reduced BoNT E for 5 min, and secretion was evoked by Ca^{2+} pulses of different duration. Incubation of permeabilized chromaffin cells with 10 μM ESUP E or 10 nM BoNT E inhibited ~60% of catecholamine release, primarily by altering the slow phase of secretion (Fig. 1B), suggesting that the vesicle pools upstream of docking and priming steps are sensitive to the action of ESUP E and BoNT E [24–26]. These data indicate that the 26-mer peptide released by BoNT E cleavage of SNAP-25 is a potent and specific uncoupler of Ca^{2+}-evoked exocytosis, and suggest that the efficiency of BoNT E to disable the fusion process may arise from the combined action of cleaving a protein critical for the assembly of the fusion complex, and by releasing a small peptide which, in turn, may interfere with the formation of the complex.

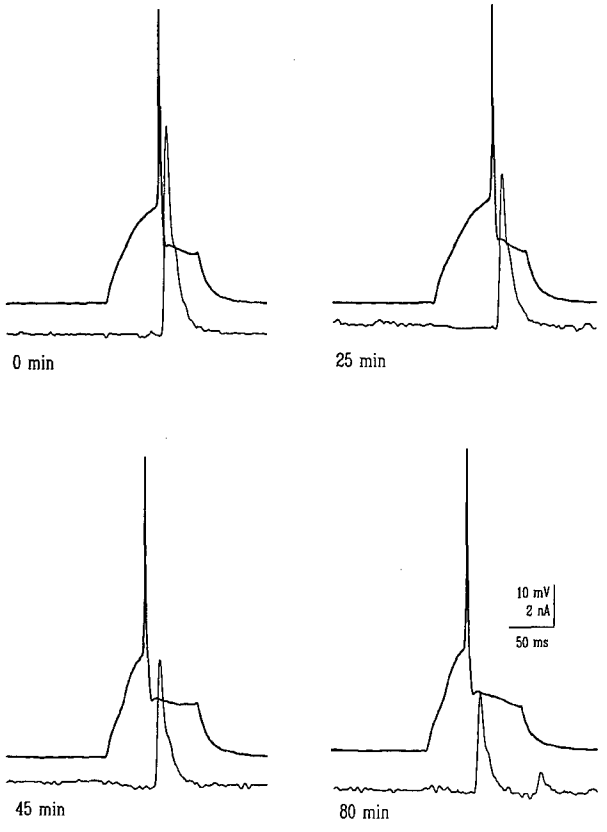

Fig. 2. ESUP E blocks ACh release by the presynaptic neuron in a cholinergic synapse in *Aplysia* buccal ganglia. ACh release was monitored as the amplitude of the IPSC (lower trace) elicited by an evoked action potential (upper trace) in the presynaptic neuron. Recordings show the decrement of the IPSC amplitude after injection of ESUP E into the presynaptic neuron at zero time.

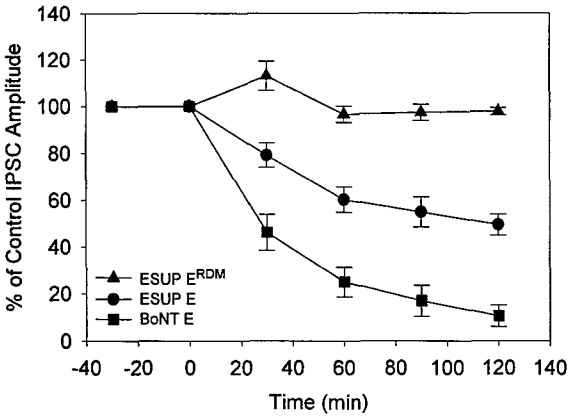

Fig. 3. ESUP E and BoNT E inhibit IPSC amplitude in *Aplysia* buccal ganglion synapses. Active ESUP E (n=10), the inactive random sequence ESUP E^{RDM} analog (n=8), or BoNT E (n=7) were injected into the presynaptic neuron at zero time. IPSC amplitude was inhibited after injection of active ESUP E and BoNT E but not by injection of the inactive analog. Mean±S.E.M.

3.2. *ESUP E and BoNT E inhibit neurotransmitter release in Aplysia cholinergic synapses in vitro*

Release of ACh by the presynaptic neuron in response to electrically evoked action potentials was assessed from the amplitudes of the evoked IPSCs in a voltage-clamped postsynaptic neuron. Fig. 2 shows superimposed action potentials and IPSCs in a typical experiment. ESUP E was injected into the presynaptic neuron at zero time (top left panel), and the resultant decline of IPSC amplitude is shown at three successive time points. The IPSC amplitude declined to 52% of the control value 120 min after the injection of ESUP E. The decrease of IPSC amplitude was gradual and incomplete, typically requiring 2 h to reach a stable value of 30–70% of the control. The time course of the effect of peptides or toxin injection on IPSC amplitude is shown in Fig. 3. BoNT E, ESUP E or ESUP E^{RDM} were injected at time zero. The increase of IPSC amplitude immediately following the injection of ESUP E^{RDM} was not considered to be significant since such increases were a frequent consequence of pressure injection of any compound, and IPSC amplitudes typically returned to control values within 20 min. No further reduction of responses occurred in cells injected with the random-sequence control peptide, whereas IPSCs in cells injected with BoNT E and active ESUP E declined to a stable level over the ensuing 120 min.

The rate and extent of IPSC inhibition caused by BoNT E was greater than that produced by ESUP E: the amplitude was attenuated by 50% in 28 min and by 90% in 120 min by BoNT E, whereas inhibition by ESUP E was only 50% at 120 min. The more rapid and nearly complete IPSC decrement caused by BoNT E supports the concept that the inhibition caused by the toxin protease is a consequence of both a decrease in available SNAP-25 and an accumulation of cleavage products.

3.3. *ESUP E inhibits vesicle docking by interfering with the formation of the ternary complex comprising SNAP-25, VAMP, and syntaxin*

Since the C-terminal domain of SNAP-25 binds tightly to VAMP and syntaxin during vesicle docking, forming a highly stable ternary complex, it is conceivable that ESUP E blocks

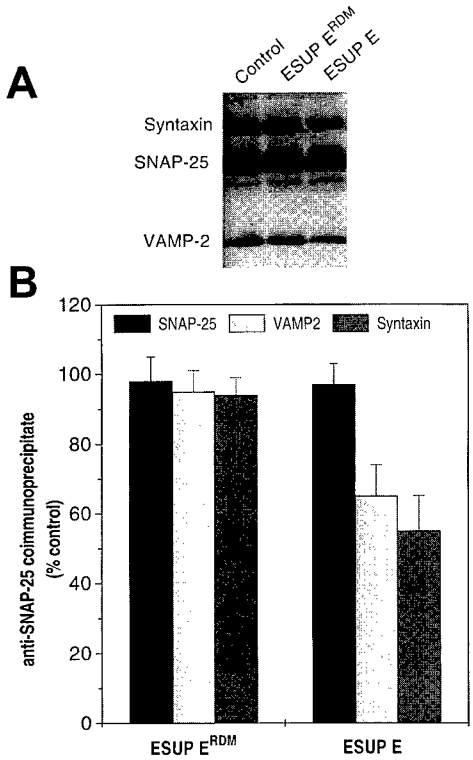

Fig. 4. ESUP E disrupts the interaction between SNAP-25, VAMP and syntaxin. A: Immunoprecipitates of the ternary complex SNAP-25/VAMP/syntaxin from rat brain synaptosomes incubated without (Control) or with 100 μM ESUP E or ESUP E^{RDM}. Immunocomplexes were analyzed using SDS-PAGE (4–20%) under non-reducing conditions, and immunoblotted with an anti-syntaxin mAb, anti-SNAP-25 mAb and anti-VAMP Ab. B: Data of three different experiments were quantified by image analysis, and values normalized with respect to that of control.

the docking process by competition with SNAP-25 for binding to the ternary complex. To examine this question, we studied the effect of ESUP E on the interaction of SNARE proteins in digitonin-permeabilized chromaffin cells. We did not observe coimmunoprecipitation of all the SNARE proteins with the anti-SNAP-25 mAb (data not shown), as reported by others [27]. We therefore turned to rat brain synaptosomes as an alternative preparation [3,20,28]. Since the SNARE complex forms spontaneously during synaptosome preparation and solubilization, we evaluated if ESUP E could displace SNAP-25 from the ternary complex and, therefore, dissociate the preformed aggregate or interfere with its assembly. The experimental protocol involved detergent solubilization of synaptosomes, incubation with ESUP E or ESUP E^{RDM}, immunopurification of the ternary complex using an anti-SNAP-25 mAb followed by separation of the components using SDS-PAGE. Immunoblots probed with specific antibodies raised against syntaxin, SNAP-25 and VAMP revealed the presence of the three proteins in the immunoprecipitate (Fig. 4A). Incubation with 100 μM ESUP E inhibited the coimmunoprecipitation of VAMP and syntaxin without affecting the immunopurification of SNAP-25.

A quantitative analysis of the immunoblots is shown in Fig. 4B. An excess of ESUP E inhibited the coimmunoprecipitation of VAMP by ~30% and of syntaxin by ~40%, whereas no effect was detected with ESUP E^{RDM}, in accord with expectations. The partial inhibition produced by ESUP E (100 μM) may be accounted for by its relatively low affinity (Fig. 1A). Nonetheless, the fact that a short peptide may interfere with the assembly or stability of an SDS-resistant complex is highly significant, and provides experimental support for the notion that ESUP E inhibits vesicle docking by preventing the formation of the essential ternary complex. These findings suggest that ESUP E may compete with SNAP-25 for binding to VAMP and interrupt the ensuing chain of protein-protein interactions that lead to vesicle fusion.

3.4. Molecular mechanism of ESUPs biological activity

The finding that the 26-mer peptide released from SNAP-25 cleavage by BoNT E mimics the inhibitory action of this neurotoxin on neurosecretion (Fig. 1), and on synaptic transmission (Figs. 2 and 3), provides support to the tenet that BoNTs abrogate vesicle fusion by the combined action of cleaving the substrate and releasing peptide products which block the docking or/and priming steps of the exocytotic cascade. The result that the ternary complex is specifically disrupted by an excess of ESUP E (Fig. 4) supports this view. The fact that the 20-mer ESUP A (SNAP-25 [187–206]: SNKTRIDEANQRATKMLGSG), corresponding to the C-terminal sequence of SNAP-25, arrests the ATP-dependent maturation of the secretory granules and promotes the accumulation of secretory vesicles near the plasma membrane is in accord with this notion [13]. Recent studies implicate the C-terminal segment of SNAP-25 encompassing residues 180–196 in vesicle docking and in a late post-docking step [29,30]. Our finding that ESUP E is a more efficient inhibitor of neurosecretion than ESUP A supports this conclusion. Thus, ESUPs mimicking specific protein domains provide novel tools to dissect their contribution to different steps of neurosecretion.

Acknowledgements: We thank B. R. DasGupta and M. Goodnough for purified BoNT E. This work was supported by Grants from the Spanish DGICYT PM-0110 (to S.V.), the US Army Medical Research and Materiel Command DAMD 17-93-C-3100 and DAMD 17-98-C-8040 (to M.M.), and a Postdoctoral Fellowship from the Dystonia Medical Research Foundation (to J.M.C.).

References

[1] Rothmann, J.E. (1994) Nature 372, 55–63.
[2] Matthews, G. (1996) Annu. Rev. Neurosci. 19, 219–233.
[3] Südhof, T.C. (1995) Nature 375, 645–653.
[4] Calakos, N. and Scheller, R.H. (1996) Physiol. Rev. 76, 1–29.
[5] Weber, T., Zemelman, B.V., McNew, J.A., Westermann, B., Gmachl, M., Parlati, F., Söllner, T.H. and Rothman, J.E. (1998) Cell 92, 759–772.
[6] Schiavo, G., Benfenati, F., Poulain, B., Rossetto, O., Polverino de Laureto, P., DasGupta, B.R. and Montecucco, C. (1992) Nature 359, 832–835.
[7] Yamasaki, S., Baumeister, A., Binz, T., Blasi, J., Link, E., Cornille, F., Rogues, B., Fykse, E.M., Sudhof, T.C., Jahn, R. and Niemann, H. (1994) J. Biol. Chem. 269, 12764–12772.
[8] Blasi, J., Chapman, E.R., Link, E., Binz, T., Yamasaki, S., De Camilli, P., Südhof, T.C., Niemann, H. and Jahn, R. (1993) Nature 365, 160–163.
[9] Schiavo, G., Santucci, A., DasGupta, B.R., Mehta, P.P., Jontes, J., Benfenati, F., Wilson, M.C. and Montecucco, C. (1993) FEBS Lett. 335, 99–103.
[10] Schiavo, G., Shone, C.C., Bennett, M.K., Scheller, R.H. and Montecucco, C. (1995) J. Biol. Chem. 270, 10566–10570.

[11] Williamson, L.C., Halpen, J.L., Montecucco, C., Brown, J.E. and Neale, E.A. (1996) J. Biol. Chem. 271, 7694–7699.
[12] Gutierrez, L.M., Canaves, J.M., Ferrer-Montiel, A.V., Reig, J.A., Montal, M. and Viniegra, S. (1995) FEBS Lett. 372, 39–43.
[13] Gutierrez, L.M., Viniegra, S., Rueda, J., Ferrer-Montiel, A.V., Canaves, J.M. and Montal, M. (1997) J. Biol. Chem. 272, 2634–2639.
[14] DeBello, W.M., Betz, H. and Augustine, G.J. (1993) Cell 74, 947–950.
[15] Geppert, M., Goda, Y., Hammer, R.E., Li, C., Rosahl, T.W., Stevens, C.F. and Südhof, T.C. (1994) Cell 79, 717–727.
[16] DeBello, W.M., O'Connor, V., Dresbach, T., Whiteheart, S.W., Wang, S.S.-H., Scheweizer, F.E., Betz, H., Rothman, J.E. and Augustine, G.J. (1995) Nature 373, 626–630.
[17] Cornille, F., Deloye, F., Fournie-Zaluski, M.-C., Roques, B.P. and Poulain, B. (1995) J. Biol. Chem. 270, 16826–16832.
[18] Martin, F., Salinas, E., Vazquez, J., Soria, B. and Reig, J.A. (1996) Biochem. J. 320, 201–205.
[19] Mochida, S., Sheng, Z.H., Baker, C., Kobayashi, H. and Catterall, W.A. (1996) Neuron 17, 781–788.
[20] Metha, P.P., Battenberg, E. and Wilson, M.C. (1996) Proc. Natl. Acad. Sci. USA 93, 10471–10476.
[21] Huttner, W.B., Schiebler, W., Greengard, P. and De Camilli, P. (1983) J. Cell Biol. 96, 1374–1378.
[22] Gardner, D. and Kandel, E.R. (1977) J. Neurophysiol. 40, 333–348.
[23] Poulain, B., Tauc, L., Maisey, E.A., Wadsworth, J.D.F., Mohan, P.M. and Dolly, J.O. (1988) Proc. Natl. Acad. Sci. USA 85, 4090–4094.
[24] Hay, J.C. and Martin, T.F.J. (1992) J. Cell Biol. 119, 139–151.
[25] Bittner, M.A. and Holz, R.W. (1992) J. Biol. Chem. 267, 16219–16225.
[26] Parsons, T.D., Coorssen, J.R., Horstmann, H. and Almers, W. (1995) Neuron 15, 1085–1096.
[27] Misono, H., Nishiki, T.-I., Sekiguchi, M., Takahashi, M., Kamata, Y., Kozaki, S., Ohara-Imaizumi, M. and Kumakura, K. (1996) Brain Res. 737, 351–355.
[28] Hayashi, T., Yamasaki, S., Nauenburg, S., Binz, T. and Niemann, H. (1995) EMBO J. 14, 2317–2325.
[29] Lawrence, G.W., Foran, P., Mohammed, N., DasGupta, B.R. and Dolly, J.O. (1997) Biochemistry 36, 3061–3067.
[30] Barnajee, A., Kowalchyk, J.A., DasGupta, B.R. and Martin, T.F.J. (1996) J. Biol. Chem. 271, 20227–20230.

10/28/98

MODULATION OF SNAP-25-SYNTAXIN-VAMP COMPLEX FORMATION AND STABILITY BY SMALL PEPTIDES

C. Blanes-Mira[1], A. Gil[2], M. Llobregat[1], G. Fernández-Ballester[1], R. Planells-Cases[1], E. Pérez-Payá[3], J. Canaves[4], L. M. Gutierrez[2], M. Montal[4], and A. Ferrer-Montiel[1].

[(1)]Centro de Biología Molecular y Celular. Universidad Miguel Hernández. 03206 Elche. Spain.
[(2)]Instituto de Neurociencias. Universidad Miguel Hernández. 03206 Elche. Spain.
[(3)]Departamento de Bioquímica y Biología Molecular. Universitat de Valencia. Burjassot. Spain.
[(4)]Department of Biology. University of California San Diego. La Jolla. CA 92093-0366.

Ca2+-dependent exocytosis is a highly regulated process in neural and endocrine cells. The SNARE model proposes that this process rely on the specificity of protein-protein interactions between vesicular (v-SNARE) and plasma membrane (t-SNARE) proteins. Thus, formation of stable protein complexes account for the efficiency and fidelity of vesicle docking and fusion. To better understand the physical basis of complex formation, we have used peptide molecules that interfere with the formation of the ternary complex between the vesicular protein VAMP (v-SNARE) and the plasma membrane proteins SNAP-25 and syntaxin 1 (t-SNARE). The results show that peptides patterned after the carboxy terminus of SNAP-25 prevent complex formation of recombinant proteins and in a rat brain synaptosomal fraction. As a result, these peptides are potent inhibitors of Ca2+-dependent exocytosis, emulating the action of botulinum neurotoxins. Thus, our results substantiate the notion that the C-end domain of SNAP-25, specifically residues 170-197, are essential for efficient neurosecretion, and provide novel tools to dissect the contribution of this protein region to the chain of protein-protein interaction events of the secretory pathway.

1998 –

Spanish Biophysical Society.

DEPARTMENT OF THE ARMY
US ARMY MEDICAL RESEARCH AND MATERIEL COMMAND
504 SCOTT STREET
FORT DETRICK MD 21702-5012

REPLY TO
ATTENTION OF:

MCMR-RMI-S (70-1y) 28 Aug 02

MEMORANDUM FOR Administrator, Defense Technical Information Center (DTIC-OCA), 8725 John J. Kingman Road, Fort Belvoir, VA 22060-6218

SUBJECT: Request Change in Distribution Statement

1. The U.S. Army Medical Research and Materiel Command has reexamined the need for the limitation assigned to technical reports written for this Command. Request the limited distribution statement for the enclosed accession numbers be changed to "Approved for public release; distribution unlimited." These reports should be released to the National Technical Information Service.

2. Point of contact for this request is Ms. Kristin Morrow at DSN 343-7327 or by e-mail at Kristin.Morrow@det.amedd.army.mil.

FOR THE COMMANDER:

Enc

PHYLIS M. RINEHART
Deputy Chief of Staff for
Information Management

ADB231838
ADB240253
ADB251610
ADB275099
ADB253637
ADB261538
ADB275186
ADB264648
ADB275102
ADB241899
ADB259033
ADB266113
ADB275663
ADB254489
ADB262700
ADB276708
ADB274345
ADB274844
ADB275154
ADB275535
ADB275101
ADB275451
ADB274597
ADB273871
ADB275145
ADB274505
ADB275851
ADB274459
ADB277942
ADB277404
ADB277494
ADB277536